Environment and participation of adolescents with autism spectrum disorder

HEART SOUNDS: FROM ANIMAL TO PATIENT AND MHEALTH

Hongxing Luo

Cover design: Hongxing Luo
Layout: Hongxing Luo
Printing: Ridderprint | www.ridderprint.nl
ISBN: 978-94-6458-520-9

Heart sounds:

From animal to patient and mHealth

Dissertation

To obtain the degree of Doctor at Maastricht University,

on the authority of the Rector Magnificus

prof. dr. Pamela Habibović,

in accordance with the decision of the Board of Deans,

to be defended in public on

Thursday, 22nd September, 2022, at 10:00 hours

By

Hongxing Luo

Born on 15th August, 1991

in Guangdong, China

Supervisors:
Prof. dr. F.W. Prinzen
Prof. dr. T. Delhaas

Co-supervisor:
Dr. R.N.M. Cornelussen

Assessment committee:
Prof. dr. J.E. Lumens (chair)
Prof. dr. H.P. Brunner-La-Rocca
Prof. dr. J. D'hooge (KU Leuven, Belgium)
Dr. D. Linz
Dr. ing. E. Remme (Oslo University Hospital, Norway)

The research in this thesis was funded by a grant from the European Union Horizon 2020 research and Innovation programme "Personalised In-silico Cardiology (PIC)" under the Marie Sklodowska-Curie grant agreement No. 764738.

Table of Contents

Chapter 1

General introduction

The heart is responsible for pumping blood to peripheral tissues to provide oxygen and nutrition and to remove waste products. Normally, the heart's electrical activation signals initiate from the sinoatrial node and spread through the right and left atria. After converging at the atrioventricular (AV) node, their propagation velocity is markedly slowed down. This AV delay allows the atria to contract to propel blood for additional ventricular filling. Once the electrical signals pass through the AV node, they quickly spread through the His-Purkinje fibers in both right ventricle (RV) and left ventricle (LV), resulting in electrical activation of the myocardial cells and synchronous contraction of the ventricles. Such coordinated electrical activation is important for maintaining normal cardiac pump function. Abnormalities such as left bundle branch block and AV block reduce pump function and cause or aggravate heart failure [1, 2].

The present thesis describes studies that explored the use of heart sounds to assess heart failure in both animals and humans. We also investigated the feasibility of using a smartphone to record heart sounds, which may have the potential to improve remote monitoring of patients and reduce costs of hospital visit.

1. Basic concepts

1.1 Heart sounds

Sounds are mechanical vibrations propagating through a medium such as air, water or solids. To be perceived by humans, sounds are required to have a minimal energy and a frequency range within 20 Hz – 20 kHz [3]. Heart sounds are audible vibrations of the cardiohemic system including blood, myocardium and valves [4-6].

Heart sounds are categorized by the phase of occurrence within the cardiac cycle: 1) the first heart sound (S1) occurring at end-diastole following closure of the atrioventricular valves; 2) the second heart sound (S2) occurring at end-systole following closure of the semilunar valves; 3) the third heart sound occurring during the early phase of ventricular filling; and 4) the fourth heart sound occurring during the late phase of ventricular filling following atrial contraction [7, 8]. S1 can be further divided into a mitral component following mitral valve closure and a tricuspid component following tricuspid valve closure. Similarly, S2 can be divided into an aortic and a pulmonic component.

Splitting of S1 and S2 occurs when closure of right- and left-sided valves is not synchronous. Physiological splitting occurs in normal subjects during respiration and changes in posture [9, 10]. Pathological

splitting is a sign of interventricular (VV) dyssynchronous contraction and relaxation such as occurs, among others, in patients with conductance disturbances like left bundle branch block [11, 12]. Though heart sound splitting may be useful for evaluation of ventricular contraction, its detection has long been challenging because of the short interval (20 ~ 60 ms) between the two components [13]. While early studies mainly relied on human ears or eyeballing (in the case of recorded heart sound signals) to identify the two components, recent researchers have adopted more advanced digital signal processing algorithms to obtain the splitting interval. Methods based on spectral observation, wavelet analysis, blind source separation, respiratory modulation, nonlinear dechirping modelling and smoothed Wigner-Ville distribution have been proposed [14-19]. However, their value in identifying VV dyssynchrony remains unclear because of the lack of validation against invasive hemodynamic parameters. In this thesis, we hypothesize that an automatic algorithm based on S-transform may help identify invasively-measured VV dyssynchrony in an animal model.

1.2 Systolic time intervals (STIs)

STIs are timing indicators of ventricular systole, including pre-ejection period (PEP) from QRS onset to aortic valve opening and ejection time (ET) from aortic valve opening to closure [20, 21]. The sum of PEP and ET is called QS2 which indicates the period from the onset of ventricular electrical activation to the end of ventricular mechanical contraction. STIs have been shown to relate to cardiac function [20, 22-25]. PEP indicates the time required for the electrically activated ventricles to accumulate sufficient force to close AV valves. The weaker the myocardial force is, the longer the PEP will be. At a constant contractile force and mean arterial pressure, a shortened ET will result in a lower stroke volume and stroke work. If the contractile force is also reduced, ET will shorten more as the myocardial contraction cannot generate a sustained pressure to keep the aortic valves open.

Recent studies have shown that STIs relate to patients' outcomes. Every 10-ms shortening of LV ET is related to 6% increase of all-cause mortality in patients with ventricular systolic dysfunction [26]. In a community-based cohort, ET was an independent predictor of incident heart failure with a hazard ratio of 1.07 per 10 ms decrease during a median follow-up of 17.6 years [27]. In an ambulatory heart failure population, a shorter ET was related to a higher risk of composite endpoint of death and heart failure hospitalization during 1-year follow-

up in patients with systolic dysfunction [28]. However, in these studies, STIs were measured using echocardiography which requires the patients to visit hospital and thus cannot be used for daily management of heart failure patients, especially in community-based cohorts. Heart sounds may prove to be a simple continuous method for the purpose. The PEP can be approximated using QS1, the interval from QRS onset to S1 onset, to reflect myocardial contractility before AV valve closure; while the LV ET can be approximated using S1S2, the interval from S1 onset to S2 onset, to reflect ventricular systole duration [25]. Similar to PEP and LV ET, heart sound-derived STIs have been shown to relate to cardiac function assessed using echocardiographic parameters such as LV ejection fraction and velocity time integral [29, 30]. Whether heart sound-derived STIs are related to invasively measured standards of myocardial contractility such as the maximal LV pressure, the maximal rate of rise of LV pressure and stroke work remains unclear. We hypothesize that heart sound-derived STIs are related to invasively measured indicators of myocardial contractility and likely serve as useful indicators for AV delay optimization.

1.3 Heart failure

Heart failure occurs when the heart cannot efficiently contract and/or relax due to structural and/or functional abnormalities, resulting in reduced stroke volume and/or elevated intracardiac pressures [31]. Heart failure is divided by LV ejection fraction to heart failure with reduced (≤ 40%, HFrEF), mildly reduced (41~49%, HFmrEF) and preserved (≥ 50%, HFpEF) ejection fraction [32].

Diagnosis of heart failure requires a comprehensive evaluation of the patient's symptoms such as dyspnea and reduced physical activities, signs such as lower-extremity edema and elevated jugular venous pressure, and risk factors such as cardiomyopathy and myocardial infarction. Serological markers including B-type natriuretic peptide and N-terminal pro-B-type natriuretic peptide can serve as a useful tool to reflect ventricular overload and to exclude acute heart failure [33]. Noninvasive assessment of heart failure patients mainly relies on imaging techniques such as echocardiography. Echocardiography provides an evaluation of cardiac structural and functional abnormalities including chamber volume, myocardial thickness, tissue velocity and blood flow. In this thesis, we investigate the relationship between echocardiography and heart sounds in outpatients suspected

of HFpEF, and hypothesize that heart sounds may serve as a useful indicator of ventricular diastolic dysfunction.

Treatments of heart failure are classified into pharmacological and device approaches. Pharmacological approach aims to modulate the renin-angiotensin-aldosterone and sympathetic nervous systems to reduce patients' mortality and hospitalization and to alleviate symptoms and signs [34]. Drugs including angiotensin-converting enzyme inhibitors or an angiotensin receptor-neprilysin inhibitor, beta-blockers, and mineralocorticoid receptor antagonists are the cornerstones of pharmacotherapy. Device therapy mainly contains implantable cardioverter-defibrillator and cardiac resynchronization therapy (CRT) [35]. The implantable cardioverter-defibrillator has been shown to reduce all-cause mortality and hospitalization in patients recovered from a ventricular arrhythmia (secondary prevention) and in patients with ischemic heart failure and a severely reduced LV ejection fraction (primary prevention) [36]. CRT aims to restore electrical and mechanical synchronies of atria and ventricles so that the heart can pump in an optimal condition. It is mainly recommended for symptomatic HFrEF patients with an LV ejection fraction ≤ 35% and a QRS duration of 130-149 ms in the presence of LBBB or an QRS duration of ≥ 150 ms in the absence of LBBB [32].

1.4 CRT optimization

Large clinical trials have shown the beneficial effects of CRT on reducing all-cause mortality and heart failure hospitalization [37]. Three major factors determined the amount of CRT benefit: patient selection, pacing electrode position and timing of atrial and ventricular stimulation [38]. Post-implantation optimization involves adjustments of AV delay and VV delay in a non-invasive way by programming the pacemaker. Conventionally, such optimization has been performed using electrocardiographic and echocardiographic techniques [39-41]. However, these methods may be time-consuming and subject to inter-operator variability. In this thesis, we hypothesize that measurement of heart sound splitting may indicate VV dyssynchrony and has the potential to guide CRT optimization. We also hypothesize that AV delay may be optimized by using heart sound-derived STIs.

1.5 Mobile health (mHealth)

mHealth refers to the use of mobile phone technologies such as audio calling, video calling, message texting and Apps for health purposes

including diagnosis and monitoring [42]. While the concept and its applications have only emerged recently, it has rapidly expanded in the past two decades thanks to the technological advancements of mobile phones and the drastic increase of mobile phone users. By 2021, there were 6.4 billion mobile phone users around the world, and the trend of using mobile phone for health purposes has been gaining its momentum in the past two years with the emergence of the coronavirus disease 2019 (COVID-19) [43-46]. Compared with conventional methods of patient management, mHealth has the advantages of wider user coverage, quicker/real-time data collection and feedbacks, daily home monitoring and cost effectiveness [47, 48]. An example is the use of the phone camera to obtain photoplethysmography for monitoring of heart rate and rhythm in patients with atrial fibrillation during teleconsultations [49].

Regardless of the diversity of mHealth applications, it consists of a few essential elements: phone sensor, user interface, algorithm and application scenario [50]. In a given application scenario, users interact with user interface and algorithms with or without the use of sensor(s). Frequently used phone sensors include camera, touch screen and microphone. In this thesis, we investigate the hypothesis that the smartphone built-in microphone can be used to collect heart sounds from general users.

2. Aims of the thesis

The ultimate goal of this thesis is to investigate the relation between heart sounds and hemodynamics in heart failure and the feasibility of turning the smartphone microphone into a digital stethoscope for heart sound measurements in the general public. To this end the following general aims are formulated:

1) Develop a novel algorithm to automatically identify the S2 splitting interval for evaluation of VV dyssynchrony;
2) Investigate the relations between heart sound-derived STIs and myocardial contractility and whether STIs can be applied to AV delay optimization;
3) Improve the evaluation of diastolic dysfunction using heart sounds in patients suspected of HFpEF;
4) Test the feasibility of using a smartphone microphone as digital stethoscope for heart sound measurement in the general public, and explore potential factors affecting heart sound quality.

3. Outline of the thesis

This thesis describes studies starting with animal experiments, followed by measurements in patients from HFrEF to HFpEF, and finalized with the possible application of heart sounds to mHealth (**Figure 1**).

In **Chapter 2**, we describe acute experiments in pigs with AV block, paced at varying VV delays. The relationship between VV dyssynchrony and S2 splitting was investigated using a novel automatic algorithm based on a time-frequency analysis algorithm called S-transform. The S2 splitting interval was then related to the invasively measured indicator of VV dyssynchrony.

In **Chapter 3**, we investigated the possibility of using heart sound-derived STIs for AV delay optimization in CRT. The study utilized data from both acute porcine experiments and a human study named Sensor Optimization of Cardiac Resynchronization Therapy Response (SOCR) Study. STIs including QS1 and S1S2 were measured and their relations to LV hemodynamics including maximal LV pressure, maximal rate of rise of LV pressure and stroke work were investigated. Using a parabolic curve fitting technique, we explored the feasibility of using heart sound-derived STIs for AV delay optimization in CRT.

In **Chapter 4**, the association between heart sounds and LV diastolic dysfunction was explored in HFpEF patients using a digital stethoscope. We obtained a series of heart sound features including amplitude, frequency and timing intervals, and compared them between patients with high and low ratios of early mitral inflow velocity over mitral annular early diastolic velocity (E/e'). Diagnostic performance to identify an E/e' ratio > 9 of these heart sound indicators, both used alone or combined, was investigated. From this data a heart sound score was proposed for noninvasive evaluation of diastolic dysfunction in HFpEF patients.

Nowadays, the wide applications of smartphones provide a unique opportunity for health monitoring in the general population. In **Chapter 5**, a smartphone was used as an electronic stethoscope for heart sound measurement in the general public. In collaboration with King's College London, we developed an App named Echoes for collecting heart sounds. In a preliminary analysis of this technique in > 1000 individuals, we focused on hardware (i.e., phone version) and users' characteristics (time of heart sound measurement, gender, age and body mass index) as potential determinants of heart sound quality.

Chapter 6 integrates the major findings of above-mentioned chapters and discusses them in a broader scientific and clinical perspective.

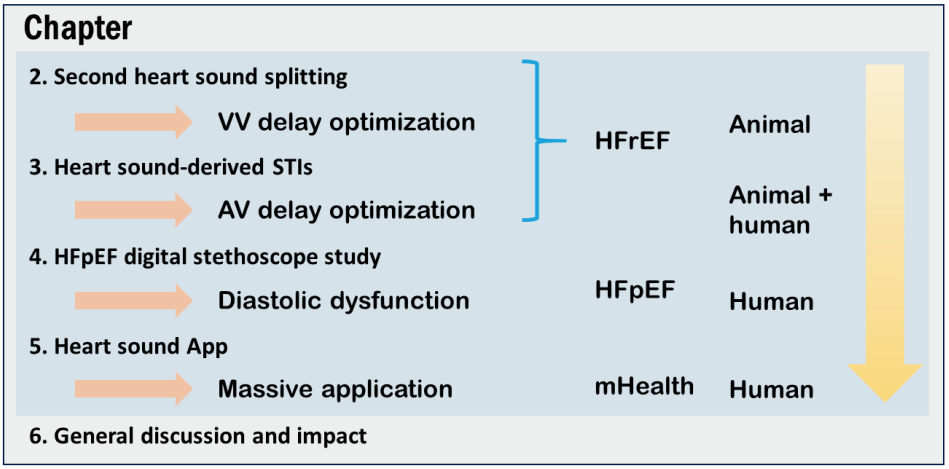

Figure 1. Overview of this thesis

AV, atrioventricular; HFrEF, heart failure with reduced ejection fraction; HFpEF, heart failure with preserved ejection fraction; mHealth, mobile health; VV, interventricular.

References:

1. Zannad F, Huvelle E, Dickstein K, van Veldhuisen DJ, Stellbrink C and Køber L, et al. Left bundle branch block as a risk factor for progression to heart failure. Eur J Heart Fail 2007; 9(1):7-14. [doi: 10.1016/j.ejheart.2006.04.011]
2. Michaelsson MRTJ. Natural history of congenital complete atrioventricular block. Pacing and clinical electrophysiology 1997; 20(8):2098-2101. [doi: 10.1111/j.1540-8159.1997.tb03636.x]
3. Gray L. Properties of sound. J Perinatol 2000; 20(8 Pt 2):S6-S11. [doi: 10.1038/sj.jp.7200442]
4. Piemme TE, Barnett GO and Dexter L. Relationship of heart sounds to acceleration of blood flow. Circ Res 1966; 18(3):303-315. [doi: 10.1161/01.res.18.3.303]
5. Kupari M. Aortic valve closure and cardiac vibrations in the genesis of the second heart sound. Am J Cardiol 1983; 52(1):152-154. [doi: 10.1016/0002-9149(83)90086-3]
6. Sabbah HN and Stein PD. Investigation of the theory and mechanism of the origin of the second heart sound. Circ Res 1976; 39(6):874-882. [doi: 10.1161/01.res.39.6.874]
7. Luisada A, Mendoza F and Alimurung M. The duration of normal heart sounds. Br Heart J 1949; 11(1):41-47. [doi: 10.1136/hrt.11.1.41]
8. Van de Werf F, Minten J, Carmeliet P, De Geest H and Kesteloot H. The genesis of the third and fourth heart sounds. A pressure-flow study in dogs. J Clin Invest 1984; 73(5):1400-1407. [doi: 10.1172/JCI111344]
9. Boyer S and Chisholm A. Physiologic splitting of the second heart sound. Circulation 1958; 18(5):1010-1011. [doi: 10.1161/01.cir.18.5.1010]
10. Breen W and Rekate A. Effect of posture on splitting of the second heart sound. JAMA 1960; 173:1326-1328. [doi: 10.1001/jama.1960.03020300038012]
11. Wolferth CC and Margolies A. Asynchronism in contraction of the ventricles in the so-called common type of bundle-branch block: Its bearing on the determination of the side of the significant lesion and on the mechanism of split first and second heart sounds. Am Heart J 1935; 10(4):425-452. [doi: 10.1016/S0002-8703(35)90213-7]
12. Xiao HB, Faiek AH and Gibson DG. Re-evaluation of normal splitting of the second heart sound in patients with classical left bundle branch block. Int J Cardiol 1994; 45(3):163-169. [doi: 10.1016/0167-5273(94)90161-9]
13. Castle R and Jones K. The mechanism of respiratory variation in splitting of the second heart sound. Circulation 1961; 24:180-184. [doi: 10.1161/01.cir.24.2.180]
14. Al-Naami B, Al-Nabulsi J, Amasha H and Torry J. Utilizing wavelet transform and support vector machine for detection of the paradoxical splitting in the second heart sound. Med Biol Eng Comput 2010; 48(2):177-184. [doi: 10.1007/s11517-009-0548-7]
15. Chen L, Wu SF, Xu Y, Lyman WD and Kapur G. Blind separation of heart sounds. Journal of Theoretical and Computational Acoustics 2018; 26(01):1750035. [doi: 10.1142/S2591728517500359]
16. Tang H, Chen H and Li T. Discrimination of aortic and pulmonary components from the second heart sound using respiratory modulation and measurement of respiratory split. Applied Sciences 2017; 7(7):690. [doi: 10.3390/app7070690]

17. Xu J, Durand LG and Pibarot P. A new, simple, and accurate method for non-invasive estimation of pulmonary arterial pressure. Heart 2002; 88(1):76-80. [doi: 10.1136/heart.88.1.76]
18. Yildirim I and Ansari R. A robust method to estimate time split in second heart sound using instantaneous frequency analysis. Annu Int Conf IEEE Eng Med Biol Soc 2007; 2007:1855-1858. [doi: 10.1109/IEMBS.2007.4352676]
19. Mckusick V, Reagan W, Santos G and Webb G. The splitting of heart sounds; A spectral phonocardiographic evaluation of clinical significance. Am J Med 1955; 19(6):849-861. [doi: 10.1016/0002-9343(55)90152-2]
20. Alhakak AS, Teerlink JR, Lindenfeld J, Böhm M, Rosano GMC and Biering Sørensen T. The significance of left ventricular ejection time in heart failure with reduced ejection fraction. Eur J Heart Fail 2021; 23(4):541-551. [doi: 10.1002/ejhf.2125]
21. Newlin DB and Levenson RW. Pre-ejection period: Measuring beta-adrenergic influences upon the heart. Psychophysiology 1979; 16(6):546-553. [doi: 10.1111/j.1469-8986.1979.tb01519.x]
22. Reant P, Dijos M, Donal E, Mignot A, Ritter P and Bordachar P, et al. Systolic time intervals as simple echocardiographic parameters of left ventricular systolic performance: Correlation with ejection fraction and longitudinal two-dimensional strain. European journal of echocardiography 2010; 11(10):834-844. [doi: 10.1093/ejechocard/jeq084]
23. Martin CE, Shaver JA, Thompson ME, Reddy PS and Leonard JJ. Direct correlation of external systolic time intervals with internal indices of left ventricular function in man. Circulation 1971; 44(3):419-431. [doi: 10.1161/01.cir.44.3.419]
24. Nakamura Y, Wiegner AW, Gaasch WH and Bing OH. Systolic time intervals: Assessment by isolated cardiac muscle studies. J Am Coll Cardiol 1983; 2(5):973-978. [doi: 10.1016/s0735-1097(83)80248-4]
25. Weissler AM, Harris WS and Schoenfeld CD. Systolic time intervals in heart failure in man. Circulation 1968; 37(2):149-159. [doi: 10.1161/01.cir.37.2.149]
26. Alhakak AS, Sengeløv M, Jørgensen P, Bruun NE, Abildgaard U and Iversen A, et al. Left ventricular systolic ejection time is an independent predictor of all-cause mortality in heart failure with reduced ejection fraction. J Am Coll Cardiol 2020; 75(11, Supplement 1):1776. [doi: 10.1016/S0735-1097(20)32403-7]
27. Biering-Sorensen T, Querejeta RG, Hegde SM, Shah AM, Claggett B and Mosley TJ, et al. Left ventricular ejection time is an independent predictor of incident heart failure in a community-based cohort. Eur J Heart Fail 2018; 20(7):1106-1114. [doi: 10.1002/ejhf.928]
28. Patel PA, Ambrosy AP, Phelan M, Alenezi F, Chiswell K and Van Dyke MK, et al. Association between systolic ejection time and outcomes in heart failure by ejection fraction. Eur J Heart Fail 2020; 22(7):1174-1182. [doi: 10.1002/ejhf.1659]
29. Zuber M, Toggweiler S, Quinn-Tate L, Brown L, Amkieh A and Erne P. A comparison of acoustic cardiography and echocardiography for optimizing pacemaker settings in cardiac resynchronization therapy. Pacing Clin Electrophysiol 2008; 31(7):802-811. [doi: 10.1111/j.1540-8159.2008.01094.x]

30. Shah SJ and Michaels AD. Hemodynamic correlates of the third heart sound and systolic time intervals. Congest Heart Fail 2006; 12 Suppl 1:8-13. [doi: 10.1111/j.0889-7204.2006.05767.x]
31. Kemp CD and Conte JV. The pathophysiology of heart failure. Cardiovasc Pathol 2012; 21(5):365-371. [doi: 10.1016/j.carpath.2011.11.007]
32. McDonagh TA, Metra M, Adamo M, Gardner RS, Baumbach A and Bohm M, et al. 2021 ESC Guidelines for the diagnosis and treatment of acute and chronic heart failure. Eur Heart J 2021; 42(36):3599-3726. [doi: 10.1093/eurheartj/ehab368]
33. Roberts E, Ludman AJ, Dworzynski K, Al-Mohammad A, Cowie MR and McMurray JJ, et al. The diagnostic accuracy of the natriuretic peptides in heart failure: Systematic review and diagnostic meta-analysis in the acute care setting. BMJ 2015; 350:h910. [doi: 10.1136/bmj.h910]
34. Iacoviello M, Palazzuoli A and Gronda E. Recent advances in pharmacological treatment of heart failure. Eur J Clin Invest 2021; 51(11):e13624. [doi: 10.1111/eci.13624]
35. Hussein AA and Wilkoff BL. Cardiac implantable electronic device therapy in heart failure. Circ Res 2019; 124(11):1584-1597. [doi: 10.1161/CIRCRESAHA.118.313571]
36. Santini M, Lavalle C and Ricci RP. Primary and secondary prevention of sudden cardiac death: Who should get an ICD? Heart 2007; 93(11):1478-1483. [doi: 10.1136/hrt.2006.095190]
37. Cleland JG, Abraham WT, Linde C, Gold MR, Young JB and Claude Daubert J, et al. An individual patient meta-analysis of five randomized trials assessing the effects of cardiac resynchronization therapy on morbidity and mortality in patients with symptomatic heart failure. Eur Heart J 2013; 34(46):3547-3556. [doi: 10.1093/eurheartj/eht290]
38. Vernooy K, van Deursen CJ, Strik M and Prinzen FW. Strategies to improve cardiac resynchronization therapy. Nat Rev Cardiol 2014; 11(8):481-493. [doi: 10.1038/nrcardio.2014.67]
39. Gold MR, Niazi I, Giudici M, Leman RB, Sturdivant JL and Kim MH, et al. A prospective comparison of AV delay programming methods for hemodynamic optimization during cardiac resynchronization therapy. J Cardiovasc Electr 2007; 18(5):490-496. [doi: 10.1111/j.1540-8167.2007.00770.x]
40. Boriani G, Muller CP, Seidl KH, Grove R, Vogt J and Danschel W, et al. Randomized comparison of simultaneous biventricular stimulation versus optimized interventricular delay in cardiac resynchronization therapy. The Resynchronization for the HemodYnamic Treatment for Heart Failure Management II implantable cardioverter defibrillator (RHYTHM II ICD) study. Am Heart J 2006; 151(5):1050-1058. [doi: 10.1016/j.ahj.2005.08.019]
41. Jansen AH, Bracke FA, van Dantzig JM, Meijer A, van der Voort PH and Aarnoudse W, et al. Correlation of echo-Doppler optimization of atrioventricular delay in cardiac resynchronization therapy with invasive hemodynamics in patients with heart failure secondary to ischemic or idiopathic dilated cardiomyopathy. Am J Cardiol 2006; 97(4):552-557. [doi: 10.1016/j.amjcard.2005.08.076]

42. Fiordelli M, Diviani N and Schulz PJ. Mapping mHealth research: A decade of evolution. J Med Internet Res 2013; 15(5):e95. [doi: 10.2196/jmir.2430]
43. Statista.Number of smartphone users from 2016 to 2021. URL: https://www.statista.com/statistics/330695/number-of-smartphone-users-worldwide/ [accessed 2021-11-29]
44. Almalki M and Giannicchi A. Health apps for combating COVID-19: Descriptive review and taxonomy. JMIR mHealth uHealth 2021; 9(3):e24322. [doi: 10.2196/24322]
45. Giansanti D. The role of the mHealth in the fight against the covid-19: Successes and failures. Healthcare (Basel) 2021; 9(1). [doi: 10.3390/healthcare9010058]
46. Ming LC, Untong N, Aliudin NA, Osili N, Kifli N and Tan CS, et al. Mobile health apps on COVID-19 launched in the early days of the pandemic: Content analysis and review. JMIR mHealth uHealth 2020; 8(9):e19796. [doi: 10.2196/19796]
47. Tate EB, Spruijt-Metz D, O'Reilly G, Jordan-Marsh M, Gotsis M and Pentz MA, et al. MHealth approaches to child obesity prevention: Successes, unique challenges, and next directions. Transl Behav Med 2013; 3(4):406-415. [doi: 10.1007/s13142-013-0222-3]
48. Iribarren SJ, Cato K, Falzon L and Stone PW. What is the economic evidence for mHealth? A systematic review of economic evaluations of mHealth solutions. Plos One 2017; 12(2):e170581. [doi: 10.1371/journal.pone.0170581]
49. Pluymaekers N, Hermans A, van der Velden R, Gawalko M, den Uijl DW and Buskes S, et al. Implementation of an on-demand app-based heart rate and rhythm monitoring infrastructure for the management of atrial fibrillation through teleconsultation: TeleCheck-AF. Europace 2021; 23(3):345-352. [doi: 10.1093/europace/euaa201]
50. Baxter C, Carroll JA, Keogh B and Vandelanotte C. Assessment of mobile health apps using Built-In smartphone sensors for diagnosis and treatment: Systematic survey of apps listed in international curated health app libraries. JMIR mHealth uHealth 2020; 8(2):e16741. [doi: 10.2196/16741]

Chapter 2

Second heart sound splitting as an indicator of interventricular mechanical dyssynchrony using a novel splitting detection algorithm

Hongxing Luo [1], Philip Westphal [1, 2], Mehrdad Shahmohammadi [3], Luuk I.B. Heckman [1], Marion Kuiper [1], Richard N. Cornelussen [1, 2], Tammo Delhaas [3], Frits W. Prinzen [1]

Physiol Rep. 2021 Jan; 9(1):e14687. doi: 10.14814/phy2.14687.

[1] Department of Physiology, Cardiovascular Research Institute Maastricht (CARIM), Maastricht University, the Netherlands
[2] Bakken Research Centre Medtronic, plc, Maastricht, the Netherlands
[3] Department of Biomedical Engineering, Cardiovascular Research Institute Maastricht (CARIM), Maastricht University, the Netherlands

Abstract

Second heart sound (S2) splitting results from non-simultaneous closures between aortic (A2) and pulmonic valves (P2) and may be used to detect timing differences (dyssynchrony) in relaxation between right (RV) and left ventricle (LV). However, overlap of A2 and P2 and the change of heart sound morphologies have complicated detection of the S2 splitting interval. This study introduces a novel S-transform amplitude ridge tracking (START) algorithm for estimating S2 splitting interval and investigates the relationship between S2 splitting and interventricular relaxation dyssynchrony (IRD). Firstly, the START algorithm was validated in a simulated model of heart sound. It showed small errors (< 5 ms) in estimating splitting intervals from 10 to 70 ms, with A2/P2 amplitude ratios from 0.2 to 5, and signal-to-noise ratios from 10 to 30 dB. Subsequently, the START algorithm was evaluated in a porcine model employing a wide range of paced RV-LV delays. IRD was quantified by the time difference between invasively measured LV and RV pressure downslopes. Between LV pre-excitation to RV pre-excitation, S2 splitting interval significantly decreased from 47 ms to 23 ms ($P < 0.001$), accompanied by a decrease in IRD from 8 ms to -18 ms ($P < 0.001$). S2 splitting interval was significantly correlated with IRD in each experiment ($P < 0.001$). In conclusion, the START algorithm can accurately assess S2 splitting and may serve as a useful tool to assess interventricular dyssynchrony.

Introduction

Heart sounds, originating from vibrations of valves and adjacent tissues following valve closure, contain information of timing differences (dyssynchrony) of contraction and relaxation between the ventricles [1-3]. Physiological splitting of the second heart sound (S2) occurs during inspiration when the difference between timing of aortic and pulmonic valve closure is accentuated because the right ventricular (RV) ejection period is extended with a temporary increase in central venous return. Wide splitting is seen in conditions that delay RV emptying like right bundle branch block. Reverse splitting, i.e., splitting during expiration, is associated, amongst others, with left bundle branch block. Because of these relations between S2 splitting behaviours and ventricular activation patterns, quantification of S2 splitting might help to assess the degree of dyssynchrony in patients eligible for cardiac resynchronization therapy (CRT) and also to specify the settings of pacemakers that aim at minimizing dyssynchrony. However, currently heart sound indicator and algorithm to monitor interventricular dyssynchrony in these patients are lacking [4-8].

Estimating heart sound splitting interval has long been a challenge because of the overlap of heart sound components. Auscultatory detection of S2 splitting is possible at intervals of at least 40 ms, whereas detection of intervals of 20 - 40 ms is only feasible with low ambient noise and extensive listener's experience [9]. Importantly, this borderline area is where normal/physiological heart sound splitting occurs. Digital recording of heart sounds and subsequent analyses obviously avoid the limitations of human ear and brain. Existing heart sound splitting detection algorithms can be mainly divided into three categories: 1) mathematical modeling of heart sound morphologies and inferring splitting interval by comparing morphology similarity between simulated and real heart sounds; 2) blind source separation using multiple-channel simultaneous recordings; and 3) time-frequency analysis followed by visual identification of splitting heart sound components [9-19]. Modeling approaches have been dampened by the lack of a unified model of heart sound genesis [15, 17]. Blind source separation requires multi-sensor recordings, hypothesis of heart sound transmission and complicated mathematical calculation [11, 14]. Time-frequency analysis approaches, such as continuous wavelet transform (CWT) and smoothed Wigner-Ville distribution (SWVD), have been popular in recent years [9, 10, 12, 13, 16, 18, 19]. However, CWT decomposes heart sounds into various scales, making further signal

processing required to translate CWT results into a time-frequency spectrum. SWVD is undermined by its cross-terms which may heavily interfere with the real heart sound components. As one of time-frequency analysis methods, S-transform has been proposed as an energy-concentrated signal processing approach which has a more direct relation with frequency compared with CWT and which has no cross-terms interference compared with SWVD [20].

It is the aim of the present study to develop a single-heartbeat S2 splitting method that may be applied to CRT. Our S2 splitting measurement is based on S-transform. We first validated the algorithm using a chirp model of simulated heart sound and subsequently applied the algorithm to an animal model of varying interventricular delays.

Methods

S-transform for signal analysis

S-transform is a signal processing technique used to analyze time-frequency features of a signal [20]. It slides a mother wavelet of a given frequency along the raw signal (**Figure 1A**). Note that the width of the mother wavelet decreases with increasing frequency and height increases with frequency. For each time point, the wavelet is multiplied with the raw signal, and the resultant values are summed as an amplitude value. Similar to the principle of fast Fourier transform, this amplitude value would be high if the raw signal has a similar shape to the mother wavelet, and vice versa. This enables to extract the frequency contents of a signal using wavelets of a given range of frequencies, resulting in a matrix of amplitude values with time as horizontal axis and frequency as vertical axis, or an S-transform amplitude spectrum (**Figure 1B**). For our purpose, we used the frequency range of 50 - 250 Hz.

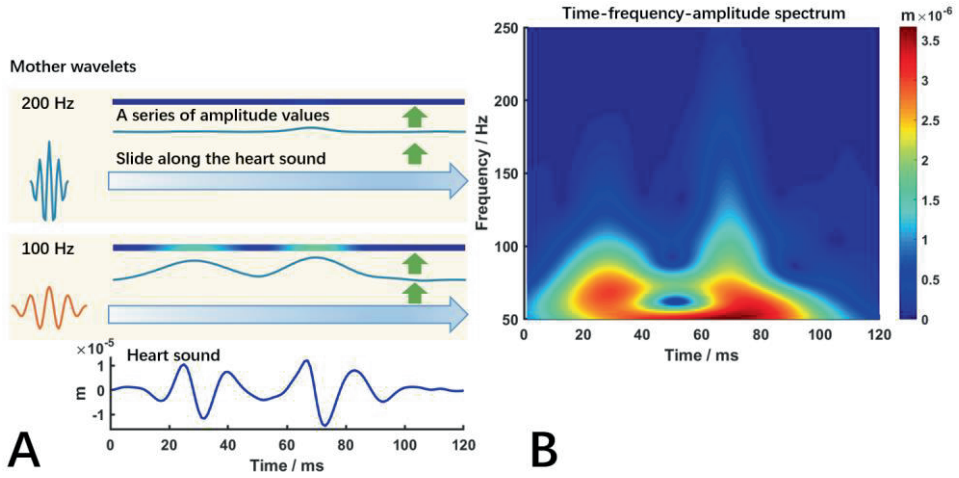

Figure 1. Demonstration of S-transform for signal analysis using an S2 from an animal experiment. *Panel A shows (from bottom to top) 1) the S2 during biventricular pacing with the right atrium to RV (A-RV) paced interval 150 ms and A-LV 50 ms, 2) a mother wavelet of 100 Hz and the resulting amplitude values with time, and 3) a mother wavelet of 200 Hz and the resulting amplitude values with time. Panel B shows the complete S-transform amplitude spectrum. In panel A, the mother wavelets of various frequencies slide along the heart sound signal, convolve with the signal, and result in amplitude values. In panel B, amplitude values of frequencies from 50 Hz to 250 Hz are plotted as an intensity map.*

S-transform amplitude ridge tracking (START)-based detection of S2 splitting interval

The START-based detection of S2 splitting interval was performed on the S-transform amplitude spectrum. It consists of two steps: ridge identification on the amplitude spectrum, and calculation of splitting interval from these ridges (**Figure 2**). 1) Ridge identification: A 50-Hz highpass filter was applied to an S2, after which it underwent an S-transform using mother wavelets with frequencies of 50 to 250 Hz, resulting in an amplitude spectrum. Local adjacent maxima of the amplitude spectrum were connected as a ridge. A ridge was used for further analysis if its frequency range covered more than 50 Hz. Doing so, in the example of **Figure 2**, 5 ridges were detected. 2) Subsequently, the importance of each ridge was graded using a weight factor which is the sum of products of amplitude and frequency of each ridge. This weight factor was indicative of the energy contained in each

ridge. After finding all ridges, the weight factors were normalized to the highest one. Then two strongest ridges were considered to stem from A2 and P2. The A2-P2 splitting interval was calculated as the median time between common frequencies of the two ridges.

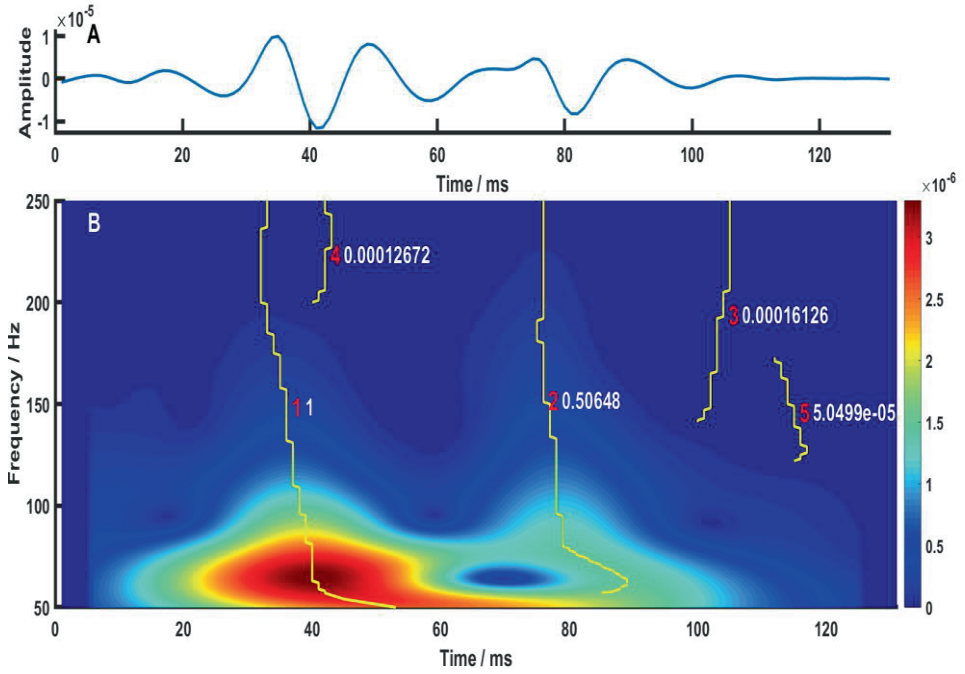

Figure 2. START algorithm for estimating A2-P2 splitting interval *A) A segmented S2 from animal experiment No.1 with A-RV delay 150 ms and A-LV delay 50 ms. B) S-transform amplitude spectrum and 5 ridges (solid yellow lines). Red number indicates the rank of each ridge. White number indicates weight factor of each ridge. The raw heart sound signal in the panel A was processed with S-transform to obtain a time-frequency-amplitude map in the panel B, then the ridges of this map were identified and ranked according to their energies. The two ridges with the highest energies were used for calculating heart sound splitting interval. In this example, the START-estimated S2 splitting interval is 44 ms.*

Validation of START algorithm in S2 simulation model

The START algorithm was validated using artificial heart sounds, generated by a widely used nonlinear transient chirp signal model of S2 [21]. It first simulates A2 and P2, and then sums them up to obtain the

entire S2. The A2 and P2 are simulated by the following equations, respectively:

$$\mathrm{A2(t)} = A_A(t)\sin\big(\varphi_A(t)\big) \qquad (1)$$

$$P2(t) = A_P(t)\sin\big(\varphi_P(t)\big) \qquad (2)$$

The duration of each component, t, is defined as $0 \le t \le 60$ ms. A and φ represent the amplitude and phase function of A2 and P2, respectively:

$$A_A(t) = \mathrm{ampA} * \left(1 - e^{\frac{-t}{8}}\right) * e^{\frac{-t}{16}} * \sin\left(\frac{\pi t}{60}\right) \qquad (3)$$

$$A_p(t) = \mathrm{ampP} * \left(1 - e^{\frac{-t}{8}}\right) * e^{\frac{-t}{16}} * \sin\left(\frac{\pi t}{60}\right) \qquad (4)$$

$$\varphi_A(t) = 24.3 * t + 451.4 * \sqrt{t+1} \qquad (5)$$

$$\varphi_p(t) = 21.8 * t + 356.3 * \sqrt{t+1} \qquad (6)$$

ampA and ampP represent the normalized amplitude of A2 and P2, respectively. In this study, we used a constant normalized amplitude of P2, so ampP = 1. Phase functions (5) and (6) control the frequency range of A2 and P2, respectively. To validate the START algorithm, we varied the splitting interval from 10 ms to 70 ms; ampA from 0.2 to 5.0; and signal-to-noise ratios (SNRs)from 10 to 30 decibels (dB).

Animal experiments

Open-chest sacrifice pig experiments were performed in accordance with the Dutch Law on Animal Experimentation and the European Directive for the Protection of Vertebrate Animals Used for Experimental and Other Scientific Purposes. The protocol was approved by the Central Committee for Animal experiments (CCD) in The Netherlands and the Animal Experimental Committee of Maastricht University.

Five male adult pigs (weight: 64 ± 1 kg) were premedicated with prophylactic antibiotics (ampicillin 1000 mg I.V.) and thiopental (5-15 mg/kg, I.V.) for induction of general anesthesia [22]. Subsequently, they were intubated and mechanically ventilated, followed by maintenance of general anesthesia using rocuronium (0.1 mg/kg/h I.V.), sufentanyl (4-8 μg/kg/h I.V.) and propofol (2.5-10 mg/kg/h, I.V.). A left thoracotomy through the fifth intercostal space was performed to completely expose the epicardial surface. LV and RV pressure signals were acquired by using 7F catheter-tip manometers, inserted into the carotid artery and jugular vein, respectively. Pacing electrodes were transvenously placed in the right atrium, RV apex and epicardially on the basal posterolateral wall of LV. Complete atrioventricular (AV) block was induced by radiofrequency ablation.

Heart sounds were collected by a triaxial accelerometer with a sample rate of 1000 Hz, positioned on the anterior RV base. This position was chosen because it was close to the pulmonic and aortic valves. After creation of AV-block, biventricular pacing was used with a fixed atrial (A) to RV (A-RV) pacing delay (150 ms) and varying A to LV (A-LV) pacing delays (50 ms to 250 ms), using 25 ms in the 1st experiment or 50 ms per step in the remaining 4 experiments.

During each pacing setting, ECG and hemodynamic signals were collected for 20 - 30 seconds using the IDEEQ data acquisition system (IDEE Maastricht University / Maastricht Instruments BV). Accelerometer signals were collected using a custom-made data acquisition system. Hemodynamic signals and accelerometer signals were aligned using a synchronous pulse signal. Hemodynamic analysis was performed using the IDEEQ software, developed at Maastricht University.

Calculation of interventricular relaxation dyssynchrony (IRD)

IRD was defined as the time difference between the downslopes of LV and RV pressure curves (**Figure 3**). Pressure data were filtered using a second-order Butterworth bandpass filter with the range of 0.5-40 Hz. After normalizing both pressure curves to the range of 0 to 1, IRD was determined as the time shift between LV and RV pressure, required to achieve the highest correlation coefficient. Positive IRD indicates the LV downslope being earlier than the RV downslope. This approach is similar to that used in our previous study to determine interventricular mechanical dyssynchrony during isovolumic contraction phase [23].

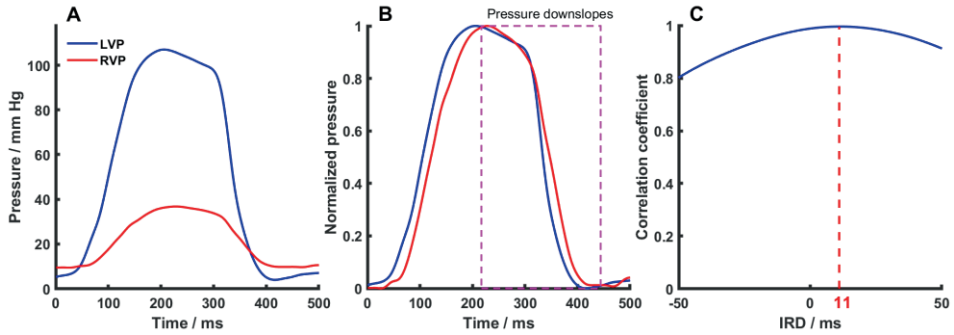

Figure 3. Demonstration of interventricular relaxation dyssynchrony calculation *A) Raw LV and RV pressures from animal experiment No.1 at A-RV delay 150 ms and A-LV delay 50 ms. B) Normalized LV and RV pressure, with their downslopes used for correlation calculation. C) Correlation coefficient curve indicating an interventricular relaxation dyssynchrony of 11 ms. Raw LV and RV pressures in the panel A were normalized in the panel B. The downslopes of the normalized pressures were cross-correlated to obtain the correlation coefficients in the panel C. The time when the correlation coefficient was the highest was used as an estimate of interventricular relaxation dyssynchrony.*
LVP, left ventricular pressure; RVP, right ventricular pressure.

Heart sound signal processing

From data acquired during the animal experiments, a combined accelerometer signal was calculated from the raw signals of X, Y and Z directions, and double integrated to obtain a displacement signal. A second-order Butterworth bandpass filter of 50-250 Hz was applied. Locations of S1 and S2 were identified with reference to lead II electrocardiogram (ECG). To reduce the effect of any sudden vibrations and background noises on manual identification, we overlapped all heartbeats and calculated a median heart sound signal as a reference. Premature ventricular contraction beats and their 2 subsequent heartbeats as well as heartbeats with too much noise were discarded. Finally, the resulting S2 signal was processed with the START algorithm to obtain splitting interval.

Comparison with existing heart sound splitting detection algorithms

To clarify the role of our START algorithm in comparison with other existing heart sound splitting detection algorithms, we searched the

PubMed database using terms of "heart sound" and "split*" on October 27, 2020. Date of publication was from the year 1970. Each publication was first judged by title and abstract. Publications including reviews, letters and case reports were excluded. Potential articles were further screened for full text. The search approach was complemented by consulting experts of the field for potential related studies. We included original studies which described heart sound splitting detection algorithms. The following information was extracted from each eligible article: first author name, year of publication, brief description of the algorithm, whether the algorithm works on a single heartbeat, and whether validation study was performed. Validation study could be any of the following: 1) validation of the algorithm in various splitting intervals; 2) validation of the algorithm in various A2/P2 amplitude ratios; or 3) validation of the algorithm in various SNRs.

Statistical analysis

Hemodynamic data and summary of correlation data were expressed as mean and standard deviation. S2 splitting interval and IRD were expressed as median (25th percentile, 75th percentile) to reduce the potential effect of respiration on our analysis. Pearson's correlation was calculated between START-estimated splitting interval and simulated splitting interval as well as between estimated splitting interval and IRD during animal experiment. Spearman's rank correlation was calculated between splitting interval and A-LV delay as well as between IRD and A-LV delay. A P value less than 0.05 was assumed to indicate a statistically significant difference. All statistical analyses were performed using MATLAB R2018b and Stata/MP 14.0.

Results

Validation of START algorithm in simulated signals

When using the simulated heart sound signals, the START algorithm had a high accuracy at a wide range of splitting intervals (10 - 70 ms; $R^2 = 1$, $P < 0.001$) (**Figure 4A**). Mean estimation error was 0.5 ms in this range. When fixing the normalized P2 amplitude at 1 and varying the A2 amplitude from 0.2 to 5, the splitting estimation was stable for the ampA/ampP ratios below 4 and slightly increased by 1 ms at ampA/ampP ratio of 5 (**Figure 4B**). From SNRs of 10 dB to 30 dB, the estimated splitting values fluctuated around the expected value by 1 to 2 ms (**Figure 4C**).

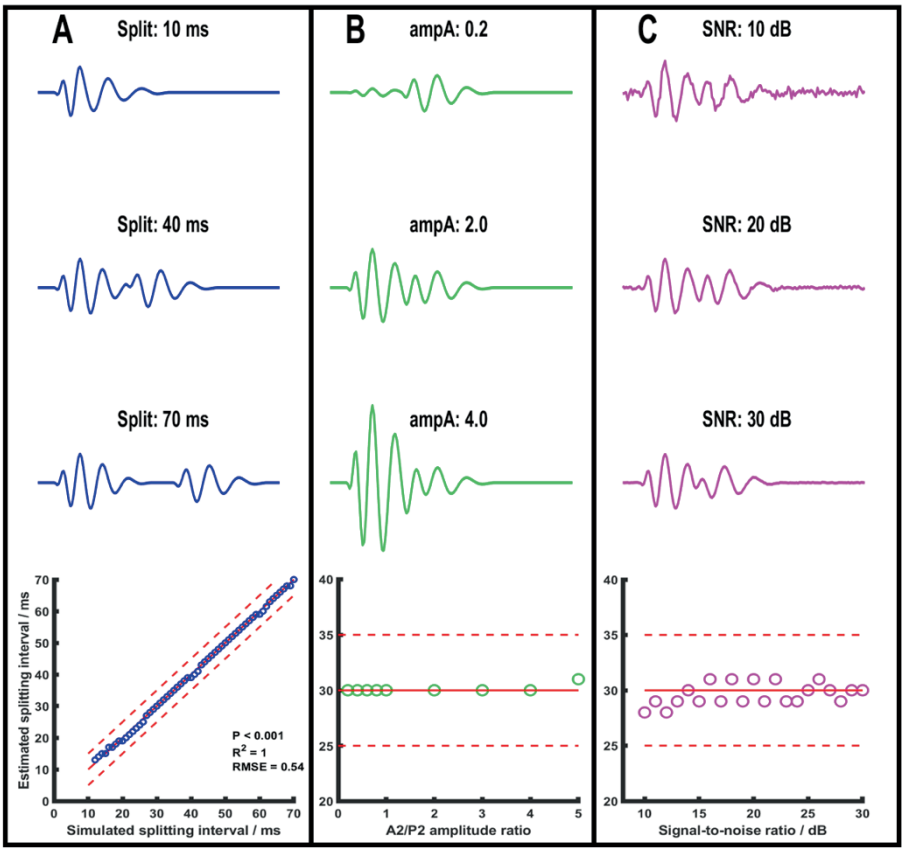

Figure 4. START algorithm in simulated second heart sounds. *Red solid line indicates line of identity in panel A and 30 ms in panels B and C. Red dash lines are 5-ms upper and lower boundaries of the expected values. Panel A (in blue) demonstrated three representative simulated heart sounds of splitting intervals 10 ms, 40 ms and 70 ms, while the bottom figure showed the relationship between simulated and START-estimated splitting intervals from 10 ms to 70 ms. Pearson's correlation was calculated. Panel B (in green) demonstrated three representative simulated heart sounds with normalized A2 amplitudes of 0.2, 2.0 and 4.0 when the normalized P2 amplitude was fixed at 1.0. In all these cases, the simulated splitting intervals were fixed at 30 ms, and the bottom figure showed the errors of splitting interval estimation using our proposed START algorithm. Panel C (in magenta) demonstrated three representative simulated heart sounds of signal-to-noise ratios of 10, 20 and 30 dB. In all these cases, the simulated splitting intervals were fixed at 30 ms, and the bottom figure showed*

the errors of START-based splitting interval estimation for signal-to-noise ratios from 10 dB to 30 dB at step of 1 dB.
ampA, normalized amplitude of aortic component of S2; dB, decibel; RMSE, root mean square error; SNR, signal-to-noise ratio.

Animal experiments

Table 1 summarizes the hemodynamic data of the 5 pigs with AV block, measured during simultaneous RV and LV pacing with an AV delay of 150 ms.

Table 1. Summary of hemodynamics (n = 5) *

Variables	Values
Heart rate (bpm)	94 ± 23
Systolic blood pressure (mmHg)	99 ± 21
Diastolic blood pressure (mmHg)	71 ± 19
LV dP/dtmax (mmHg / sec)	1337 ± 206
LV dP/dtmin (mmHg / sec)	-1685 ± 447
RV dP/dtmax (mmHg / sec)	337 ± 25
RV dP/dtmin (mmHg / sec)	-358 ± 75

bpm, beats per minute; LV, left ventricle; RV, right ventricle.
** Data were measured during biventricular pacing with AV delay of 150 ms.*

The left panels of **Figure 5** show examples of the measurements of RV and LV pressure as well as heart sounds at three A-LV delays (75 ms, 150 ms and 225 ms) when A-RV delay was fixed at 150 ms. Note that at an A-LV of 75 ms LV pressure rises before RV pressure and that this is accompanied by a clear S2 splitting. S2 splitting becomes smaller with longer A-LV delays, i.e., more simultaneous LV and RV activation (A-LV 150 ms) and earlier RV activation (A-LV 225 ms). Note that the amplitudes of S2 also became higher as A2 and P2 merged. The most significant changes of A2 and P2 occurred from A-LV delay of 100 ms to 200 ms. This is further demonstrated in all five experiments in **Figure 6**. S2 splitting interval significantly decreased from low to high A-LV intervals (representing changes from LV preexcitation to RV preexcitation) (all $P < 0.001$).

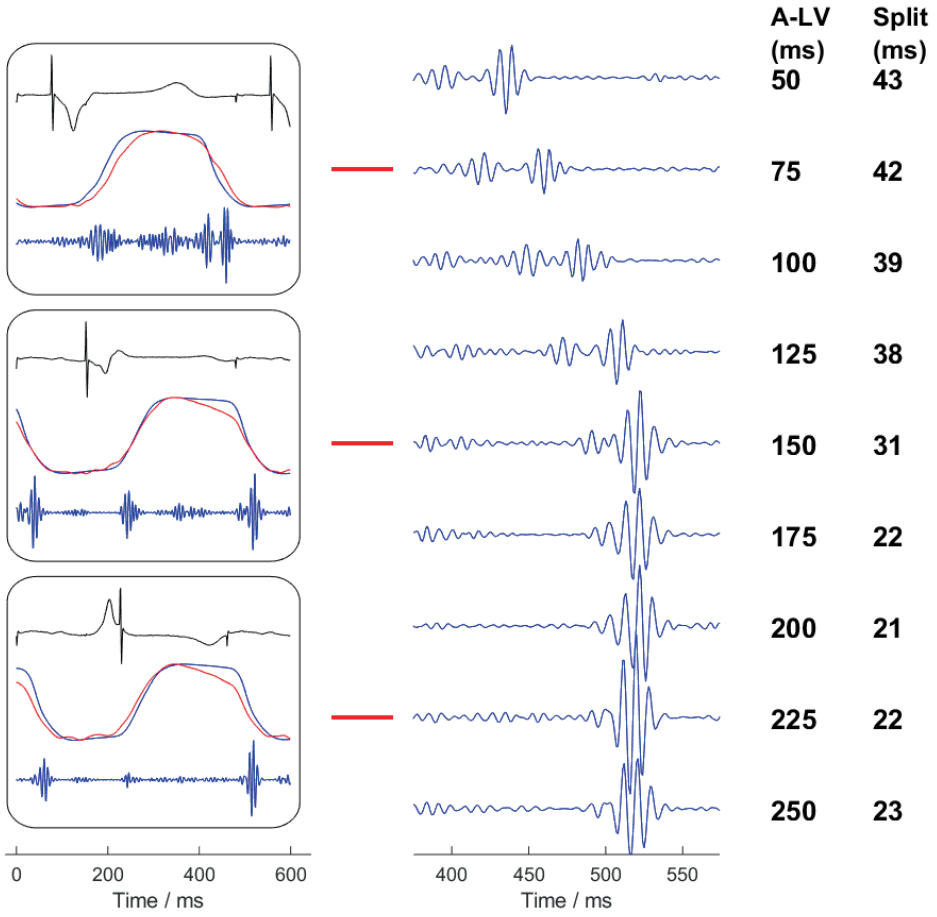

Figure 5. Representative examples of second heart sound splitting at various paced interventricular delays. *When A-RV delay was fixed at 150 ms, A-LV delays were varied from 50 ms to 250 ms with 25 ms per step. Representative heart sounds from experiment No.1. In the left panels, three situations with A-LV delays of 75, 150 and 225 ms are shown with recordings of electrocardiogram, LV pressure (blue), RV pressure (red) and heart sounds. In the right panel, S2 is shown at higher temporal resolution. Note that S2 splitting decreases from A-LV delays of 50 ms to 150 ms, but remains virtually constant at longer A-LV delays.*

S1, the first heart sound; S2, the second heart sound; LV, left ventricle; RV, right ventricle; A-LV, right atrium to left ventricle paced delay.

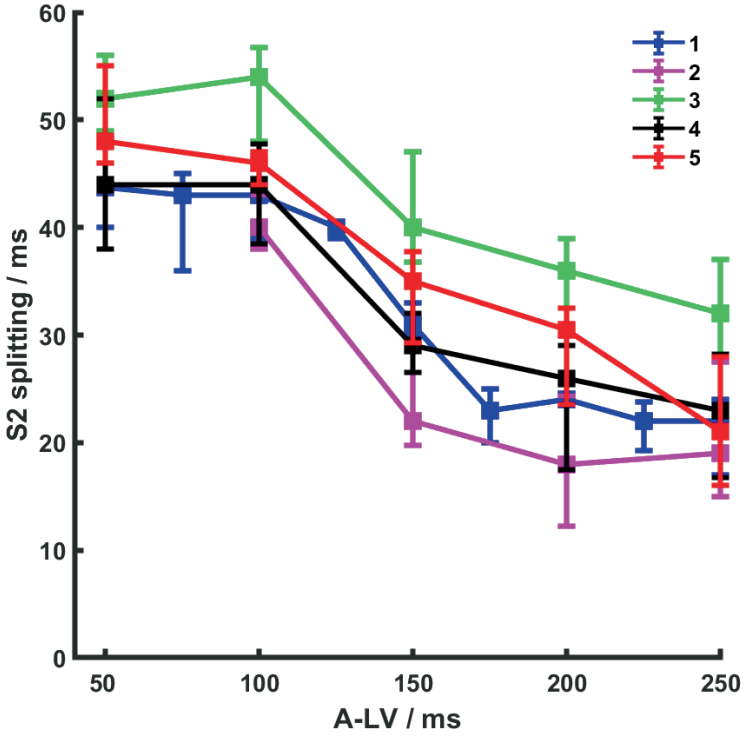

Figure 6. Second heart sound splitting interval as a function of atrio-left ventricular stimulation interval (A-LV). *Each colour represents a different animal. Median values and 25-75% percentiles of all beats at each A-LV interval are presented (A-RV delay was fixed at 150 ms). From experiments No. 1 to 5, the median number of heartbeats was 38, 43, 34, 29 and 33, respectively, for each A-LV delay group. From A-LV delay of 50 ms to 250 ms at step of 50 ms, the overall S2 splitting interval was 47 (41, 52) ms, 44 (39, 47) ms, 32 (27, 37) ms, 25 (17, 30) ms and 23 (16, 28) ms, respectively. Data were presented as median (25 percentile to 75 percentile). For all 5 experiments, Spearman's rank correlation was calculated. R^2 value was 0.71, 0.41, 0.63, 0.64 and 0.72 from experiment 1 to 5, respectively, and all P values were < 0.001.*
S2, second heart sound.

Figure 7A showed decreasing IRDs as A-LV delays changed from 50 ms to 250 ms, when A-RV delay was fixed at 150 ms (all P < 0.001). It is noteworthy that like S2 splitting interval in the **Figure 6**, the most significant changes of IRD occurred from A-LV delay of 100 ms to 200 ms. **Figure 7B** demonstrated that for each animal experiment, there was a strong correlation between START-estimated S2 splitting intervals and invasively measured IRDs (all P < 0.001). **Table 2** presented a summary of results of linear curve fitting and correlation coefficient between S2 splitting and IRD.

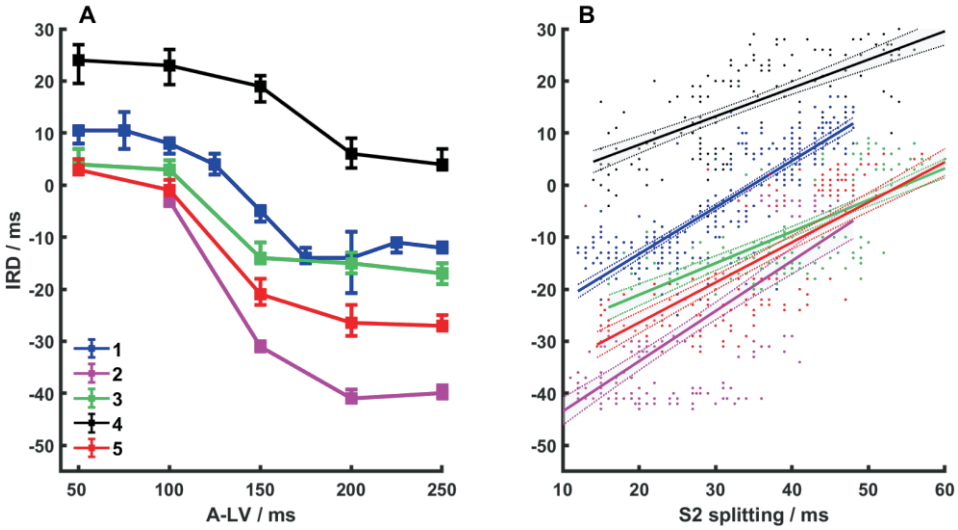

Figure 7. A: Changes of interventricular relaxation dyssynchrony (IRD) as a function of A-LV delay (n = 5). *A-RV delay was fixed at 150 ms. From A-LV delay of 50 ms to 250 ms at step of 50 ms, the overall IRD was 8 (4,12) ms, 2 (-2,8) ms, -14 (-24, -5) ms, -20 (-39, -11) ms and -18 (-28,-11) ms, respectively. Data were presented as median (25 percentile, 75 percentile). For all 5 experiments, Spearman's rank correlation was calculated. R2 value was 0.72, 0.73, 0.75, 0.64 and 0.82 from experiment 1 to 5, respectively, and all P values were < 0.001.* ***B: Correlation between IRD and S2 splitting.*** *Each point represents a heartbeat. Each colour represents an experiment, the same as in* ***Figure 6****. Equations and Pearson's correlation coefficients of the correlation plots are summarized in* ***Table 2****). A-LV, right atrium to left ventricle paced delay; S2, the second heart sound.*

Table 2. Pearson's Correlation of second heart sound splitting interval with interventricular relaxation dyssynchrony

Exp.	No. of heartbeats	Slope	Intercept	R^2	P value
1	346	0.90	-31	0.72	< 0.001
2	172	0.96	-53	0.54	< 0.001
3	163	0.61	-33	0.56	< 0.001
4	143	0.55	-3	0.49	< 0.001
5	150	0.77	-42	0.63	< 0.001

Exp., Experiment; No., total number.

Comparison of START algorithm with other splitting detection algorithms

Searching the PubMed database using "heart sound" and "split*" resulted in 120 publications. After excluding 6 reviews, 3 letter and 35 case reports, the remaining 76 publications were checked for description of heart sound splitting detection algorithm. Two publications were recommended by experts of the field [11, 24]. Finally, 13 publications on 12 splitting detection algorithms were included for analysis (**Table 3**).

Early efforts were focused on using modeling approaches to simulate heart sound morphologies and further to extract splitting interval [15, 17]. Blind source separation was proposed only for multiple-channel simultaneous recordings [11, 14]. Many later studies employed CWT and SWVD to identify A2 and P2 on time-frequency spectrum [9, 10, 12, 13, 16, 18, 19]. However, both methods relied on visual identification of two well separated components of heart sound on time-frequency spectrum, making the detection threshold exceeding 20 ms. Moreover, the SWVD method was complicated by cross-terms which interfered with the identification of A2 and P2. Validation of splitting detection algorithm in various splitting intervals was provided only in 4 studies [13, 14, 16, 24]. Validation of algorithm in various SNRs was provided only in 1 study [16]. No studies provided validation on various A2/P2 amplitude ratios.

Table 3. Summary of publications of heart sound splitting detection algorithm

Author [Ref.]	Year	Description	DT (ms)	Detect single heartbeat?	Validation?
Xu J [17]	2002	Nonlinear transient chirp signal modeling	--	Y	N
Popov B [15]	2004	Gaussian chirplet modeling	--	Y	N
Nigam V [14]	2006	Blind source separation	≥ 0	N	Y
Debbal SM [12, 18]	2006	Continuous wavelet transform	--	Y	N
Yildirim I [16]	2007	Smoothed Wigner-Ville distribution	≥ 20	Y	Y
Al-Naami B [9]	2010	Continuous wavelet transform and support vector machine	--	Y	N
Hamza Cherif L [25]	2013	Hilbert transform envelope	--	Y	N
Djebbari A [13]	2013	Reassigned smoothed pseudo Wigner-Ville distribution	≥ 30	Y	Y
Thiyagaraja SR [19]	2014	Continuous wavelet transform	--	Y	N
Barma S [10]	2015	Hilbert vibration decomposition and reassigned smoothed pseudo Wigner-Ville distribution	≥ 20	Y	N
Tang H [24]	2017	Respiration-modulated splitting measurement	≥ 25	N	Y
Chen L [11]	2018	Blind source separation	--	N	N
Proposed method	2020	S-transform	≥ 10	Y	Y

DT, detection threshold; N, no; Y, yes.

Discussion

We introduced a time-frequency-based START method to estimate S2 splitting, validated it with simulated heart sounds, and employed it to observe S2 splitting in porcine experiments. Major findings of our study are: 1) the START algorithm for estimating S2 splitting interval is accurate in a wide range of splitting intervals, A2/P2 amplitude ratios, and SNRs; and 2) START-estimated S2 splitting interval is significantly correlated with paced interventricular delays and IRD, though no correlations are observed for long A-LV delays in porcine models probably because of the fact that the LV is activated even before the moment of pacing. To our knowledge, our study is the first to investigate the possibility of using a heart sound indicator to monitor interventricular dyssynchrony in CRT-like settings. As a simple measurement, heart sound is likely to serve as a promising real-time monitoring approach for patients with interventricular dyssynchrony.

Comparison of START algorithm with other splitting detection methods

Distinguishing the time difference between the two components of S2, i.e., A2 and P2, has long been a challenge because of their overlap within a short period of time. Our proposed algorithm works for a small splitting interval down to 10 ms, for various A2/P2 amplitude ratios and for low SNRs. Previous studies using modeling approaches to extract splitting interval assumed a standard template of heart sound which remains debatable [15, 17]. Blind source separation method required at least 4 simultaneous recordings to obtain a satisfactory splitting estimation [14]. Respiration-modulated splitting measurement method required a continuous recording of at least 200 heartbeats to obtain a relatively robust estimation [24]. Our proposed START algorithm does not rely on theories about genesis, transmission or statistical characteristics of heart sound, making it adaptable for heart sounds of various shapes from different individuals. This is supported by the consistency of decreasing trends of S2 splitting during varying paced interventricular delays in the 5 pigs. The START algorithm works on a single-sensor single heartbeat, enabling it to be applicable to a short heart sound recording. Though previous time-frequency algorithms including CWT and SWVD could also work on a single heartbeat, they relied on two well separated components on time-frequency spectrum to label A2 and P2 [9, 10, 12, 13, 16, 18, 19]. Moreover, for SWVD method, the clear identification of A2 and P2 on time-frequency spectrum was interfered by the unavoidable introduction of cross-terms during signal processing. Our proposed START algorithm improves the efficiency and accuracy of existing time-frequency algorithms by automatically tracking the ridges of A2 and P2 on time-frequency spectrum. This avoids the bias of identifying A2 and P2 by human eyeballs, especially for low splitting intervals.

Furthermore, lack of validation is likely to render many existing splitting detection algorithms to be unclear for challenging conditions such as extremely low or high A2/P2 amplitude ratios, or low SNRs. Among the various algorithms proposed to assess S2 splitting, our algorithm is unique also in the sense that it has been evaluated not only in simulated heart sounds of various conditions, but more importantly, in heart sounds acquired from an *in-vivo* porcine model of varying VV delays. In animal studies, the proposed method captured all the decreasing trends of S2 splitting within a narrow range from around 40 ms to around 20 ms during changing paced interventricular intervals.

Relationship between S2 splitting and IRD

Our study demonstrates a good correlation between S2 splitting interval and IRD, confirming its value as a non-invasive indicator of interventricular dyssynchrony. Using a highly accurate splitting detection algorithm and an animal model with adjustable paced interventricular delays, our study for the first time provides direct experimental evidence to an old assumption that S2 splitting is associated with synchronism at the end of the ejection period of the two ventricles [26]. Current methods of evaluating IRD mainly rely on echocardiography which is time-consuming, operator-dependent and is commonly performed in the recumbent position [27]. Moreover, the echocardiography-derived IRD is confined to a few cardiac cycles and thus cannot be used for continuous monitoring of the patient's status. In contrast, S2 splitting interval derived from heart sounds may be collected continuously using sensors on the chest or incorporated in implantable devices.

One initially surprising observation of this study is that while there was a clear S2 splitting during LV preexcitation, no reverse splitting was observed during RV preexcitation. At long A-LV delays, the LV was already activated by means of myocardial conduction coming from the paced RV. The explanation for this observation may also be found in the fact that in general, ejection time is shorter in the LV than in the RV. In the synchronously activated heart, this leads to earlier aortic than pulmonic valve closure and consequently an earlier onset of A2 than P2. LV pre-excitation most likely increases the time interval between aortic and pulmonary valve closure and thus S2 splitting. RV pre-excitation on its turn shifts the pulmonic valve closure to earlier time points, but apparently not before aortic valve closure in our porcine animal model. This finding implies that S2 splitting interval is more sensitive to detect LV than RV preexcitation. This is further supported by findings of Xiao *et al*. who showed that 88% (21/24) of patients with RV pacing did not show any reversed splitting of S2 [28]. In CRT the aim is to synchronize contraction of the two ventricles. As part of this approach, pacemaker settings can be adjusted to vary the activation time of RV and LV. The data of the present study show that S2 splitting can be used to detect LV preexcitation associated with pacing. Though respiration may also affect the detection, in the current experimental setting, with open chest and mechanical ventilation, respiratory variations were negligible.

Comparison with other heart sound measures

Several other heart sound-based indicators have been used for CRT optimization. These include electromechanical activation time (time between onset of electrical activation and onset of S1), left ventricular systolic time (time difference between S1 and S2), and S3 strength [4-7]. The only heart sound approach that has progressed to clinical application is the SonR algorithm, which uses the amplitude of S1 as an indicator. This algorithm is used for repetitive and automated optimization of CRT. The SonRtip Lead and Automatic AV-VV Optimization Algorithm in the Paradym RF SonR CRT-D (RESPOND CRT) Trial showed that SonR-guided optimization of atrioventricular and interventricular timings significantly improves CRT responder rate and reduces risk of heart failure hospitalization as compared with the conventional, inconsistently applied optimization [8, 29].

While these parameters mainly reflect contractility, the START-based S2 splitting is the only indicator of interventricular dyssynchrony from heart sound so far and may therefore be of additional value on top of the aforementioned indicators. It can be imagined that S2 splitting can be used to guide pacing lead location during CRT implantation as well as in CRT optimization during follow-up, either manually during outpatient visits or, when accelerometers are incorporated in pacing leads and or pacemakers, in ambulatory fashion.

Limitations:

Translating results from animal experiments to clinical applications should be done with caution. First of all, the conduction system in the pigs differs to some extents from that of humans, resulting in narrower QRS complexes during ventricular pacing. This likely also results in smaller interventricular dyssynchrony. The fact that START algorithm can detect the small S2 splitting intervals in pigs suggests therefore, that this certainly will be possible in humans. Secondly, the pigs had normal cardiac function, while humans eligible for pacing treatments may have depressed cardiac function. Thirdly, the number of experiments was small and measurements were performed during anaesthesia and with open chest.

Conclusions

The proposed START algorithm is accurate in estimating S2 splitting under a wide range of conditions as shown by heart sound simulation.

Our pilot animal experiment in the AV block porcine model demonstrates that the START-estimated S2 splitting interval can be used as an indicator of interventricular dyssynchrony. The estimated S2 splitting is well correlated with paced interventricular delays and with invasively measured IRD.

References:

1. Luisada AA, Feigen LP and Mori K. On the unitary nature of cardiac vibrations. Jpn Heart J 1973; 14(5):406-413. [doi: 10.1536/ihj.14.406]
2. FABER JJ. Origin and conduction of the metral sound in the heart. Circ Res 1964; 14:426-435. [doi: 10.1161/01.res.14.5.426]
3. Leatham A. Splitting of the first and second heart sounds. The Lancet 1954; 264(6839):607-614. [doi: https://doi.org/10.1016/S0140-6736(54)90399-2]
4. Zuber M, Toggweiler S, Quinn-Tate L, Brown L, Amkieh A, Erne P. A comparison of acoustic cardiography and echocardiography for optimizing pacemaker settings in cardiac resynchronization therapy. Pacing and Clinical Electrophysiology 2008; 31(7):802-811. [doi: 10.1111/j.1540-8159.2008.01094.x]
5. Taha N, Zhang J, Ranjan R, Daneshvar S, Castillo E and Guillen E, et al. Biventricular pacemaker optimization guided by comprehensive echocardiography—preliminary observations regarding the effects on systolic and diastolic ventricular function and third heart sound. J Am Soc Echocardiog 2010; 23(8):857-866. [doi: 10.1016/j.echo.2010.04.022]
6. Toggweiler S, Zuber M and Erne P. Optimization of atrioventricular and interventricular delay with acoustic cardiography in biventricular pacing. Congest Heart Fail 2006; 12 Suppl 1:37-40. [doi: 10.1111/j.1527-5299.2006.05771.x]
7. Toggweiler S, Zuber M, Kobza R, Roos M, Jamshidi P and Meier R, et al. Improved response to cardiac resynchronization therapy through optimization of atrioventricular and interventricular delays using acoustic cardiography: A pilot study. J Card Fail 2007; 13(8):637-642. [doi: 10.1016/j.cardfail.2007.05.008]
8. Brugada J, Delnoy PP, Brachmann J, Reynolds D, Padeletti L and Noelker G, et al. Contractility sensor-guided optimization of cardiac resynchronization therapy: Results from the RESPOND-CRT trial. Eur Heart J 2016:w526. [doi: 10.1093/eurheartj/ehw526]
9. Al-Naami B, Al-Nabulsi J, Amasha H and Torry J. Utilizing wavelet transform and support vector machine for detection of the paradoxical splitting in the second heart sound. Med Biol Eng Comput 2010; 48(2):177-184. [doi: 10.1007/s11517-009-0548-7]
10. Barma S, Chen BW, Man KL and Wang JF. Quantitative measurement of split of the second heart sound (S2). IEEE/ACM Trans Comput Biol Bioinform 2015; 12(4):851-860. [doi: 10.1109/TCBB.2014.2351804]
11. Chen L, Wu SF, Xu Y, Lyman WD and Kapur G. Blind separation of heart sounds. Journal of Theoretical and Computational Acoustics 2018; 26(01):1750035. [doi: 10.1142/S2591728517500359]
12. Debbal SM and Bereksi-Reguig F. Automatic measure of the split in the second cardiac sound by using the wavelet transform technique. Comput Biol Med 2007; 37(3):269-276. [doi: https://doi.org/10.1016/j.compbiomed.2006.01.005]
13. Djebbari A and Bereksi-Reguig F. Detection of the valvular split within the second heart sound using the reassigned smoothed pseudo Wigner-Ville distribution. Biomed Eng Online 2013; 12:37. [doi: 10.1186/1475-925X-12-37]

14. Nigam V and Priemer R. A dynamic method to estimate the time split between the A2 and P2 components of the S2 heart sound. Physiol Meas 2006; 27(7):553-567. [doi: 10.1088/0967-3334/27/7/001]
15. Popov B, Sierra G, Durand LG, Xu J, Pibarot P and Agarwal R, et al. Automated extraction of aortic and pulmonary components of the second heart sound for the estimation of pulmonary artery pressure. Conf Proc IEEE Eng Med Biol Soc 2004; 2004:921-924. [doi: 10.1109/IEMBS.2004.1403310]
16. Yildirim I and Ansari R. A robust method to estimate time split in second heart sound using instantaneous frequency analysis. Annu Int Conf IEEE Eng Med Biol Soc 2007; 2007:1855-1858. [doi: 10.1109/IEMBS.2007.4352676]
17. Xu J, Durand LG and Pibarot P. A new, simple, and accurate method for non-invasive estimation of pulmonary arterial pressure. Heart 2002; 88(1):76-80. [doi: 10.1136/heart.88.1.76]
18. Debbal SM and Bereksi-Reguig F. Analysis and study of the variation of splitting in the second heartbeat sound of wavelet transform. Journal of Medical Engineering & Technology 2006; 30(5):298-305. [doi: 10.1080/03091900500256164]
19. Thiyagaraja SR, Vempati J, Dantu R, Sarma T and Dantu S. Smart phone monitoring of second heart sound split. Annu Int Conf IEEE Eng Med Biol Soc 2014; 2014:2181-2184. [doi: 10.1109/EMBC.2014.6944050]
20. Stockwell RG, Mansinha L and Lowe RP. Localization of the complex spectrum: The S transform. Ieee T Signal Proces 1996; 44(4):998-1001. [doi: 10.1109/78.492555]
21. Xu J, Durand L and Pibarot P. Nonlinear transient chirp signal modeling of the aortic and pulmonary components of the second heart sound. Ieee T Bio-Med Eng 2000; 47(10):1328-1335. [doi: 10.1109/10.871405]
22. Heckman LIB, Kuiper M, Anselme F, Ziglio F, Shan N and Jung M, et al. Evaluating multisite pacing strategies in cardiac resynchronization therapy in the preclinical setting. Heart Rhythm O2 2020; 1(2):111-119. [doi: https://doi.org/10.1016/j.hroo.2020.03.003]
23. Verbeek XAAM, Vernooy K, Peschar M, Van der Nagel T, Van Hunnik A and Prinzen FW. Quantification of interventricular asynchrony during LBBB and ventricular pacing. Am J Physiol-Heart Circ 2002; 283(4):H1370-H1378. [doi: 10.1152/ajpheart.00051.2002]
24. Tang H, Chen H and Li T. Discrimination of aortic and pulmonary components from the second heart sound using respiratory modulation and measurement of respiratory split. Applied Sciences 2017; 7(7):690. [doi: 10.3390/app7070690]
25. Hamza CL and Debbal SM. Algorithm for detection of the internal components of the heart sounds and their split using a Hilbert transform. J Med Eng Technol 2013; 37(3):220-230. [doi: 10.3109/03091902.2013.786154]
26. Wolferth CC and Margolies A. The influence of varying As-Vs intervals on split first heart sounds: Its bearing on the cause of split sounds and the mechanism of the first sound. J Clin Invest 1935; 14(5):605-618. [doi: 10.1172/JCI100710]
27. Dreger H, Antonow G, Spethmann S, Bondke H, Baumann G and Melzer C.

Dyssynchrony parameter-guided interventricular delay programming. Europace 2012; 14(5):696-702. [doi: 10.1093/europace/eur376]

28. Xiao HB, Brecker SJ and Gibson DG. Differing effects of right ventricular pacing and left bundle branch block on left ventricular function. Br Heart J 1993; 69(2):166-173. [doi: 10.1136/hrt.69.2.166]

29. Brugada J, Brachmann J, Delnoy PP, Padeletti L, Reynolds D and Ritter P, et al. Automatic optimization of cardiac resynchronization therapy using SonR—rationale and design of the clinical trial of the SonRtip lead and automatic AV-VV optimization algorithm in the paradym RF SonR CRT-D (RESPOND CRT) trial. Am Heart J 2014; 167(4):429-436. [doi: 10.1016/j.ahj.2013.12.007]

Chapter 3

Heart sound-derived systolic intervals for atrioventricular delay optimization in cardiac resynchronization therapy

Hongxing Luo [1], Philip Westphal [1, 2], Mehrdad Shahmohammadi [3], Luuk I.B. Heckman [1], Marion Kuiper [1], Richard N. Cornelussen [1, 2], Tammo Delhaas [3], Frits W. Prinzen [1]

Under review at *Heart Rhythm.*

[1] Department of Physiology, Cardiovascular Research Institute Maastricht (CARIM), Maastricht University, the Netherlands
[2] Bakken Research Centre Medtronic, plc, Maastricht, the Netherlands
[3] Department of Biomedical Engineering, Cardiovascular Research Institute Maastricht (CARIM), Maastricht University, the Netherlands

Abstract

Introduction:

Phonocardiography (PCG) can be used to determine systolic time intervals (STIs) like the interval between ventricular pacing spike and the first heart sound (VS1) and the interval between the onsets of S1 and second heart sound (S1S2). We investigated the relations between PCG-derived STIs and hemodynamics during optimization of atrioventricular (AV) delay of biventricular pacing (BiVP) in animals and patients.

Methods:

Animal studies were performed in 5 pigs with complete AV block during BiVP under various hemodynamic conditions while PCG was determined from an epicardially positioned accelerometer. In 21 patients undergoing CRT device implantation, PCG was measured using a microphone embedded in a pulse generator. Optimal AV delay was identified at the shortest VS1 and longest S1S2, and compared with the largest values of hemodynamic variables.

Results:

In the animal study, VS1 and S1S2 predicted the AV delay associated with highest LV pressure, maximal rate of rise of LV pressure and stroke work, with median errors ranging from 2 ms to 28 ms, resulting in < 2% underestimation of the maximal values of these variables. In the entire patient cohort, VS1 and S1S2 underestimated the optimal hemodynamics-based AV delay by 32.5 ms and 37.5 ms, respectively, which was reduced to 21 ms and 24 ms in the 8 patients with full BiVP capture at AV delays ≥ 180 ms. PCG-derived optimal AV delay related to a 0.2%-0.9% loss in optimal hemodynamics.

Conclusions:

During BiVP at varying AV delays, close relations exist between PCG-derived STIs and hemodynamic variables. These relations are particularly clear during full capture. PCG predictions of optimal AV delays cause only minimal losses in optimal hemodynamics.

Introduction

Systolic time interval (STI) is the period from the onset of ventricular depolarization to the end of ventricular systole [1]. It can be divided into two phases: pre-ejection period (PEP: interval from QRS onset to opening of aortic valves), and left ventricular (LV) ejection time (LVET: interval from opening to closure of the aortic valves). Both PEP and LVET have been proposed as temporal indicators of ventricular systolic function [2, 3]. A prolonged PEP indicates more time required for the ventricles to develop sufficient forces to open the aortic and pulmonic valves, thus implying impaired contractility. A shortened LVET indicates an abbreviated period of the LV to eject blood, indicating low myocardial forces relative to the afterload. Previous echocardiographic studies have shown short LVET to be an independent predictor of all-cause mortality and heart failure hospitalization in heart failure with reduced ejection fraction [4, 5]. In a community cohort, every 10 ms decrease of LVET was associated with an increment of 7% of risk of incident heart failure [6].

STIs can also be obtained using the first (S1) and second heart sounds (S2) on phonocardiography (PCG). Both S1 and S2 are the result of abrupt cessation of blood flow by valve closure which sets the viscoelastic cardiovascular system including valve leaflets, myocardial tissues and blood columns into vibrations [7]. The PEP can be approximated using QS1, the interval between the onsets of QRS complex and S1, while LVET can be approximated using S1S2, the interval between the onsets of S1 and S2. Prolonged QS1 interval and shortened S1S2 interval are indicative of reduced stroke volume and cardiac output in heart failure patients [8]. The QS1 interval (also referred to as electromechanical activation time (EMAT)) has been proposed as a measure to guide optimization of cardiac resynchronization therapy (CRT). A feasibility study showed high correlations between QS1- and echocardiography-guided optimization of AV delay and interventricular (VV) delay [9].

This study aimed to comprehensively investigate whether heart sound-derived STIs are related to invasively measured hemodynamics in animals and humans, and further whether they can be used for AV delay optimization in CRT. To this purpose, measurements were performed in a preclinical porcine model where an epicardially positioned accelerometer was used to measure myocardial vibrations during normal and depressed myocardial contractility, while we analyzed the data from a previously performed clinical study where a

pulse generator-integrated microphone was used to measure heart sounds in various paced AV delays.

Methods

Study approvals and ethics

This study consisted of both animal and human investigations. The animal study was an acute sacrifice porcine study approved by the Central Committee for Animal experiments (CCD) in the Netherlands and the Animal Experimental Committee of Maastricht University. A part of the study results has already been reported in a study on using second heart sound splitting as an indicator of VV dyssynchrony in CRT [10]. The human study was a multicentre, prospective, non-randomized acute feasibility study named Sensor Optimization of Cardiac Resynchronization Therapy (CRT) Response (SOCR) Study [11]. The study was sponsored by Medtronic Cardiac Rhythm and Heart Failure group and conducted in four countries (Canada, Hong Kong, United Kingdom and United States) between 2013 and 2016.

Animal study and data collection

Five male adult pigs (weight: 64 ± 1 kg) were used. The animals were injected with antibiotics (ampicillin 1000 mg IV), followed by thiopental (5-15 mg/kg IV) for induction of general anesthesia. After intubation, the animals were mechanically ventilated. General anesthesia was maintained by continuous IV infusion of rocuronium (0.1 mg/kg/h), sufentanyl (4-8 μg/kg/h) and propofol (2.5-10 mg/kg/h). A left thoracotomy through the fifth intercostal space was performed to expose the heart. A triaxial accelerometer with a sampling frequency of 1000 Hz was positioned on the anterior RV base to record heart sounds.

Two 7F catheter-tip manometers were inserted through the carotid artery and jugular vein to measure LV and RV pressures, respectively. LV volume was measured using the conductance catheter technique [12]. Pacing electrodes were transvenously placed in the right atrium and RV apex, and epicardially on the basal posterolateral wall of LV. Radiofrequency ablation of the atrioventricular (AV) node was performed to induce complete AV block. Immediately after creation of AV block, biventricular pacing was configured with an AV delay of 100 ms, which condition served as a reference in this study. To investigate the effect of varying AV delay on heart sounds, AV delay was increased from 50 ms to 250 ms, in steps of 50 ms. After obtaining these data, isoflurane was added to the ventilatory gases to reduce myocardial

contractility as indicated by a reduction of LV dP/dtmax by at least 30%. Subsequently, the aforementioned pacing protocol was repeated.

During each pacing setting, ECG and hemodynamics were recorded for 20 to 30 seconds using the IDEEQ data acquisition system (IDEE Maastricht University / Maastricht Instruments BV). Heart sounds were collected using a custom-made data acquisition system [10]. The hemodynamic data and heart sound signals were synchronized using pulse signals that appeared on both systems.

Human SOCR study and data collection

The SOCR study was conducted to determine whether heart sounds obtained subcutaneously via a piezoelectric microphone incorporated in a pulse generator could be used to determine the optimal paced AV interval in CRT patients [11]. The included patients underwent implant of a new or replacement/upgrade Medtronic CRT-P or CRT-D device. A patient was excluded if one or more of the following conditions were met: 1) ECG quality was too low to visually identify QRS complexes or pacing spikes; 2) heart sound recordings were too noisy to visually identify any S1 and S2; or 3) LV ejection fraction was above 35%.

Baseline cardiac function data (e.g., LV ejection fraction, end-diastolic and end-systolic LV volume) were obtained using echocardiography before CRT implantation. During the implant procedures, a modified CRT device was temporarily placed in the pacemaker pocket. The circuit of this device was specifically designed to contain the Biopac Data Acquisition System (BIOPAC Systems Inc, CA, USA) for measurements of heart sounds and single-lead ECG. Heart sounds were resampled from 128 Hz to 1000 Hz and stored together with ECG at 1000 Hz. The CRT device was connected to standard right atrial and right ventricular (RV) pacing leads. LVP was measured using a Millar catheter (Millar, TX, USA) introduced through the femoral artery. ECG, heart sound and LVP were measured during biventricular pacing with an AV delay ranging from 60 ms to 330 ms, in steps of 30 ms. After the end of the measuring protocol, the modified device was removed and a regular device was implanted.

Data processing

For both animal and patient studies, ten consecutive heartbeats at the end of each paced AV delay were used for analysis. Systolic and diastolic blood pressures were obtained from the aortic pressure tracing in animal study. The maximal LV pressure (LVP max) was calculated

from the LVP tracing. The maximal rates of rise (LV dP/dtmax) and fall (LV dP/dtmin) of LVP were calculated from the first derivative of LVP which was first filtered using a series of mean filters with window size from 2 ms to 40 ms. This smoothing process was performed to reduce the potential effect of high-frequency intracardiac pressure fluctuations caused by valve closures on calculation of dP/dtmax or min. SW was calculated from the LV pressure-volume loop area.

In the animal experiments, the epicardially measured heart sounds were bandpass-filtered using a second-order Butterworth filter between 20 Hz and 250 Hz. For the patient study, heart sounds were more noisy because they were collected by the pulse generator on the chest. Therefore, a signal processing algorithm called harmonic regeneration noise reduction was utilized to remove the baseline noises of the heart sounds [13]. The algorithm firstly manually sets a level of background noise based on the signal envelope, and then removes the background noise from the data.

Denoised heart sounds were plotted to visually identify S1 and S2, with reference to the synchronously recorded ECG. The onsets of S1 and S2 were identified as the first deflection whose absolute height was over 1/3 of the maximal amplitude of S1 or S2, respectively. RR interval was calculated from the interval between two consecutive ventricular pacing spikes on ECG.

The following systolic intervals were calculated: 1) VS1: interval between ventricular pacing spike and S1 onset; 2) S1S2: interval between onsets of S1 and S2; 3) VS2: interval between ventricular pacing spike and S2 onset (= VS1 + S1S2).

In this study, only AV delays with full capture of BiV pacing were analyzed. In the animal experiments, these comprised all AV delays, because of the AV-block that was performed prior to starting the protocol. In the patient study, the number of AV delays with full capture of BiV pacing was variable. AV delays with fusion pacing were not used for this study in order to focus on the relation between PCG-derived STIs and AV dyssynchrony and excluding an effect of VV dyssynchrony. Full capture was identified from the QRS morphology on ECG.

Determination of optimal AV delay

Optimal AV delay was determined for each of hemodynamic indicators (LVP max, LV dP/dtmax and SW) and PCG-derived STIs (VS1 and S1S2). To improve accuracy of determining the optimal AV delay, a parabola was utilized to fit the measured median values of each indicator for AV

delays ranging from 50 ms to 250 ms [14]. The optimal AV delay was identified as the lowest vertex for VS1 and the highest vertex for the remaining indicators. If the fitted parabola was monotonous, the value at the shortest or the longest AV delay was used. With optimal hemodynamics determined using LVP max, LV dP/dtmax and SW as "gold standards", loss of cardiac pump function using STIs-derived optimal AV delays for CRT optimization was also calculated.

Statistical analysis

Normally distributed data were expressed as mean and standard deviation. Skewed data were expressed as median (25th percentile, 75th percentile). Count data were expressed as absolute number. Continuous variables were compared using an independent sample *t* test between groups. A two-sided P value < 0.05 was assumed to indicate a statistically significant difference. All statistical analyses were performed using MATLAB R2018b (The MathWorks, Inc., MA, USA).

Results

Animal study

Hemodynamics and PCG at reference AV delay

Table 1 summarizes the hemodynamic and PCG characteristics during biventricular pacing at the reference AV delay of 100 ms during baseline and isoflurane-depressed myocardial contractility. Isoflurane ventilation significantly reduced myocardial contractility as evidenced by 41% reduction in LV dP/dtmax. VS1, S1S2 and VS2 did not significantly change between baseline and isoflurane.

Table 1. Hemodynamics and PCG in the porcine study*

	Baseline (n = 5)	Isoflurane (n = 5)	P value
Hemodynamics			
Heart rate (bpm)	91 ± 24	108 ± 24	0.31
RR interval (ms)	694 ± 175	577 ± 116	0.25
SBP (mmHg)	99 ± 19	67 ± 15	< 0.001
DBP (mmHg)	71 ± 17	41 ± 12	< 0.001
LVP max (mmHg)	102 ± 17	67 ± 16	< 0.001
LV dP/dtmax (mmHg / sec)	706 ± 94	419 ± 128	< 0.001
LV dP/dtmin (mmHg / sec)	-754 ± 143	-464 ± 140	< 0.001
SW (mmHg·mL)	4534 ± 441	1678 ± 591	< 0.001
Systolic time intervals			
VS1 (ms)	76 ± 15	75 ± 23	0.76
S1S2 (ms)	292 ± 42	292 ± 26	1.00
VS2 (ms)	369 ± 46	367 ± 39	0.89

Values are mean ± SD.

** Data during biventricular pacing with an AV delay of 100 ms.*

bpm, beats per minute; DBP, diastolic blood pressure; LV, left ventricle; LVP max, maximal LV pressure; S1S2, interval from S1 onset to S2 onset; SBP, systolic blood pressure; SW, stroke work; VS1, interval from ventricular pacing spike to S1 onset; VS2, interval from ventricular pacing spike to S2 onset.

Changes of heart sound with AV delay

Figure 1 shows a representative example of heart sound and ECG signals during paced AV delays ranging from 50 to 250 ms. With prolonging AV delays, VS1 monotonously increased from 66 ms to 76 ms, while S1S2 firstly increased from 272 ms to 278 ms and then gradually decreased to 265 ms. LVP max and SW were the highest at an AV delay of 100 ms, when the S1S2 was the longest. LV dP/dtmax peaked at an AV delay of 150 ms. Using parabolic curve fitting, optimal AV delay was calculated to be 118 ms based on the longest S1S2 and 128 ms based on the highest LVP max (**Figure 1**, lower panels).

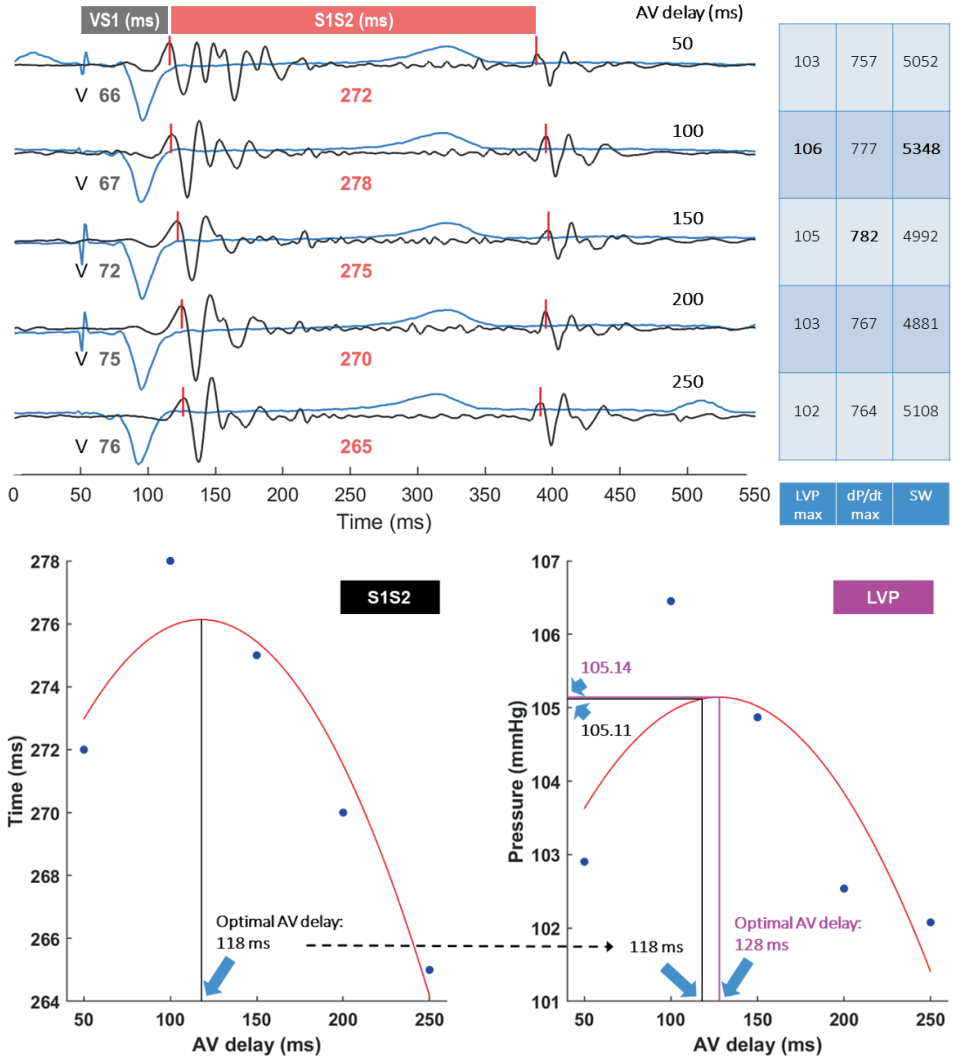

Figure 1. An example of heart sounds and hemodynamics at varying AV delays

Units of LVP max, LV dP/dtmax and SW are mmHg, mmHg/sec and mmHg·mL, respectively.

*Optimal AV delay was identified at the vertex of each fitted parabola (red curve). S1S2-determined optimal AV delay (**lower left panel**) was compared with the LVP-determined optimal AV delay (**lower right panel**), showing negligible "loss" of hemodynamics in this example (105.11 mmHg vs. 105.14 mmHg).*

LVP max, maximal LV pressure; S1S2, interval from S1 onset to S2 onset; SW, stroke work; V, position of ventricular pacing spike; VS1, interval from ventricular pacing spike to S1 onset.

Figure 2 shows STIs and hemodynamic variables during the paced AV delays in 2 experiments. The first experiment (**A**) showed a clear parabolic curve for all variables, indicating an optimal AV delay for highest LVP max of 126 ms, for LV dP/dtmax of 129 ms and for SW of 122 ms, while VS1 and S1S2 indicated an optimal AV delays of 103 ms and 131 ms, respectively. The second experiment (**B**) showed monotonous parabola resulting in the estimation of the optimal AV delay at 50 ms, based on both STIs and hemodynamics.

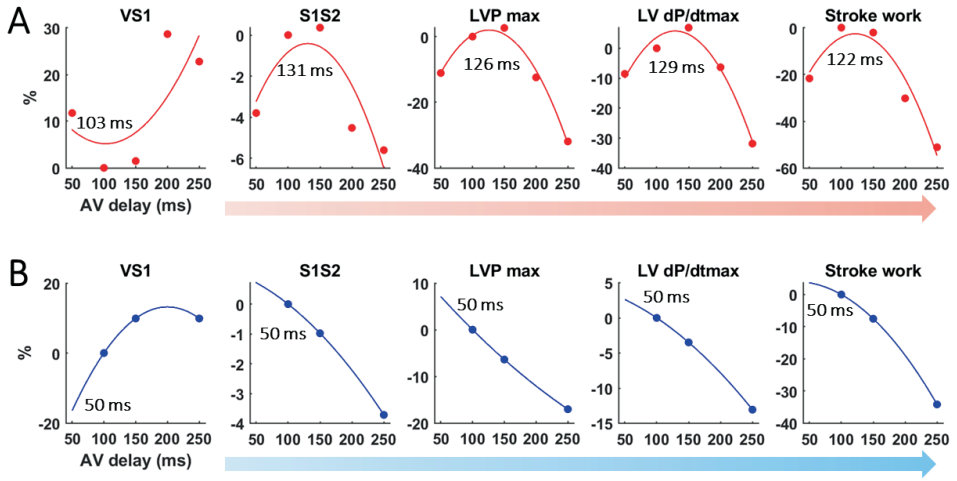

Figure 2. Changes of systolic intervals and hemodynamics with AV delay in two representative experiments

Y-axis shows the percent difference from the value of AV delay of 100 ms. Each point represents the median value of 10 heartbeats for a given AV delay. Parabolic curve fitting and optimal AV delay were indicated in each panel.

LVP max, maximal LV pressure; S1S2, timing interval from S1 onset to S2 onset; VS1, timing interval from ventricular pacing spike to S1 onset.

Prediction of optimal AV delay using STIs

Table 2 summarizes the deviations of the PCG-predicted optimal AV delay from the optimal delays obtained using LVP max, dp/dtmax and SW. VS1 and S1S2 intervals underestimated LVP max-based optimal AV delay by median values of -10 ms and -13 ms, respectively. The

underestimation appeared to be more pronounced for LV dP/dtmax, with median differences being -27 ms and -28.5 ms using VS1 and S1S2, respectively. The optimal AV delay according to SW was slightly overestimated by VS1 (8 ms) and S1S2 (2 ms). These deviations in optimal timing of pacing resulted in loss of maximal hemodynamic function ("Loss" in table 2) normalized to that of AV delay of 100 ms. Median loss was below 1% for LVP max and below 2% for LV dP/dtmax and SW.

Table 2. Prediction of optimal AV delay using systolic time intervals

	LVP max	LV dP/dtmax	SW
VS1 (ms)	-10 (-34, 17)	-27 (-66, 6)	8 (-82, 21)
Loss (%)	-0.8 (-1.2, -0.3)	-1.9 (-2.4, -0.2)	-2.0 (-5.6, -0.6)
S1S2 (ms)	-13 (-34, 34)	-28.5 (-64, 2)	2 (-58, 37)
Loss (%)	-0.5 (-1.0, -0.1)	-1.2 (-2.5, -0.1)	-1.0 (-5.6, -0.2)

Presented are the differences between PCG- and hemodynamics-determined optimal AV delays, expressed as median values and the 25 and 75 percentiles. In the rows of VS1 and S1S2, a positive value indicates overestimation of the optimal AV delay by PCG, while a negative value indicates underestimation. Loss indicates the % reduction in the value of the hemodynamic between the actual maximal value and the one obtained at the optimal AV delay according to PCG variables, normalized to the value of AV delay of 100 ms.
LV, left ventricle; LVP max, maximal LV pressure; S1S2, timing interval from S1 onset to S2 onset; SW, stroke work; VS1, timing interval from ventricular pacing spike to S1 onset.

Human study

Baseline characteristics

Of the 30 patients enrolled in the SOCR study, we excluded 4 patients without usable ECG, 3 patients with bad-quality heart sound recordings and 1 patient with an ejection fraction above 35%. In addition, 1 patient without at least two consecutive paced AV delays of full capture judged by QRS morphology was also excluded. Finally, 21 patients were included for our analysis, of whom 15 had left bundle branch block. **Table 3** summarizes the patients' baseline characteristics measured during biventricular pacing with a reference AV delay of 90 ms.

Table 3. Baseline characteristics (n = 21)

	Values
Patient	
Male (n)	14
Age (yrs.)	59 ± 15
Heart rate (bpm)	81 ± 11
RR interval (ms)	755 ± 106
LBBB	15
Ischemic heart disease	4
Hypertension	6
LV lead location	
Posterior lateral vein	9
Anterior lateral vein	5
Lateral marginal vein	3
Unknown	4
Hemodynamics	
LVP max (mmHg)*	109 ± 19
LV dP/dtmax (mmHg / sec)*	563 ± 117
LV dP/dtmin (mmHg / sec)*	-599 ± 104
LVEF (%)	24 ± 6
EDV (ml)	232 ± 101
ESV (ml)	171 ± 80
Phonocardiography*	
VS1 (ms)	231 ± 33
S1S2 (ms)	324 ± 35
VS2 (ms)	555 ± 33

Values are mean ± SD or n.
** Values during biventricular pacing with an AV delay of 90 ms.*
bpm, beats per minute; DBP, diastolic blood pressure; EDV, end-diastolic volume; ESV, end-systolic volume; LBBB, left bundle branch block; LV, left ventricle; LVEF, left ventricular ejection fraction; LVP max, maximal LV pressure; S1S2, interval from S1 onset to S2 onset; VS1, interval from ventricular pacing spike to S1 onset; VS2, interval from ventricular pacing spike to S2 onset.

Changes of heart sounds and hemodynamics with AV delay

Figure 3 illustrates the changes of heart sounds and hemodynamics with AV delay in a representative patient. With paced AV delay increasing from 60 ms to 180 ms, VS1 progressively shortened from 257 ms to 166 ms, accompanied by a progressive lengthening of S1S2

from 315 ms to 401 ms. Note that between AV delays of 120 ms and 150 ms, an inversion of the main QRS axis occurred, along with a marked change of S1 morphology, indicating significant changes of electrical activation patterns and ventricular contraction pattern, respectively. As explained in the method section, only AV delays with a full ventricular capture, in this case AV delays 60, 90 and 120 ms, were used for further analysis. The right columns of **Figure 3** indicate that the optimal LVP max and LV dP/dtmax occurred at an AV delay of 150 ms and 120 ms, respectively.

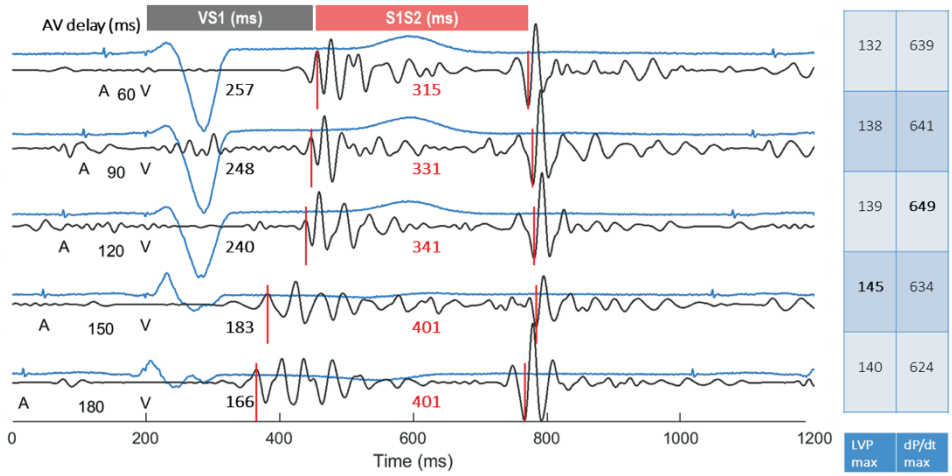

Figure 3. Changes of heart sounds (black), ECG (blue) and hemodynamics with AV delay *ECGs were aligned at ventricular pacing spikes ("V") at 200th ms. Note the marked changes of QRS complex between AV delays of 120 and 150 ms.*
Units of LVP max and LV dP/dtmax are mmHg and mmHg/sec, respectively.
A, position of atrial pacing spike; LVP max, maximal LV pressure; S1S2, interval from S1 onset to S2 onset; V, position of ventricular pacing spike; VS1, interval from ventricular pacing spike to S1 onset.

Prediction of optimal AV delay using parabolic curve fitting

Figure 4 shows the parabolic curve fitting results of PCG-derived STIs and hemodynamics in two representative patients, having short (60-120 ms) and long (60-180 ms) ranges of AV delays of full ventricular capture. In patient **A**, the predicted optimal AV delays using VS1 (110 ms) and S1S2 (120 ms) underestimated the AV delays providing the highest LVP max (207 ms) and LV dP/dtmax (221 ms). This was

because the LVP max and LV dP/dtmax continued to rise beyond the AV delay where fusion pacing started. However, the data also show that VS1 and S1S2 captured the steep rising part of the hemodynamics curve. In patient **B,** with a wide range of full capture AV delays**,** the optimal AV delays predicted by VS1 (145 ms) and S1S2 (153 ms) were close to the values judged by LVP max (152 ms) and LV dP/dtmax(143 ms).

Table 4 summarizes the differences between PCG- and hemodynamics-predicted optimal AV delays, stratified by whether a full capture occurred after an AV delay of 180 ms. Overall, both VS1 and S1S2 underestimated the real optimal AV delays and were better in predicting the optimal LV dP/dtmax than LVP max. The median underestimation of the optimal AV delay was 20~30 ms for LVP max, and around 13 ms for LV dP/dtmax. Comparing AV delays of ≤ 150 ms and ≥ 180 ms showed a decreasing prediction error by ~ 1/3 when full capture occurred at a longer AV delay, though the improvement was less pronounced for LV dP/dtmax. The median percent underestimation of LVP max and LV dP/dtmax (Loss%) using PCG was within 1% in all cases, and mostly around 0.3%. Consistent with the observations of the optimal AV delays, the loss was also lower for LV dP/dtmax than LVP max.

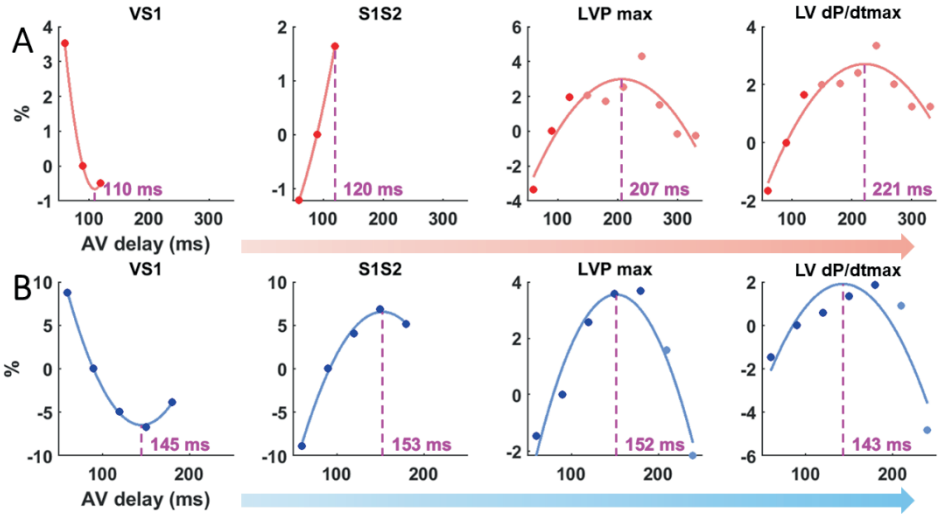

Figure 4. Optimal AV delays judged by systolic time intervals and hemodynamics *Panels A and B represent data of two patients. Each parabolic line connects the median values of 10 heartbeats. The optimal AV delay is also indicated by a dashed line in each panel. On*

the Y-axis, "%" showed the percent change relative to the value at AV delay of 90 ms.
LVP max, maximal LV pressure; S1S2, interval from S1 onset to S2 onset; VS1, interval from ventricular pacing spike to S1 onset.

Table 4. Prediction of optimal AV delays using systolic time intervals

	Full capture ⩽ 150 ms (n = 13)		Full capture ≥ 180 ms (n = 8)	
	LVP max	**LV dP/dtmax**	**LVP max**	**LV dP/dtmax**
VS1 (ms)	-32.5 (-58, -22)	-13.5 (-22.5, 4)	-21 (-26, -7)	-10 (-14, 2)
Loss (%)	-0.7 (-1.1, -0.4)	-0.3 (-1.0, -0.1)	-0.3 (-0.4, -0.2)	-0.2 (-0.7, -0.1)
S1S2 (ms)	-37.5 (-59, -22.5)	-13.5 (-22.5, 1.5)	-24 (-28, -6)	-14 (-20, 10)
Loss (%)	-0.9 (-1.3, -0.4)	-0.3 (-1.1, -0.1)	-0.3 (-0.6, 0)	-0.2 (-0.5, -0.1)

Presented are the differences between PCG- and hemodynamics-determined optimal AV delays, expressed as median values and the 25 and 75 percentiles. In the rows of VS1 and S1S2, a positive value indicates overestimation of the optimal AV delay by PCG, while a negative value indicates underestimation. Loss was normalized to the value of AV delay of 90 ms.
LVP max, maximal LV pressure; S1S2, interval from S1 onset to S2 onset; VS1, interval from ventricular pacing spike to S1 onset.

Discussion

The main findings of this combined animal and human study are: 1) shortened VS1 and prolonged S1S2 are associated with improved myocardial contractility, evaluated by LVP max and LV dP/dtmax in both animal and human studies, 2) these relations between heart sound-derived STIs (VS1 and S1S2) and invasively-measured hemodynamics (LVP max and LV dP/dtmax) are particularly clear at AV-delays with full capture of BiV pacing, and 3) the existence of these relations during protocols of AV-delay optimization in CRT indicates the potential use of PCG indicators for CRT optimization in a continuous and low-cost manner.

Relationship between STIs and cardiac pump function

Our findings support evidence from literature that a shorter VS1 and a longer S1S2 relate to better cardiac pump function during AV delay optimization [9, 15]. Furthermore, the animal study showed that these relations persist even when myocardial contractility is depressed by isoflurane. Since the ventricular electrical activities indicated by QRS

morphology were relatively unchanged throughout the paced AV delays for each study subject, changes in STIs can be attributed to the effect of changing diastolic ventricular filling when adjusting paced AV delay in our study.

Diastolic ventricular filling affects VS1 in two ways: AV valve position at the moment of ventricular depolarization and myocardial contractility at the time of valve closure. The relationship can be expressed in an equation: $t = d/v$, in which t represents the VS1, d the distance that AV valves need to travel to be closed, and v the average velocity of AV valves driven by the blood column which derives its energy from ventricular contraction. At a short AV delay, the diastolic filling has not completed, thus the valves are still at a widely open position (a larger d in the equation) at the moment of ventricular depolarization. Moreover, the incompletely filled ventricles generate a lower contractile force according to the Frank-Starling relation, causing a lower velocity of valve movements (a lower v in the equation) [16]. As a result, t, representing VS1 in our study, becomes longer. As the paced AV delay prolongs, the valves are apposed to each other, thus d becomes gradually smaller. While the ventricles are better filled, the contractile force also becomes stronger, causing a higher velocity v of valve closure, leading to a shorter t. The proposed hypothesis is supported by observations in previous studies [17-20]. Regarding valve position, a previous study of patients with congenital AV block and right ventricular pacing showed that as PR interval increased from ~ 50 ms to ~ 500 ms, the time from Q wave to closure of the mitral valves (Q-MC) evaluated by echocardiogram progressively shortened [17]. In normal subjects, a linear negative relation is also found between Q-MC and PR intervals of 100 ms to 220 ms [18]. Regarding contractile force, studies on patients with dilated congestive heart failure showed that LV dP/dtmax as a proxy for myocardial contractility was highest at optimal paced AV delay [19, 20]. Moreover, it is noteworthy that VS1 tended to prolong with AV delay in 3 of 10 conditions in our animal study. The reason might be that in these conditions the value at the shortest paced AV delay of 50 ms was missing, leading to a monotonous increase of VS1 from AV delays of 100 ms.

The S1S2 interval is the period from AV valve closure to semilunar valve closure, and thus includes two phases: isovolumic contraction phase (ICP) from the closure of AV valves to the opening of semilunar valves and the ventricular ejection phase (VEP) from opening to closure of semilunar valves. Previous tissue- and pulse-Doppler imaging studies

showed that ICP ranges between 60-80 ms and VEP between 280-400 ms [6, 23, 24]. The much shorter ICP compared with VEP indicates a narrower potential range of change for ICP when hemodynamics fluctuates. This is important because ICP and VEP usually change in an opposite direction as myocardial contractility changes. Since S1S2 is the sum of ICP and VEP, in our study it was largely determined by the longer VEP. The potential of S1S2 to indicate ventricular ejection duration may provide an easy-to-use solution to monitor cardiac pumping function, compared with both tissue- and pulse-Doppler imaging techniques.

Heart sound for CRT optimization

Both animal and patient studies showed that the PCG-predicted optimal AV delay was close to that identified by the invasive hemodynamic measurements. Our study results are supported by a previous study which optimized AV delay from 60 ms to intrinsic conduction and reported a high correlation between QS1- and echocardiogram-predicted optimal AV delays [9].

In the human study, the PCG-predicted optimal AV delay underestimated its hemodynamic equivalent by a median of 35 ms (LVP max) and 13.5 ms (LV dP/dtmax), when the patients with a full-capture AV delay less than 150 ms were considered. The underestimation was reduced by 1/3 when only the patients with the largest range of AV delays with full-capture of biventricular pacing (≥ 180 ms) were considered. The different findings in these two groups of patients can be explained by the fact that the AV delay with highest values of LVP max and LV dP/dtmax was in the range of 120-200 ms but that we limited our analysis to the range of AV delays with full capture. Consequently, the STI-derived optimum was shortened in patients with a smaller range of AV delays with full capture. However, even when the optimal AV delay was not identical with the PCG predictions, the loss of cardiac pump function was small (< 2% in animal studies and < 1% in human studies), because the parabolically shaped optimization curves were relatively flat around the optimum. Moreover, it is noteworthy that in our human studies, the improvements of hemodynamics during AV delay optimization seem to be smaller than previous studies. In the two examples in Figure 4, the ranges of change of LV dP/dtmax were around 5% and 7%, respectively, in comparison to a mean increase of 12% during conventional CRT optimization [25]. This may be due to the selection of an AV delay of 90 ms as reference setting rather than the

baseline condition without any pacing where LV dP/dtmax is supposed to be lower and thus the percent change based on it becomes higher. Nevertheless, the fact that PCG performed well in the patients with less response of CRT indicates that it will also be applicable to super-responders.

Other heart sound parameters have also been proposed to optimize AV delay in CRT. S1 amplitude has been previously used for AV delay optimization. In a pilot study of 6 patients with AV block, heart sounds were recorded using an acceleration-type microphone on the cardiac apex when paced AV delay was set from 50 ms to 250 ms [26]. A cubic curve was applied to fitting S1 amplitudes, and the optimal AV delay was defined at the inflection point of the fitted curve. A high correlation was found between PCG- and echocardiography-determined optimal AV delays. The finding was later confirmed in another study of similar protocol in 12 CRT patients and 8 patients with dual-chamber pacemakers (R = 0.83; 161 ms *vs*. 148 ms) [27]. The randomized RESPOND-CRT trial extended this experience in CRT patients [28, 29]. The optimal AV delay was identified at inflection point of the sigmoid curve-fitted S1 amplitude during AV delay optimization. Randomization of 998 patients at a 2:1 ratio to either automatic and repeated CRT optimization with this "SonR" algorithm or a single conventional echocardiography-guided optimization showed a 35% risk reduction in heart failure hospitalization in the former. An advantage of our patient study is that heart sounds were collected in a pulse generator rather than from a pacemaker lead like in the SonR studies. This design avoids the complexity and bulkiness of implementing an accelerometer in the relatively slender pacing lead. The feasibility of measuring heart sounds from a pulse generator has been supported by a previous study in 30 heart failure patients and 10 normal subjects [30]. The study used an accelerometer enclosed within a pulse generator which was taped to the skin surface over left and right pectoral regions to measure heart sounds. Fundamental heart sound components including S1, S2 and third heart sound were recorded using the device, with a higher signal-to-noise ratio on the left pectoral region. In our human study, the pulse generator was subcutaneously implanted on the left pectoral region, thus providing sufficient quality of heart sounds for analysis of STIs.

Future perspectives

In this combined animal and human study, we found that heart sound-derived STIs like VS1 and S1S2 may serve as useful indicators for AV

delay optimization in CRT. An important next step will be to validate these findings in a larger study. This may be a non-inferiority study comparing STIs with conventional echocardiography. A larger sample size allows to identify potential confounding factors such as myocardial scar that may affect STIs. Secondly, long-term follow-up of patients is crucial to establish relations between STIs and patients' outcomes. STIs estimated using conventional echocardiography have been shown to relate to the patients' heart failure incident, heart failure hospitalization and all-cause mortality [4-6]. However, no similar findings have been reported for heart sound-derived STIs. Lastly, in the SOCR study, the sampling frequency of heart sounds was low (128 Hz). With the development of newer sensor technologies in recent years, more accurate and consistent results may be obtained.

Conclusions

Heart sound-derived STIs may serve as useful indicators for AV delay optimization in CRT. Shortened interval between onsets of ventricular pacing and S1 (VS1) and prolonged interval between onsets of S1 and S2 (S1S2) are associated with better myocardial contractility evaluated by LVP max and LV dP/dtmax.

References:

1. Boudoulas KD and Boudoulas H. Time and left ventricular function: The forgotten dynamic factor. Eur J Heart Fail 2021; 23(4):552-554. [doi: 10.1002/ejhf.2165]
2. Reant P, Dijos M, Donal E, Mignot A, Ritter P and Bordachar P, et al. Systolic time intervals as simple echocardiographic parameters of left ventricular systolic performance: Correlation with ejection fraction and longitudinal two-dimensional strain. European journal of echocardiography 2010; 11(10):834-844. [doi: 10.1093/ejechocard/jeq084]
3. Alhakak AS, Teerlink JR, Lindenfeld J, Böhm M, Rosano GMC and Biering Sørensen T. The significance of left ventricular ejection time in heart failure with reduced ejection fraction. Eur J Heart Fail 2021; 23(4):541-551. [doi: 10.1002/ejhf.2125]
4. Alhakak AS, Sengeløv M, Jørgensen P, Bruun NE, Abildgaard U and Iversen A, et al. Left ventricular systolic ejection time is an independent predictor of all-cause mortality in heart failure with reduced ejection fraction. J Am Coll Cardiol 2020; 75(11, Supplement 1):1776. [doi: 10.1016/S0735-1097(20)32403-7]
5. Patel PA, Ambrosy AP, Phelan M, Alenezi F, Chiswell K and Van Dyke MK, et al. Association between systolic ejection time and outcomes in heart failure by ejection fraction. Eur J Heart Fail 2020; 22(7):1174-1182. [doi: 10.1002/ejhf.1659]
6. Biering-Sorensen T, Querejeta RG, Hegde SM, Shah AM, Claggett B and Mosley TJ, et al. Left ventricular ejection time is an independent predictor of incident heart failure in a community-based cohort. Eur J Heart Fail 2018; 20(7):1106-1114. [doi: 10.1002/ejhf.928]
7. Shahmohammadi M, Luo H, Westphal P, Cornelussen RN, Prinzen FW and Delhaas T. Hemodynamics-driven mathematical model of first and second heart sound generation. Plos Comput Biol 2021; 17(9):e1009361. [doi: 10.1371/journal.pcbi.1009361]
8. Weissler AM, Harris WS and Schoenfeld CD. Systolic time intervals in heart failure in man. Circulation 1968; 37(2):149-159. [doi: 10.1161/01.CIR.37.2.149]
9. Zuber M, Toggweiler S, Quinn-Tate L, Brown L, Amkieh A and Erne P. A comparison of acoustic cardiography and echocardiography for optimizing pacemaker settings in cardiac resynchronization therapy. Pacing Clin Electrophysiol 2008; 31(7):802-811. [doi: 10.1111/j.1540-8159.2008.01094.x]
10. Luo H, Westphal P, Shahmohammadi M, Heckman L, Kuiper M and Cornelussen RN, et al. Second heart sound splitting as an indicator of interventricular mechanical dyssynchrony using a novel splitting detection algorithm. Physiol Rep 2021; 9(1):e14687. [doi: 10.14814/phy2.14687]
11. SOCR Clinical Trial Leader. Sensor optimization of cardiac resynchronization therapy response (SOCR). URL: https://clinicaltrials.gov/ct2/show/record/NCT01832493 [accessed 2021-12-22]
12. Baan J, van der Velde ET, de Bruin HG, Smeenk GJ, Koops J and van Dijk AD, et al. Continuous measurement of left ventricular volume in animals and humans by conductance catheter. Circulation 1984; 70(5):812-823. [doi: 10.1161/01.cir.70.5.812]
13. Plapous C, Marro C and Scalart P. Improved Signal-to-Noise ratio estimation for

speech enhancement. IEEE transactions on audio, speech, and language processing 2006; 14(6):2098-2108. [doi: 10.1109/TASL.2006.872621]
14. Whinnett ZI, Davies JE, Willson K, Manisty CH, Chow AW and Foale RA, et al. Haemodynamic effects of changes in atrioventricular and interventricular delay in cardiac resynchronisation therapy show a consistent pattern: Analysis of shape, magnitude and relative importance of atrioventricular and interventricular delay. Heart 2006; 92(11):1628-1634. [doi: 10.1136/hrt.2005.080721]
15. Bashour TT, Naughton JP and Cheng TO. Systolic time intervals in patients with artificial pacemakers: Noninvasive technique for assessing atrial contribution to stroke volume at various P-R intervals. The American Journal of Cardiology 1973; 32(3):287-290. [doi: https://doi.org/10.1016/S0002-9149(73)80135-3]
16. Little WC. The left ventricular dP/dtmax-End-Diastolic volume relation in Closed-Chest dogs. Circ Res 1985; 56(6):808-815. [doi: 10.1161/01.RES.56.6.808]
17. Burggraf GW and Craige E. The first heart sound in complete heart block. Phono-echocardiographic correlations. Circulation 1974; 50(1):17-24. [doi: 10.1161/01.cir.50.1.17]
18. Leech G, Brooks N, Green-Wilkinson A and Leatham A. Mechanism of influence of PR interval on loudness of first heart sound. Br Heart J 1980; 43(2):138-142. [doi: 10.1136/hrt.43.2.138]
19. Auricchio A, Stellbrink C, Block M, Sack S, Vogt J and Bakker P, et al. Effect of pacing chamber and atrioventricular delay on acute systolic function of paced patients with congestive heart failure. The Pacing Therapies for Congestive Heart Failure Study Group. The Guidant Congestive Heart Failure Research Group. Circulation 1999; 99(23):2993-3001. [doi: 10.1161/01.cir.99.23.2993]
20. Kass DA, Chen CH, Curry C, Talbot M, Berger R and Fetics B, et al. Improved left ventricular mechanics from acute VDD pacing in patients with dilated cardiomyopathy and ventricular conduction delay. Circulation 1999; 99(12):1567-1573. [doi: 10.1161/01.cir.99.12.1567]
21. Zamorano J, Wallbridge DR, Ge J, Drozd J, Nesser J and Erbel R. Non-invasive assessment of cardiac physiology by tissue Doppler echocardiography. Eur Heart J 1997; 18(2):330-339. [doi: 10.1093/oxfordjournals.eurheartj.a015236]
22. Moreno R, Zamorano J, Almeria C, Perez-Gonzalez JA, Mataix L and Rodrigo JL, et al. Isovolumic contraction time by pulsed-wave Doppler tissue imaging in aortic stenosis. Eur J Echocardiogr 2003; 4(4):279-285. [doi: 10.1016/s1525-2167(03)00009-x]
23. Zweerink A, Salden OAE, van Everdingen WM, de Roest GJ, van de Ven PM and Cramer MJ, et al. Hemodynamic optimization in cardiac resynchronization therapy. JACC: Clinical Electrophysiology 2019; 5(9):1013-1025. [doi: 10.1016/j.jacep.2019.05.020]
24. Miki Y, Ishikawa T, Matsushita K, Yamakawa Y, Matsumoto K and Sumita S, et al. Novel method of predicting the optimal atrioventricular delay in patients with complete AV block, normal left ventricular function and an implanted DDD pacemaker. Circulation journal : official journal of the Japanese Circulation Society 2009; 73(4):654-

657. [doi: 10.1253/circj.CJ-08-0351]
25. Miki Y, Ishikawa T, Matsushita K, Yamakawa Y, Matsumoto K and Sumita S, et al. Optimal programming of the atrioventricular delay using the phonocardiogram. Pacing Clin Electrophysiol 2009; 32 Suppl 1:S81-S85. [doi: 10.1111/j.1540-8159.2008.02258.x]
26. Brugada J, Brachmann J, Delnoy PP, Padeletti L, Reynolds D and Ritter P, et al. Automatic optimization of cardiac resynchronization therapy using SonR—rationale and design of the clinical trial of the SonRtip lead and automatic AV-VV optimization algorithm in the paradym RF SonR CRT-D (RESPOND CRT) trial. Am Heart J 2014; 167(4):429-436. [doi: https://doi.org/10.1016/j.ahj.2013.12.007]
27. Brugada J, Delnoy PP, Brachmann J, Reynolds D, Padeletti L and Noelker G, et al. Contractility sensor-guided optimization of cardiac resynchronization therapy: Results from the RESPOND-CRT trial. Eur Heart J 2017; 38(10):730-738. [doi: 10.1093/eurheartj/ehw526]
28. Siejko KZ, Thakur PH, Maile K, Patangay A and Olivari MT. Feasibility of heart sounds measurements from an accelerometer within an ICD pulse generator. Pacing Clin Electrophysiol 2013; 36(3):334-346. [doi: 10.1111/pace.12059]

Chapter 4

Association between phonocardiography and echocardiography in heart failure patients with preserved ejection fraction

Hongxing Luo [1*], Jerremy Weerts [2*], Anja Bekkers [2], Anouk Achten [2], Sien Lievens [1,2], Kimberly Smeets [2], Vanessa van Empel [2], Tammo Delhaas [3], Frits W. Prinzen [1]

*Contributed equally.

Under review at *European Heart Journal – Digital Health*

[1] Department of Physiology, Cardiovascular Research Institute Maastricht (CARIM), Maastricht University, the Netherlands.
[2] Department of Cardiology, Cardiovascular Research Institute Maastricht (CARIM), Maastricht University Medical Centre (MUMC+), Maastricht, the Netherlands.
[3] Department of Biomedical Engineering, Cardiovascular Research Institute Maastricht (CARIM), Maastricht University, the Netherlands.

Abstract

Aims:

Heart failure with preserved ejection fraction (HFpEF) is associated with stiffened myocardium and elevated filling pressure that may be captured by heart sound. We investigated relationship between phonocardiography (PCG) and echocardiography in symptomatic patients suspected of HFpEF.

Methods and results:

Consecutive symptomatic patients with sinus rhythm and left ventricular ejection fraction > 45% were enrolled. Echocardiography was performed to evaluate the patients' diastolic function, accompanied by PCG measurements. PCG features including heart sound amplitude, frequency and timing intervals were calculated. A PCG-based score was developed to stratify E/e' ≤ or > 9 and its diagnostic performance was investigated. Of 45 patients, variable ratio matching was applied to obtain two groups of patients with similar characteristics but different E/e'. Patients with a higher E/e' showed higher S1 frequency, S2 frequency and S4 occurrence and longer systolic time intervals. QRS onset to S1 (QS1) interval was the best feature for prediction of E/e' > 9 (area under curve (AUC): 0.72 (0.51 - 0.88)) in the matched patients. The PCG score showed an AUC of 0.85 (0.65 - 0.96) and 0.74 (0.59 - 0.86) in the matched and all patients, respectively, both of which were not significantly improved by adding N-terminal pro-B-type natriuretic peptide (NT-proBNP, P > 0.05).

Conclusions:

PCG features can stratify E/e' in symptomatic patients suspected of HFpEF at a diagnostic performance similar to NT-proBNP. Heart sound may serve as a simple non-invasive tool for prescreening HFpEF patients.

Graphical abstract

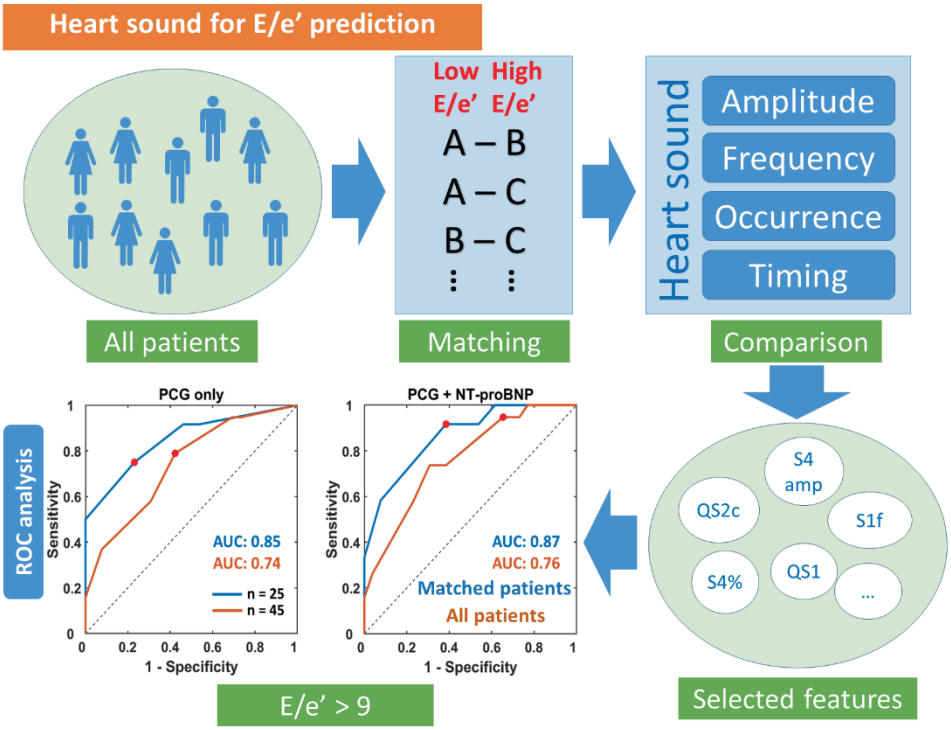

Introduction

Heart failure with preserved ejection fraction (HFpEF) accounts for approximately 50% of heart failure [1]. It is associated with ageing, hypertension and obesity and characterized by an elevated left ventricular (LV) filling pressure [2]. Current HFpEF diagnosis mainly relies on echocardiographic parameters such as the ratio between early mitral inflow velocity and early diastolic mitral annular velocity (E/e') and serological biomarkers such as N-terminal pro-brain natriuretic peptide (NT-proBNP) [3]. E/e' has been recommended as a sensitive marker of LV filling pressure elevation in current European heart failure guideline [3]. NT-proBNP is a highly sensitive but moderately specific marker of heart failure in acute settings [4]. Its level is affected by multiple factors such as patient's age and kidney function. Neither E/e' nor NT-proBNP can be used by patients at home, making early recognition of heart failure challenging.

Heart sound may serve as a simple noninvasive tool for home monitoring of heart failure with the recent emergence of portable digital stethoscopes and wearable acoustic sensing devices [5, 6]. The relationship between heart sound and heart failure has been widely investigated in both animal and human studies [7, 8]. However, these studies have focused on the third heart sound (S3) in systolic ventricular dysfunction. The changes of heart sound in diastolic ventricular dysfunction remain incompletely understood. Recently, several studies utilized machine learning to differentiate HFpEF from normal subjects by heart sound, but no relations between heart sound and echocardiography have been demonstrated [9-11]. Considering the widespread use and importance of echocardiography nowadays, it may be valuable to link heart sound to echocardiographic parameters such as E/e' for evaluation of LV filling pressure elevation.

This pilot study is dedicated to exploration of the association between phonocardiography (PCG) and echocardiography in a patient cohort suspected of HFpEF. To this purpose, we used a three-step approach:

- Investigate whether heart sound features differ between patients with low and high E/e', irrespective of potential confounding factors;
- Compose a heart sound score to predict E/e' > 9, based on features significantly different between low- and high-E/e' patients; and
- Investigate the diagnostic performance of this score in a group of matched patients and in all patients.

Methods

Study approval

This prospective observational study was approved by medical ethics committee of Maastricht University Medical Center+ (MUMC+). Data were collected from consecutive patients suspected with HFpEF and referred to a diagnostic work-up including echocardiography in the MUMC+ between January 2020 and May 2021. All study participants provided a written consent.

Patient inclusion and exclusion

Patients meeting the following criteria were included: 1) symptoms and/or signs of heart failure such as dyspnea and lower-extremity edema, 2) sinus rhythm, 3) a preserved LV ejection fraction (LVEF, > 45%) and E/e' ratio evaluated by echocardiography, and 4) serum NT-proBNP test performed during the hospital visit.

Clinical data was obtained from routine clinical care blinded for heart sound results (A.A., K.S., J.W). All patients underwent a systematic diagnostic work-up for HFpEF as described before, including echocardiography and extensive blood analysis [12]. The final diagnosis of HFpEF was determined according to the European Society of Cardiology guideline in an expert panel meeting including heart failure cardiologists and echocardiographers [3].

Echocardiographic examination

Echocardiographic examinations including 2-dimensional measurements, Doppler and tissue Doppler imaging were performed using a Philips iE33 system (Philips Medical Systems, Andover, MA) with the patients in resting supine position. LV function and structure, peak mitral inflow velocity (E wave and A wave), deceleration time, isovolumic relaxation time, early diastolic mitral annulus velocity (e') at the septal and lateral aspects, and left atrial volume were assessed according to the American Society of Echocardiography and the European Association of Cardiovascular Imaging recommendations during routine clinical care [13]. All stored image data were analyzed by experienced sonographers using Philips IntelliSpace Cardiovascular echocardiographic analysis software during routine clinical care. The sonographers were blinded to the patients' heart sound data.

Heart sound and electrocardiogram (ECG) collections

Heart sounds were recorded on the left fourth intercostal space along midclavicular line while the patients were in sitting resting condition with the body leaning forward at the same day of the echocardiography. A digital stethoscope EKO DUO (frequency range: 20-2000 Hz; Eko Devices Inc., US) was used to simultaneously record heart sound and single-lead ECG for 15 ~ 30 seconds. The collected data were transferred via Bluetooth from the EKO device to the cloud, from which data could be downloaded for further offline analysis. Heart sounds were collected by researchers (A.B., S.L., A.A., K.S.) who were blinded to both echocardiographic and PCG features of the patients.

Location of heart sound components

Signal processing procedures are shown in **Figure 1** and further described in the **Supplementary Methods**. In brief, both ECG and PCG recordings were resampled to 1000 Hz. Then ECG was used as a reference to find S1 and S2. To identify the low-frequency S3 and S4, the raw heart sound recordings were lowpass-filtered with a cut-off frequency of 50 Hz. Occurrences of S3 (S3%) and S4 (S4%) among the 10 to 15 heart beats analyzed were calculated.

Heart sound features

For each patient, heart sound features were calculated from median value of 10-15 consecutive heart beats. S1 and S2 features were calculated after lowpass-filtering the raw heart sound signals at 200 Hz, and S3 and S4 at 50 Hz.

Amplitude: Amplitudes of S1 and S2 were automatically identified as the maximal value within 80 ms following their onsets. Amplitudes of S3 and S4 were identified as the maximal value within 60 ms around their respective locations.

Frequency: The dominant frequency was calculated for each heart sound component. For S1 and S2, a 60-ms segment after their onset was used for fast Fourier transform to avoid potential heart sound splitting occurring at a later time. For S3 and S4, the onsets were generally difficult to be identified due to the low amplitude, therefore a 60-ms segment around their envelope peaks was used for calculation of dominant frequency based on fast Fourier transform.

Timing intervals: The following heart sound-derived systolic time intervals (STIs) were analyzed: 1) QS1: from the onset of the Q-wave to

the onset of S1; 2) S1S2: from S1 onset to S2 onset; and 3) QS2: from QRS onset to S2 onset. In analogy to QT, we also applied the Fridericia equation to correct QS2 for heart rate as follows: $QS2c = QS2/RR^{1/3}$, in which QS2 and QS2c are in unit of ms and RR in sec [14, 15].

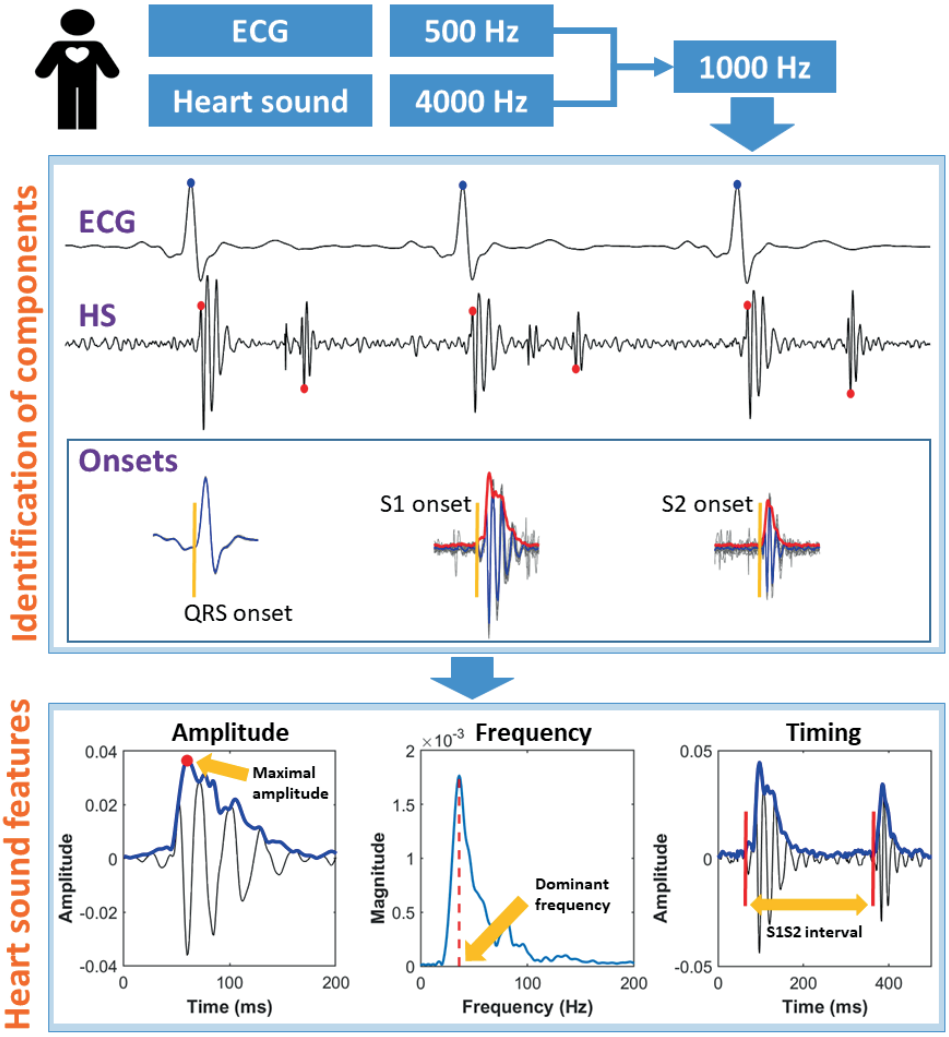

Figure 1. Demonstration of signal processing procedures

Upper panel: *Reference points were identified for ECG QRS (blue dot), S1 (red dot) and S2 (red dot), respectively. Onsets of ECG QRS, S1 and S2 were identified using a median signal (in blue) calculated from all heartbeats (in grey) aligned at the reference points.* ***Lower panel:*** *Multiple heart sound features were calculated.*

ECG, electrocardiogram; HS, heart sound; S1, first heart sound; S1S2, timing interval from S1 onset to S2 onset; S2, second heart sound.

Statistical analysis

The overarching goal of the statistical analyses was to investigate the relationship between PCG and echocardiography while reducing the effects of confounders as much as possible. To this purpose, a matching procedure was applied as described in literature [16]. The steps are as follows (**Figure 2**):

1) Each patient was matched to the other(s) if both had the same sex and similar body mass indexes (BMIs, difference ≤ 3 kg/m^2) and heart rates (difference ≤ 5 beats per minute). Doing so a patient might be matched with multiple patients who satisfied the three conditions above [16]. On the other hand, a patient might also not be matched with any other patients, and thus classified into "unmatched" group.

2) Identification of E/e'-related PCG features: For each match, the two patients were assigned by E/e' ratio to either low- or high-E/e' group. After assigning all patients, the two groups were compared for the PCG features. The features showing a P value ≤ 0.10 in the comparison were defined as E/e'-related.

3) Prediction of E/e' > 9 using PCG features: The selected PCG features were tested for their performance to predict an E/e' > 9 the matched, unmatched and all enrolled patients. The E/e' cut-off was set at 9 because a higher value at rest generally indicates LV diastolic dysfunction and raised LV filling pressure according to current heart failure guideline [3]. Receiver operating curve (ROC) analysis was performed and sensitivity, specificity and area under the curve (AUC) were calculated. The optimal cut-off value was identified at the maximal Youden's index (= sensitivity + specificity - 1) [17].

4) Prediction of E/e' > 9 using the PCG score: Each PCG feature was assigned a weight as follows:

$$Weight = \frac{AUC - 0.50}{0.05}, rounded\ to\ the\ nearest\ integer.$$

The weight, ranging from 0 (AUC = 0.50) to 10 (AUC = 1.00), evaluated the diagnostic power of each feature as compared with an AUC of 0.50 which indicates no discriminative power. To reduce the total number of features, only the features with a weight ≥ 2 were included in the calculation of a PCG score. Then the PCG score was applied to the unmatched patients and all patients to test its diagnostic performance.

Continuous and normally distributed data were expressed as mean ± standard deviation, and skewed data as median (interquartile range). Count data were expressed as number (%). Chi-squared test was performed to compare the difference in count data between two groups. Independent sample *t* test was used to compare normally distributed continuous variables, while Wilcoxon rank sum test was applied for comparison of skewed continuous data. The AUCs and 95% confidence intervals were calculated and compared with DeLong test using MedCalc (MedCalc Software Ltd, Belgium). Statistical significance was defined as a two-tailed P value <0.05. All analyses were performed using MATLAB R2018b (MathWorks Inc., US).

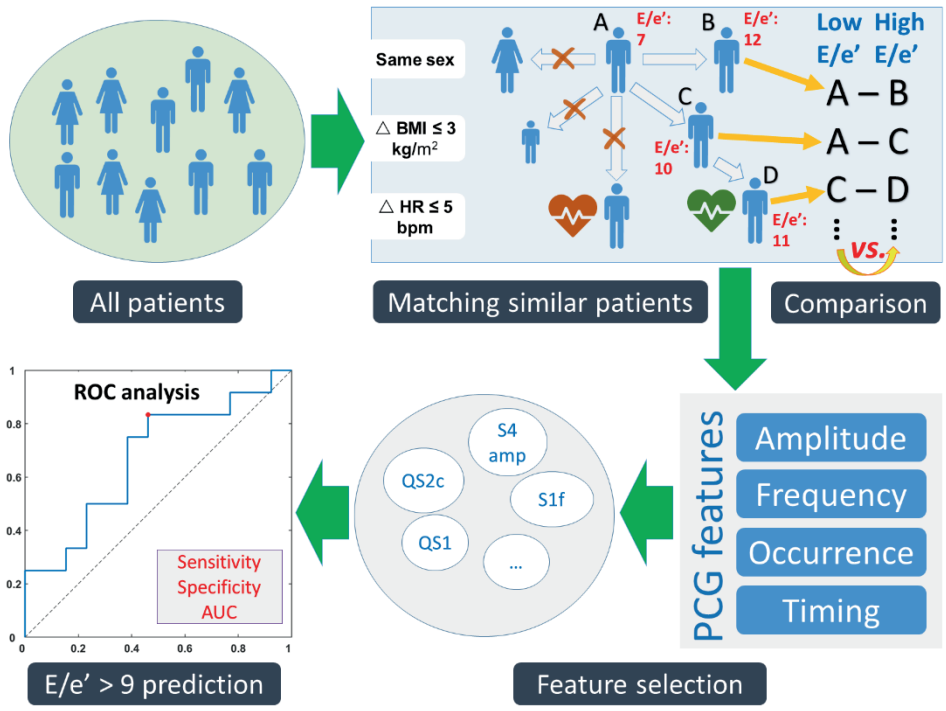

Figure 2. Illustration of statistical analyses

All patients were matched by sex, body mass index and heart rate and divided into low- and high-E/e' groups. Phonocardiographic features were compared between the two groups, and the ones showing a significant difference were identified for prediction of E/e' > 9.

AUC, area under the curve; BMI, body mass index; bpm, beats per minute; E/e', the ratio between early mitral inflow velocity and early diastolic mitral annular velocity; HR, heart rate; QS1, Q to S1 onset; QS2c, QS2 corrected

for RR interval; ROC, receiver operating curve; S1f, S1 dominant frequency; S4, fourth heart sound.

Results

Baseline characteristics

A total of 61 patients were screened in our study. After excluding 11 patients with AF during echocardiographic or phonocardiographic measurement, 2 patients without E/e' data, 1 patient without NT-proBNP data, and 2 patients with too-noisy heart sound recordings, the remaining 45 patients were matched according to sex, BMI and heart rate, resulting in 25 patients that gave rise to 32 matched pairs.

Baseline characteristics of the low- and high-E/e' groups did not significantly differ regarding age, sex, BMI, heart rate, blood pressure, history of hypertension, history of AF or PR interval (**Table 1**). One patient had heart failure with recovered LVEF. No patients had prior heart failure hospitalization. NT-proBNP was significantly higher in the high-E/e' group. Significantly more patients were diagnosed with HFpEF in the high- than low-E/e' group. Regarding echocardiographic parameters, mean E/e' was 8.3 and 13.9 in the low- and high-E/e' group, respectively. E/A ratio was similar in both groups.

Table 1. Population and echocardiographic characteristics of the matched pairs

	Low E/e' (n = 32)	High E/e' (n = 32)	P value
Patient			
Age, years	72 ± 7	74 ± 5	0.11
Female, n (%)	27 (84)	27 (84)	1.00
BMI, kg/m^2	27.5 ± 3.1	27.9 ± 3.0	0.63
Heart rate, bpm	71 ± 9	71 ± 8	0.85
PR interval, ms	185 ± 31	183 ± 26	0.75
Systolic BP, mm Hg	146 ± 17	150 ± 18	0.30
Diastolic BP, mm Hg	78 ± 14	76 ± 13	0.70
NYHA class ≥ III, n (%)	16 (50)	9 (28)	0.07
NT-proBNP, pg/ml	211 ± 172	367 ± 291	0.01
Hypertension, n (%)	24 (75)	20 (63)	0.28
History of AF, n (%)	14 (44)	12 (38)	0.61
Diabetes, n (%)	2 (6)	6 (19)	0.13
Chronic kidney disease, n (%)	1 (3)	5 (16)	0.09
COPD, n (%)	4 (13)	2 (6)	0.39
HFpEF diagnosis, n (%)	21 (66)	30 (94)	0.005
Echocardiography			
LV mass, g	123 ± 33	158 ± 46	< 0.001
LVMI, g/m^2	67 ± 14	83 ± 17	< 0.001
LAV, ml	60 ± 20	78 ± 19	< 0.001
LAVI, ml/m^2	33 ± 10	41 ± 9	< 0.001
LVEF, %	58 ± 4	62 ± 5	< 0.001
LVEDD, mm	44 ± 4	49 ± 5	< 0.001
LVESD, mm	30 ± 5	31 ± 6	0.19
Peak E-wave, cm/s	66 ± 19	87 ± 31	0.001
Peak A-wave, cm/s	63 ± 21	83 ± 23	< 0.001
E/A	1.15 ± 0.59	1.15 ± 0.62	1.00
e' lateral, cm/s	10.0 ± 4.0	6.8 ± 2.6	< 0.001
e' septal, cm/s	6.5 ± 2.1	5.9 ± 1.5	0.21
E/e' average	8.3 ± 2.2	13.9 ± 3.4	< 0.001
E-wave DT, ms	212 ± 38	209 ± 30	0.81
A-wave DT, ms	102 ± 19	118 ± 18	0.004
IVRT, ms	96 ± 20	114 ± 24	0.007

AF, atrial fibrillation; A wave, peak velocity of mitral valve inflow after atrial contraction; BMI, body mass index; BP, blood pressure; COPD, chronic obstructive pulmonary disease; DT, deceleration time; e', early diastolic mitral annulus velocity by Doppler tissue imaging; E wave, peak velocity of early diastolic mitral inflow; HFpEF, heart failure with preserved ejection fraction; IVRT, isovolumic relaxation time; LA, left atrium; LAVI, left atrial volume index; LV, left ventricle; LVEDD, left ventricular end-diastolic diameter; LVEF, left ventricular ejection fraction; LVESD, left ventricular end-systolic diameter; LVMI, left ventricular mass index; NT-proBNP, N-terminal pro-brain natriuretic peptide; NYHA, New York Heart Association.

Phonocardiographic characteristics

Figure 3 shows examples of heart sound and ECG recordings from patients of the low- and high-E/e' groups. Though QS1 did not markedly differ between low and high E/e', QS2 was longer in the latter (355 ms *vs*. 424 ms), even after correcting for RR interval (QS2c: 405 ms *vs*. 461 ms), accompanied by an higher S1 frequency (39 Hz *vs*. 42 Hz) and S2 frequency (42 Hz *vs*. 53 Hz) in the high E/e' patient.

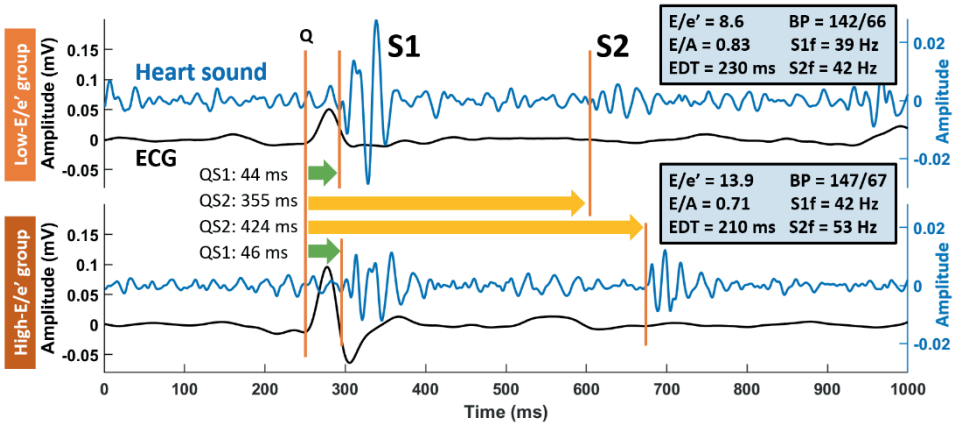

Figure 3. Examples of ECG and heart sound in patients with low vs. high E/e' *Both examples were aligned at QRS onset at 250th ms. Note the sharper S1 and S2 morphologies in the lower than the upper panel, indicating higher frequencies at a higher E/e' ratio.*

BP, blood pressure in unit of mmHg; ECG, electrocardiogram; EDT, E-wave deceleration time; Q, QRS onset; QS1, Q to S1 onset; QS2, Q to S2 onset; S1, first heart sound; S1f, S1 dominant frequency; S2, second heart sound; S2f, S2 dominant frequency.

Table 2 summarizes the phonocardiographic characteristics of the patients in the two groups. Heart sound amplitude was not significantly different between the two groups, except that S4 amplitude was significantly higher in the high-E/e' group. Frequencies of S1, S2 and S4 were significantly higher in the high- than the low-E/e' group. The occurrence of S4 and combined S3 and S4 was higher in the high-E/e' group, but the occurrence of S3 did not differ between the two groups. Regarding timing intervals, RR interval was nearly identical between the two groups. QS1 tended to be longer in the high-E/e' group (P = 0.10). QS2 and QS2c were longer in the high than in the low-E/e' group.

Table 2. Phonocardiographic characteristics of the matched pairs

	Low E/e' (n = 32)	High E/e' (n = 32)	P value
Total heartbeat, n	410	390	
Avg. heartbeat, n	13	12	
Amplitude, x 10^{-4}			
S1	243 (105 - 322)	184 (138 - 220)	0.14
S2	101 (73 - 151)	100 (57 - 224)	1.00
S3	16 (8 - 24)	16 (10 - 23)	0.99
S4	6 (0 - 20)	15 (8 - 21)	0.03
Frequency			
S1, Hz	42 ± 3	46 ± 8	0.003
S2, Hz	48 ± 6	55 ± 14	0.008
S3, Hz	34 (32 - 34)	33 (32 - 34)	0.17
S4, Hz	28 (0 - 34)	34 (31 - 34)	0.02
Occurrence			
S3, %	93 ± 18	91 ± 14	0.67
S4, %	58 ± 34	78 ± 29	0.01
S3 and S4, %	54 ± 34	71 ± 30	0.04
Time interval			
RR, ms	860 ± 115	861 ± 104	0.98
QS1, ms	69 ± 23	78 ± 19	0.10
S1S2, ms	320 ± 36	333 ± 47	0.21
QS2, ms	389 ± 42	412 ± 48	0.05
QS2c, ms	410 ± 33	433 ± 41	0.01

Avg., average; QS1, Q to S1 onset; QS2, Q to S2 onset; QS2c, QS2 corrected for RR interval; S1, first heart sound; S1S2, S1 to S2 onset; S2, second heart sound; S3, third heart sound; S3%, percentage of heartbeats with S3; S3 and S4%, percentage of heartbeats with both S3 and S4; S4, fourth heart sound; S4%, percentage of heartbeats with S4.

Prediction of E/e' using PCG features

PCG features that differed between low and high E/e' groups with a P value ≤ 0.10 in **Table 2** were included in classification of E/e' by 9. Of note, QS2c instead of QS2 was used to correct for heart rate. **Table 3** summarizes the optimal cut-off values, diagnostic performance and scores of the PCG features and NT-proBNP in predicting E/e' > 9 in matched patients. The sensitivity was the same (0.83) for all S4-related features including S4 amplitude, S4 frequency, S4% and S3 and S4%, while the specificity was the highest for S4% (0.77). Both S4 amplitude and frequency were dependent on S4% because both were set to 0 when S4 was undetected for a heartbeat. Hence, only the S4% was selected for the PCG score. S1 frequency was the highest specific feature for E/e' prediction. QS1 had the highest sensitivity (0.83) and AUC (0.72) among all features. Each feature was assigned a score, and eligible features with an AUC ≥ 0.60 (in bold in **Table 3**) were included in the final PCG score. NT-proBNP showed a similar diagnostic performance to any eligible PCG features (P > 0.05). Addition of NT-proBNP increased the total PCG score to 18.

The PCG score was applied to the matched, unmatched and all patients (**Table 4**). At the cut-off value of 152 pg/ml, NT-proBNP was a sensitive marker of E/e' > 9 in all 3 groups. PCG score showed higher absolute AUCs than NT-proBNP in the matched and all patients, though the statistical significance was not reached (P > 0.05). Addition of NT-proBNP to the PCG score did not significantly improve the prediction of E/e' as evidenced by comparisons of AUCs (P > 0.05). Of note, the absolute value of sensitivity increased by 0.15 - 0.30 from PCG only to PCG + NT-proBNP.

Figure 4 shows the ROC curves for predicting E/e' > 9 using PCG features alone (**left panel**) and with NT-proBNP (**right panel**). In both panels, the drop of AUC from the matched (blue curve) to all patients (orange curve) was insignificant (P > 0.05).

Table 3. Phonocardiography for prediction of E/e' > 9 in matched patients (n = 25)

	Cut-off value	Sensitivity	Specificity	AUC	Score*
S4 amplitude	6.6×10^{-4}	0.83	0.62	0.69 (0.47 - 0.86)	4
S1 frequency	**46.9 Hz**	**0.50**	**0.92**	**0.68 (0.47 - 0.85)**	**4**
S2 frequency	45.9 Hz	0.67	0.54	0.56 (0.35 - 0.76)	0
S4 frequency	31.3 Hz	0.83	0.69	0.69 (0.48 - 0.86)	4
S4%	**73**	**0.83**	**0.77**	**0.69 (0.48 - 0.86)**	**4**
S3 and S4%	53	0.83	0.62	0.70 (0.48 - 0.86)	4
QS1	**64 ms**	**0.83**	**0.69**	**0.72 (0.51 - 0.88)**	**4**
QS2c	**415 ms**	**0.67**	**0.77**	**0.67 (0.46 - 0.85)**	**3**
Total					***15***
NT-proBNP	**152 pg/ml**	**0.83**	**0.54**	**0.67 (0.46 - 0.85)**	**3**
Total					***18***

AUC, area under the curve; *NT-proBNP, N-terminal pro-brain natriuretic peptide; QS1, Q to S1 onset; QS2c, Q to S2 onset corrected for RR interval; S1, first heart sound; S2, second heart sound; S4%, percentage of heartbeats with S4.*

Table 4. Phonocardiography and NT-proBNP for predicting E/e' > 9

Patients	Matched (n = 25)	Unmatched (n = 20)	All (n = 45)
NT-proBNP (cut-off: 152 pg/ml)			
Average score	1.8 ± 1.5	2.4 ± 1.2	2.1 ± 1.4
Sensitivity	0.83	1.00	0.84
Specificity	0.54	0.46	0.46
AUC	0.67 (0.46 - 0.85)	0.78 (0.54 - 0.93)*	0.68 (0.52 - 0.81)
PCG only (cut-off: 7)			
Average score	5.6 ± 4.8	7.1 ± 3.2	6.3 ± 4.1
Sensitivity	0.75	0.57	0.79
Specificity	0.77	0.46	0.55
AUC	0.85 (0.65 - 0.96)	0.58 (0.34 - 0.79)*	0.74 (0.59 - 0.86)
PCG + NT-proBNP (cut-off: 7)			
Average score	7.4 ± 5.4	9.5 ± 3.5	8.4 ± 4.6
Sensitivity	0.92	0.86	0.95
Specificity	0.62	0.38	0.31
AUC	0.87 (0.67 - 0.97)	0.67 (0.43 - 0.86)*	0.76 (0.61 - 0.88)

** Compared with matched patients: P > 0.05, DeLong test.*

AUC, area under the curve; NT-proBNP, N-terminal pro-brain natriuretic peptide; PCG, phonocardiography.

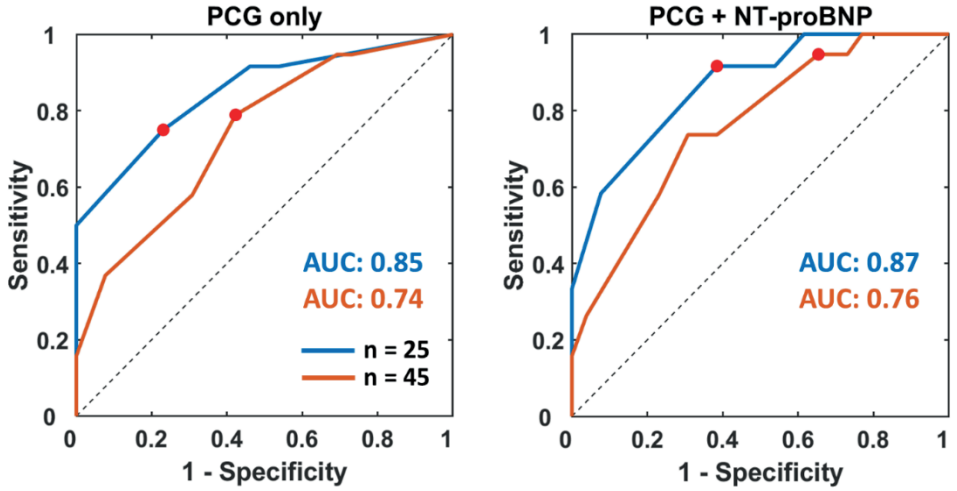

Figure 4. PCG-only and PCG + NT-proBNP scores in prediction of E/e' > 9 in matched (blue line) and all patients (orange line) *For each ROC curve, red dot indicates the sensitivity and specificity at a score of 7.*

Discussion

The main findings of this pilot study on the relationship between heart sound and echocardiography in patients suspected with HFpEF are: 1) an E/e' ratio over 9 was related to higher heart sound frequencies (S1, S2 and S4), S4 amplitude and occurrence, and a longer QS2c; 2) QS1 was the best prediction marker for E/e' > 9; and 3) PCG score showed a better prediction performance than any single feature, which was insignificantly improved by adding NT-proBNP. Our findings provide clues for using heart sound to screen and monitor HFpEF patients.

Heart sound as a novel marker of HFpEF

Our findings support heart sound as a novel simple marker of E/e' elevation in patients suspected with HFpEF. The higher S1 and S2 frequencies in the patients with an elevated E/e' ratio are consistent with the idea that stiffened ventricles are linked to higher heart sound frequencies [18]. Further evidence came from the more frequent occurrence of S4 which has been well established as a marker of less compliant ventricles [19-21].

The reasons for the stiffened ventricles are multifaceted. Firstly, the structural cause may come from myocardial hypertrophy. In our matched patients, the LV mass and mass index were significantly higher in the patients with a high E/e' ratio. Secondly, the higher stiffness may relate to

an increased ventricular wall tension, as suggested by a larger end-diastolic diameter and left atrial volume in the patients with a high E/e'. A high E/e' *per se* also indicates an increased LV filling pressure [22]. This relationship has been supported by a recent open-chest porcine study in which ventricular vibrations were collected using an epicardially attached accelerometer [23]. The study demonstrated a close relation between changes in S1 frequency and changes in end-diastolic volume during fluid administration to alter ventricular preload and myocardial tension. Compared with hypertrophy, wall tension is likely reversed as the patients' conditions are improved with treatments, indicating the value of heart sound frequency in monitoring the patients' disease conditions, yet this idea awaits further investigation.

Causes of longer QS1 and QS2 in high E/e'

Another finding of the present study was that HFpEF patients with a higher E/e' also tended to have longer QS1 and QS2 intervals. QS1 reflects the time required for the ventricles to build up sufficient intracardiac pressure to close the atrioventricular valves. Thus, prolongation of QS1 is associated with a slower myocardial force development and/or an elevated atrial pressure. Weakened myocardial force does not seem to be a major contributor of a longer QS1 in the high E/e' group because this group had a higher LVEF compared with the low-E/e' group (62% *vs*. 58%). Therefore, the prolonged QS1 interval in patients with high E/e' is most likely related to an increased left atrial pressure. The elevated left atrial pressure not only increases the trans-atrioventricular-valve pressure gradient, but also widely separates the atrioventricular valves at the moment of ventricular electrical activation. Prolongation of QS1 may also come from a shortened PR-interval, but this possibility seems unlikely because the matched groups had similar PR intervals [24]. Therefore, QS1 may be a marker tailored for differentiating HFpEF patients who are characterized by an increased LV filling pressure rather than a weakened myocardial force. This hypothesis is confirmed by the highest diagnostic performance of QS1 among all PCG features and NT-proBNP for prediction of E/e' over 9.

A longer QS2 in the high-E/e' group indicates a delayed total electro-mechanical systolic time. QS2 lengthening appears to be the results of both prolonged QS1 and S1S2 intervals. While the prolongation of QS1 has been discussed above, the prolongation of S1S2 is likely caused by longer ejection time, supported by the higher LVEF in the high-E/e' group.

Another cause of a longer QS2 and QS2c may be hypertrophy which has been shown to prolong QT interval on ECG [25]. However, this relation needs to be further investigated.

Perspectives for disease screening using heart sound

Our findings show that PCG features are non-inferior to NT-proBNP in differentiating E/e' ratios. In the matched patients, S4% and QS1 showed the same sensitivity as NT-proBNP. However, heart sound is advantageous in its noninvasiveness compared with serum NT-proBNP measurement. Secondly, heart sound measurement is time-efficient. In our study, a heart sound recording took 15 to 30 seconds. This short time enables a simple evaluation of E/e' elevation in an acute setting feasible. Thirdly, heart sound measurement is cost-effective. The device used for heart sound collection such as the EKO digital stethoscope in the current study costs only a few hundreds of dollars and can be used as long as the device is charged. In comparison, NT-proBNP measurement requires buying the detection kit, while an echocardiography machine is generally sold at a much higher price than a digital stethoscope. Finally, the EKO device can be used by patients at home to record ECG and heart sound which may be remotely interpreted by the cardiologist/nurse, reducing hospital visits and thus healthcare cost. The above advantages make heart sound a promising tool for HFpEF evaluation. Hence, future studies focusing on implementing digital stethoscopes for HFpEF diagnosis are warranted.

Current heart sound studies of HFpEF

Overall, studies of heart sound in HFpEF patients have been clearly overlooked considering the long history of studying heart sound in patients with ventricular systolic dysfunction. Recent popularity of machine learning has enabled the data-driven studies of heart sound for classification of heart failure by LVEF (i.e., normal, reduced and preserved) [9-11, 26]. Early machine learning studies relied on manual extraction of heart sound features for training the algorithm. For example, extreme learning machine trained by heart sound features such as diastolic-to-systolic duration ratio showed high sensitivity (95%) and specificity (97%) in classification between HFpEF patients and healthy controls [9]. Deep learning takes the advantage of automatic feature extraction from raw heart sound signals for training the model. Gated recurrent unit has been used to automatically learn the deep features from the raw signals and shown an accuracy of

99% in classification among HFpEF, HFrEF and normal controls [11]. Convolutional neural network trained with short-time Fourier transform spectrum is reported to show 99% of sensitivity and specificity in distinguishing LV diastolic dysfunction (n = 30) from healthy controls (n = 41) in a small sample size study [10]. The LV diastolic dysfunction group was a mixture of HFrEF and HFpEF patients (LVEF: 45% ± 16%) with a high E/e' ratio (18.6 ± 6.7).

Although machine learning is not investigated in our current study, given its high accuracy reported in other studies, it is conceivable that it will further improve the prediction power of our proposed heart sound score. Our findings on the relationship between heart sound and echocardiography provide interpretable PCG features which may be useful inputs for training the machine learning models. The fact that a simple linear combination of selected PCG features into a score already showed a relatively high AUC (0.85) provides a basis to utilize machine learning which is known for its classification of nonlinear relations inherent in the features. Deep learning may be another promising approach for prediction of E/e' and classification of HFpEF from the normal. In this case, time-frequency representation of heart sound may be useful to better visualize heart sound patterns and serve as an input to the deep learning model. However, deep learning requires a larger sample size in future studies.

Limitations

Several limitations need to be addressed in the future. Firstly, this single-center pilot study had a small sample size which to some extent limited the validation of our proposed diagnostic score. It seems that the performance of the heart sound score was damped from matched to unmatched patients, though the DeLong tests did not show a significant difference. This is likely caused by difference in patients' characteristics between the two groups. A larger sample size may help minimize this difference by enrolling a more representative group of patients in the matching cohort. A larger-scale study would also allow revealing the relationship between PCG features and patients' outcomes. Secondly, a cut-off value of 45% rather than 50% was chosen for LVEF in this study to include patients suspected of HFpEF who, in the end, appeared to have heart failure with midrange EF in a borderline region with HFpEF. In fact, only 1 patient had an LVEF between 45% ~ 50% (48%). This patient did not differ from the other patients regarding baseline characteristics,

echocardiographic parameters or PCG features, and did not lead to notably different diagnostic performances. Thirdly, the patients included in the current study appeared to have a mild degree of diastolic dysfunction, while HFpEF patients of an advanced stage or during a decompensated state may present an E/e' over 15 [27]. However, the fact that heart sound can differentiate "borderline" E/e' values may also prove valuable for preliminary assessment of the patients. Moreover, considering E/e' as a continuous variable rather than dichotomizing E/e' may be more valuable to clinical practice, but also requires a larger sample size. Lastly, our diagnostic score was only based on measurements during resting status which may not be optimal for displaying diastolic dysfunction. Interventions such as exercise may help further uncover diastolic dysfunction in some patients suspected of HFpEF.

Conclusions

PCG features such as heart sound frequency and timing intervals are related to E/e' in patients suspected with HFpEF. Heart sound-derived score may help improve classification and monitoring of diastolic dysfunction among HFpEF patients.

Funding:

This study was funded by a grant from the European Union Horizon 2020 research and Innovation programme "Personalised In-silico Cardiology (PIC)" under the Marie Sklodowska-Curie grant agreement No. 764738.

Acknowledgements:

We would like to thank Jaeson Bang, founder of Future Cardia for providing the EKO digital stethoscopes for this study.

References:

1. Dunlay SM, Roger VL, Redfield MM. Epidemiology of heart failure with preserved ejection fraction. Nat Rev Cardiol 2017;14:591-602.
2. Borlaug BA. The pathophysiology of heart failure with preserved ejection fraction. Nat Rev Cardiol 2014;11:507-15.
3. McDonagh TA, Metra M, Adamo M, et al. 2021 ESC Guidelines for the diagnosis and treatment of acute and chronic heart failure. Eur Heart J 2021;42:3599-726.
4. Hill SA, Booth RA, Santaguida PL, et al. Use of BNP and NT-proBNP for the diagnosis of heart failure in the emergency department: a systematic review of the evidence. Heart Fail Rev 2014;19:421-38.
5. Bachtiger P, Petri CF, Scott FE, et al. Point-of-care screening for heart failure with reduced ejection fraction using artificial intelligence during ECG-enabled stethoscope examination in London, UK: a prospective, observational, multicentre study. Lancet Digit Health 2022;4:e117-25.
6. Inan OT, Baran PM, Javaid AQ, et al. Novel Wearable Seismocardiography and Machine Learning Algorithms Can Assess Clinical Status of Heart Failure Patients. Circ Heart Fail 2018;11:e4313.
7. Drazner MH, Rame JE, Stevenson LW, Dries DL. Prognostic Importance of Elevated Jugular Venous Pressure and a Third Heart Sound in Patients with Heart Failure. New Engl J Med 2001;345:574-81.
8. Kono T, Rosman H, Alam M, Stein PD, Sabbah HN. Hemodynamic correlates of the third heart sound during the evolution of chronic heart failure. J Am Coll Cardiol 1993;21:419-23.
9. Liu Y, Guo X, Zheng Y. An Automatic Approach Using ELM Classifier for HFpEF Identification Based on Heart Sound Characteristics. J Med Syst 2019;43:285.
10. Yang Y, Guo XM, Wang H, Zheng YN. Deep Learning-Based Heart Sound Analysis for Left Ventricular Diastolic Dysfunction Diagnosis. Diagnostics (Basel) 2021;11.
11. Gao S, Zheng Y, Guo X. Gated recurrent unit-based heart sound analysis for heart failure screening. Biomed Eng Online 2020;19:3.
12. Weerts J, Barandiarán Aizpurua A, Henkens MTHM, et al. The prognostic impact of mechanical atrial dysfunction and atrial fibrillation in heart failure with preserved ejection fraction. Euro Heart J Cardio Imag 2021;23:74-84.
13. Lang RM, Badano LP, Mor-Avi V, et al. Recommendations for cardiac chamber quantification by echocardiography in adults: an update from the American Society of Echocardiography and the European Association of Cardiovascular Imaging. Eur Heart J Cardiovasc Imaging 2015;16:233-70.
14. Vandenberk B, Vandael E, Robyns T, et al. Which QT Correction Formulae to Use for QT Monitoring? J Am Heart Assoc 2016;5.
15. Weissler AM, Harris WS, Schoenfeld CD. Systolic time intervals in heart failure in man. Circulation (New York, N.Y.) 1968;37:149-59.

16. Chen JW, Maldonado DR, Kowalski BL, et al. Best Practice Guidelines for Propensity Score Methods in Medical Research: Consideration on Theory, Implementation, and Reporting. A Review. Arthroscopy 2021.
17. Youden WJ. Index for rating diagnostic tests. Cancer - Am Cancer Soc 1950;3:32-5.
18. Adolph RJ, Stephens JF, Tanaka K. The clinical value of frequency analysis of the first heart sound in myocardial infarction. Circulation 1970;41:1003-14.
19. Shah SJ, Nakamura K, Marcus GM, et al. Association of the fourth heart sound with increased left ventricular end-diastolic stiffness. J Card Fail 2008;14:431-6.
20. Wen-Chol Voon SSYH. Doppler Study of Transmitted Transmitral A Wave in Patients with a Fourth Heart Sound. Echocardiography (Mount Kisco, N.Y.) 1997;14:243-9.
21. Van de Werf F, Minten J, Carmeliet P, De Geest H, Kesteloot H. The genesis of the third and fourth heart sounds. A pressure-flow study in dogs. J Clin Invest 1984;73:1400-7.
22. Mitter SS, Shah SJ, Thomas JD. A Test in Context: E/A and E/e' to Assess Diastolic Dysfunction and LV Filling Pressure. J Am Coll Cardiol 2017;69:1451-64.
23. Krogh MR, Halvorsen PS, Grymyr O, et al. Continuous Estimation of Acute Changes in Preload Using Epicardially Attached Accelerometers. IEEE Trans Biomed Eng 2021;68:2067-75.
24. Bashour TT, Naughton JP, Cheng TO. Systolic time intervals in patients with artificial pacemakers. Noninvasive technique for assessing atrial contribution to stroke volume at various P-R intervals. Am J Cardiol 1973;32:287-90.
25. Dritsas A, Sbarouni E, Gilligan D, Nihoyannopoulos P, Oakley CM. QT-interval abnormalities in hypertrophic cardiomyopathy. Clin Cardiol 1992;15:739-42.
26. Zheng Y, Guo X, Qin J, Xiao S. Computer-assisted diagnosis for chronic heart failure by the analysis of their cardiac reserve and heart sound characteristics. Comput Methods Programs Biomed 2015;122:372-83.
27. Pieske B, Tschope C, de Boer RA, et al. How to diagnose heart failure with preserved ejection fraction: the HFA-PEFF diagnostic algorithm: a consensus recommendation from the Heart Failure Association (HFA) of the European Society of Cardiology (ESC). Eur Heart J 2019;40:3297-317.

SUPPLEMENTARY MATERIALS

Location of heart sound components

Signal processing procedures are shown in **Figure 1** of the manuscript. The researcher (H.L.) analyzing heart sounds was blinded to the patients' echocardiographic data until all heart sound features had been calculated. The raw EKO recordings had a sampling frequency of 500 Hz and 4000 Hz for ECG and heart sound, respectively. Both recordings were resampled to 1000 Hz before further processing. Data from patients with too noisy heart sound recordings not showing clear S1 and S2 were excluded from analysis.

ECG was used as a reference to find S1 and S2. S1 was defined as the major vibrations immediately following QRS onset, while S2 occurred around the end of T wave. To reduce noise, a reference point was first set for all 10 – 15 selected consecutive heart beats, and then a median signal was calculated after aligning all heart beats at the reference point. Subsequently, the onsets of the QRS complex, S1 and S2 were determined. For S1 and S2, their signal envelopes were calculated, their onsets being defined as the moment of the start of the rise of the envelopes.

To identify the low-frequency S3 and S4, the raw heart sound recordings were lowpass-filtered with a cutoff frequency of 50 Hz. Subsequently, the signal envelope was calculated and S3 was automatically identified as the highest peak within 100-250 ms following the onset of S2 if its amplitude was >10% of S2 amplitude [1-5]. S4 was defined as the highest peak occurring 50-200 ms after the onset of the P wave on the ECG and at least 50 ms before the onset of S1 and was only accepted as S4 if its amplitude was > 10% of the next S1. With the single-lead ECG used in this study, sometimes the P wave onset could not be identified with sufficient confidence. Therefore, for all patients, PR interval of ECG limb lead II was also obtained from clinical ECG recordings for identification of S4. If S3 or S4 was not detected, the corresponding amplitude and frequency were set to 0. Occurrences of S3 (S3%) and S4 (S4%) among the 10 to 15 heart beats analyzed were calculated.

References:

1. Abe H, Yokouchi M, Deguchi F, Saitoh F, Yoshimi H and Arakaki Y, et al. Measurement of left atrial systolic time intervals in hypertensive patients using Doppler echocardiography: Relation to fourth heart sound and left ventricular wall thickness. J Am Coll Cardiol 1988; 11(4):800-805. [doi: 10.1016/0735-1097(88)90214-8]

2. Wen-Chol Voon SSYH. Doppler study of transmitted transmitral a wave in patients with a fourth heart sound. Echocardiography (Mount Kisco, N.Y.) 1997; 14(3):243-249. [doi: 10.1111/j.1540-8175.1997.tb00716.x]

3. Denef B, De Geest H and Kesteloot H. The clinical value of the calibrated apical a wave and its relationship to the fourth heart sound. Circulation (New York, N.Y.) 1979; 60(6):1412-1421. [doi: 10.1161/01.CIR.60.6.1412]

4. Pozzoli M, Febo O, Tramarin R, Pinna G, Cobelli F and Specchia G. Pulsed Doppler evaluation of left ventricular filling in subjects with pathologic and physiologic third heart sound. Eur Heart J 1990; 11(6):500-508. [doi: 10.1093/oxfordjournals.eurheartj.a059742]

5. Van de Werf F, Minten J, Carmeliet P, De Geest H and Kesteloot H. The genesis of the third and fourth heart sounds. A pressure-flow study in dogs. J Clin Invest 1984; 73(5):1400-1407. [doi: 10.1172/JCI111344]

Chapter 5

Smartphone as an electronic stethoscope: Factors influencing heart sound quality

Hongxing Luo [1*], Pablo Lamata [2*], Salomé Bazin [3], Thea Bautista [2], Natsuki Barclay [2], Mehrdad Shahmohammadi [4], Jolijn M. Lubrecht [1], Tammo Delhaas [4], Frits W. Prinzen [1]

* Contributed equally.

Under review at *European Heart Journal – Digital Health*

[1] Department of Physiology, Cardiovascular Research Institute Maastricht (CARIM), Maastricht University, the Netherlands
[2] Biomedical Engineering Department, King´s College London, London, United Kingdom.
[3] Cellule Studio, London, United Kingdom.
[4] Department of Biomedical Engineering, Cardiovascular Research Institute Maastricht (CARIM), Maastricht University, the Netherlands

Abstract

Aims:

Smartphones are equipped with a high-quality microphone which may be used as an electronic stethoscope. We aim to investigate the factors influencing quality of heart sound recorded using a smartphone by general users.

Methods and results:

An app named Echoes was developed for recording heart sounds using iPhone. Information on phone version and users' characteristics including sex, age and body mass index (BMI) was collected. Heart sound quality was visually assessed and its relation to phone version and users' characteristics was analyzed. A total of 1148 users contributed to 7597 heart sound recordings. Over 80% of users were able to make at least 1 good-quality recording. Good-, unsure- and bad-quality recordings amounted to 5647 (74.6%), 466 (6.2%) and 1457 (19.2%), respectively. Most good recordings were collected in the first 3 attempts of the users. Phone version did not significantly change the users' success rate of making a good recording, neither was sex in the first attempt ($P = 0.41$) or the first 3 attempts ($P = 0.21$). Success rate tended to decrease with age in the first attempt ($P = 0.06$) but not the first 3 attempts ($P = 0.70$). BMI did not significantly affect the heart sound quality in a single attempt ($P = 0.73$) or in three attempts ($P = 0.14$).

Conclusions:

Smartphone can be used by general users to record heart sounds in good quality. Age may affect heart sound recording, but hardware, sex and BMI do not alter the recording.

Graphical abstract

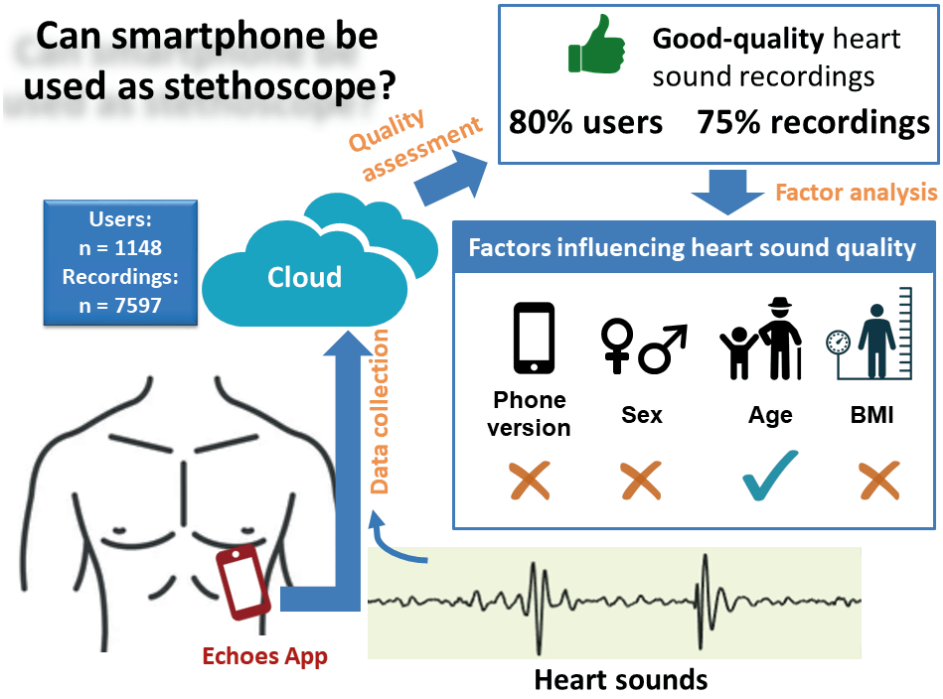

Introduction

The stethoscope has a history of over 200 years and still serves as a simple noninvasive tool to listen to patient's sounds from lungs, heart and intestines [1]. Conventional binaural stethoscopes comprise of a chestpiece and two earpieces. By putting the chestpiece against the patient's skin, the doctor can listen to the patient's sounds through the two earpieces. The electronic stethoscope was invented in the 1970s, allowing storage, replay and processing of sounds [2, 3]. However, the digital phonocardiogram has not been widely adopted, partly because of the emergence and popularity of novel imaging techniques such as echocardiography in the 1980s [4].

Recent research is creating new interest in cardiac sounds, thanks to the miniaturization of sound sensors, development of signal processing techniques and popularization of artificial intelligence algorithms [5]. The electronic stethoscope has now been shown to deliver a higher sensitivity to sound than its conventional counterpart [6]. Some handheld electronic stethoscopes allow simultaneous recordings of heart sound and electrocardiogram and are marketed to help in remote monitoring [7].

All electronic stethoscopes have the same mechanism of action that converts mechanical vibrations to digital signals. Since a decade the widely used smartphones are equipped with a high-quality microphone which may be used for recording heart sounds. This possibility will create some promising applications for the public to learn heart disease and for remote monitoring of patients at home. Several mobile App prototypes such as iStethoscope and CPstethoscope have been proposed to record heart sounds [8, 9]. Nevertheless, the central question to a large-scale deployment of a mobile phone as a digital stethoscope has not been answered: what are the factors that may affect the user's experience on using the App for heart sound recording? These factors may come from hardware such as phone version and from user's characteristics such as age, sex and body mass index (BMI).

To this purpose the Echoes app was designed for recording, processing and storage of heart sounds by means of an iPhone. The specific objective of this study is to investigate the effect of phone version as well as user characteristics on the quality of recorded heart sounds.

Methods

Echoes app

The Echoes app is the result of a primarily public-engagement study, aiming to convert a smartphone microphone into an electronic stethoscope so that general people can listen to their own heart sounds and learn more about cardiovascular disease. It does not provide any diagnosis or treatment information. The study has been approved by ethical committee of King's College London (LRS-20/21-20985) and conforms to the European Union General Data Protection Regulation on data protection and privacy. Information sheet for participants is available online [10].

The Echoes app, utilizing built-in microphone of smartphone to record heart sounds, is currently available for iPhone only. On launching the app, the users are asked to provide consent for data collection and management. Then a few tips pop up to guide the user to better record heart sounds. These tips include asking the user to remove phone case, finding one of four spots for recording, adjusting microphone amplification factor, placing the phone on the skin, taking a breath out, pressing start recording button, replaying to listen to heart sound, and if possible, retrying the recording. More details on the user's instructions can be found in **Figure S1** of ***Supplementary files***. After the user's completion of recording, the heart sounds are filtered using homemade signal processing algorithms to remove background noises. The filtered heart sounds are then replayed to allow the user to listen. Raw data stored in .wav audio format are uploaded through the Internet to Google Firebase database. The user is also asked to voluntarily provide anonymous basic demographics including age, sex, height, weight and if applicable any cardiac conditions. An illustration of data collection and storage is shown in **Figure 1**.

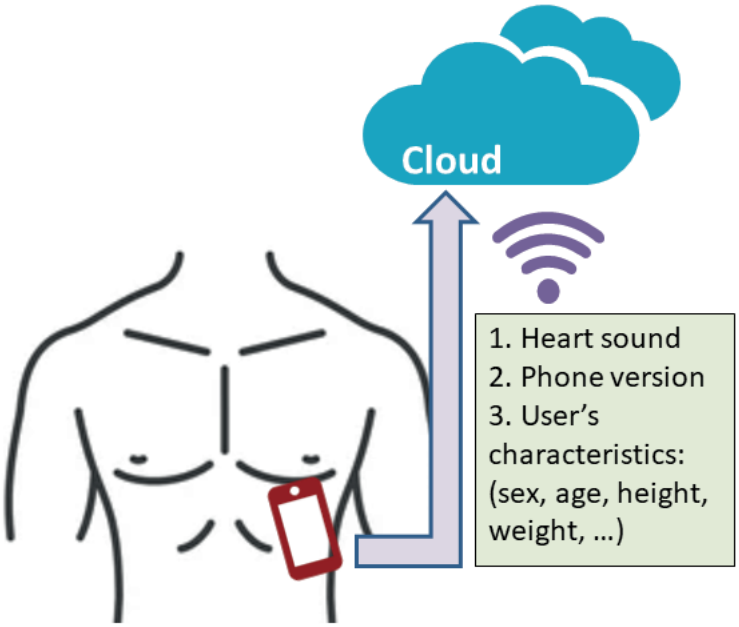

Figure 1. Demonstration of recording heart sound using Echoes app

Data processing

The users' demographic data and raw heart sound recordings were automatically downloaded using Python Firebase API called Pyrebase for offline analysis [11]. During the whole analysis, data were only accessible by a researcher (HL).

Visual assessment of heart sound quality

All raw heart sound recordings were plotted using Python software to observe signal morphologies. Then the heart sound quality was visually assessed per recording by one observer (HL). Each recording was assigned to one of the following three categories: good quality, unsure quality and bad quality. Good-quality signal was defined by at least 1 heartbeat where both the first (S1) and the second heart sound (S2) were clearly visible in the raw recordings. Bad-quality signal was defined by absence of any heartbeat with S1 and S2. Unsure-quality signal was defined if the observer deemed the signal to be in need of further processing for reliable identification of any heartbeats. To test the inter-observer variability of this visual quality assessment approach, the second assessor (JL) independently evaluated a subsample of 1000 heart sound

recordings randomly selected from the heart sound database according to the criteria above.

For validation purpose, examples of good-, unsure- and bad-quality heart sounds were processed using a time-frequency analysis method called S-transform [12]. The S-transform projects the one-dimensional heart sound signals to a two-dimensional time-frequency plane for better observations of signal components. S-transform was only used for representative heart sound examples of good, unsure and bad quality in order to confirm whether our proposed visual assessment of heart sound quality was consistent with the advanced signal processing technique.

Factors affecting heart sound quality

Heart sounds classified as good quality were deemed interpretable for analysis. Success rate was defined by the proportion of users who made at least 1 good-quality recording within a given number of attempts. We analysed the factors affecting the users' success rate, including hardware (i.e., iPhone version) and the users' demographics including sex, age and body mass index (BMI, calculated by weight (kilogram) divided by height (meter) squared). We could not analyse the effect of recording location on heart sound quality because all recordings from those users who indicated recording location were at the same area (Spot 1 of the app) on the chest.

Statistical analysis

Count data were expressed as number (percentage). Skewed data including number of recordings per user were expressed as median (interquartile range). Time-frequency analysis was performed using MATLAB R2018b (MathWorks). To reduce the effect of level of education on our analysis, all known users including university researchers, app programmers, app designers and intern students were excluded from the heart sound database. Relations between success rate and time of measurement, phone version, sex, age and BMI were analysed using Mann-Kendall trend test. Comparisons between two groups (male vs. female, age group and BMI group) were performed with chi-square test. When analysing the relations between iPhone version, sex, age, BMI and heart sound quality, we excluded groups with less than 10 users. All statistical analyses were performed using PyCharm 2021.2.2 (JetBrains s.r.o.). Statistical significance was defined as a two-tailed P value <.05.

Results

Data processing

The Echoes app was officially released on 21 May 2021 and advertised through social media channels such as Twitter and several newsletters [13-16]. For the current analysis, data were collected between 21 May and 4 October 2021. A total of 7597 recordings from 1148 users were obtained (**Figure 2**). The median number of recordings was 3 (IQR 2-6) per user. After excluding 27 recordings with a duration less than 5 seconds, 7570 recordings were visually assessed for heart sound quality.

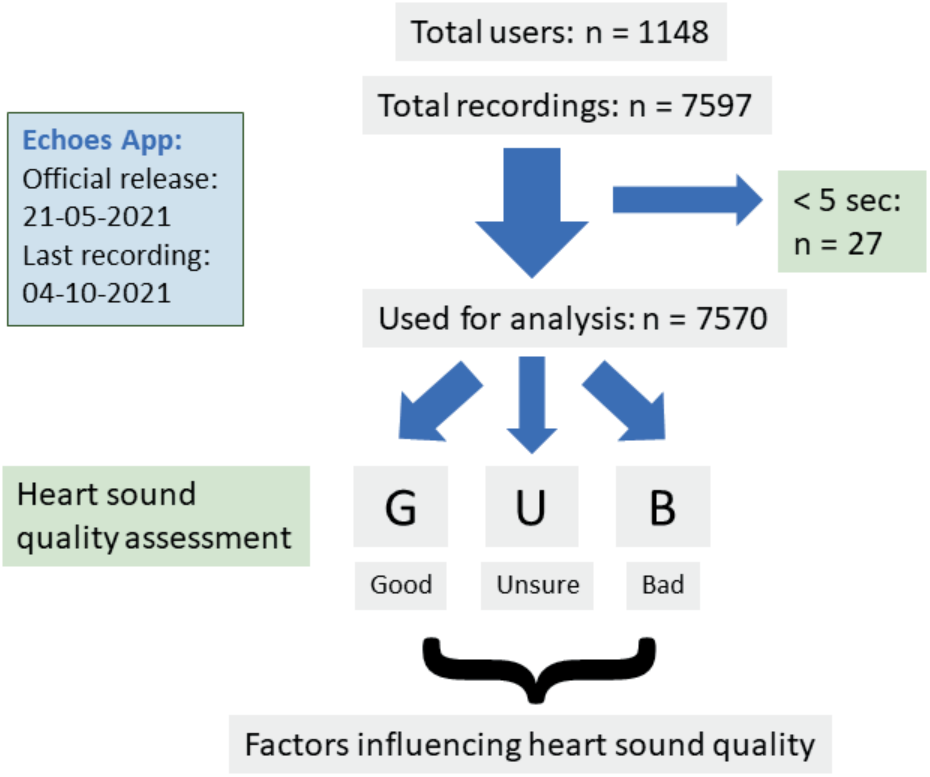

Figure 2. Overview of data processing

G, good-quality recording; U, unsure-quality recording; B, bad-quality recording.

Visual heart sound quality assessment

Good-, unsure- and bad-quality recordings amounted to 5647 (74.6%), 466 (6.2%) and 1457 (19.2%), respectively. A total of 80.1% (919/1148)

users were able to make at least 1 good-quality recording. Median number of attempts needed to make the first good-quality recording was 1 (IQR 1-1) per user. Inter-observer agreement of heart sound quality was 84.7% in the 1000 randomly-selected subsamples (**Table S1**). For good-, unsure- and bad-quality recordings, the agreements of the second assessor with the first assessor were 89.1% (672/754), 41.0% (25/61) and 81.1% (150/185), respectively. Most (61.4%, 94/153) of disagreements occurred in the category of "Unsure-quality".

Examples of good- (**A**), unsure- (**B**) and bad-quality (**C**) heart sounds are shown in **Figure 3**, including time-frequency spectrum (upper strip) and raw signals (lower strip). Audio files of these examples are also available online [17]. The good-quality recording (**3A**) clearly showed two major heart sound components (i.e., S1 and S2). Sound energies of S1 were preponderant below 100 Hz, while S2 had energies spreading beyond 100 Hz. In some heartbeats, the third (S3) and/or fourth heart sound (S4) that usually have a low signal amplitude, were also visible. The unsure-quality recording (**3B**) did not show clear S1 and S2 heart sound components in raw signals, though a few high-amplitude vibrations seemed to appear regularly. Using time-frequency analysis in these unsure-quality signals, S1 showed as low-frequency clusters occurring at a regular interval, followed by S2 in high-frequency regions. The bad-quality recording (**3C**) did not show any recurring components, neither in raw signals nor in the time-frequency spectrum.

Time of measurement

The influence of increasing user experience on sound quality was evaluated using the Mann-Kendall trend test. The proportion of users who made a good-quality recording significantly increased with the number of attempts to measure heart sound ($P < 0.001$; **Figure 4**). For the first attempt, ~ 60% of new users made a good-quality recording, which percentage increased to ~ 75% in the subsequent two attempts. From the 4th attempt and further, the success rate barely improved and approached ~ 80%, indicating that most users "learned" how to use the app within the first 3 attempts.

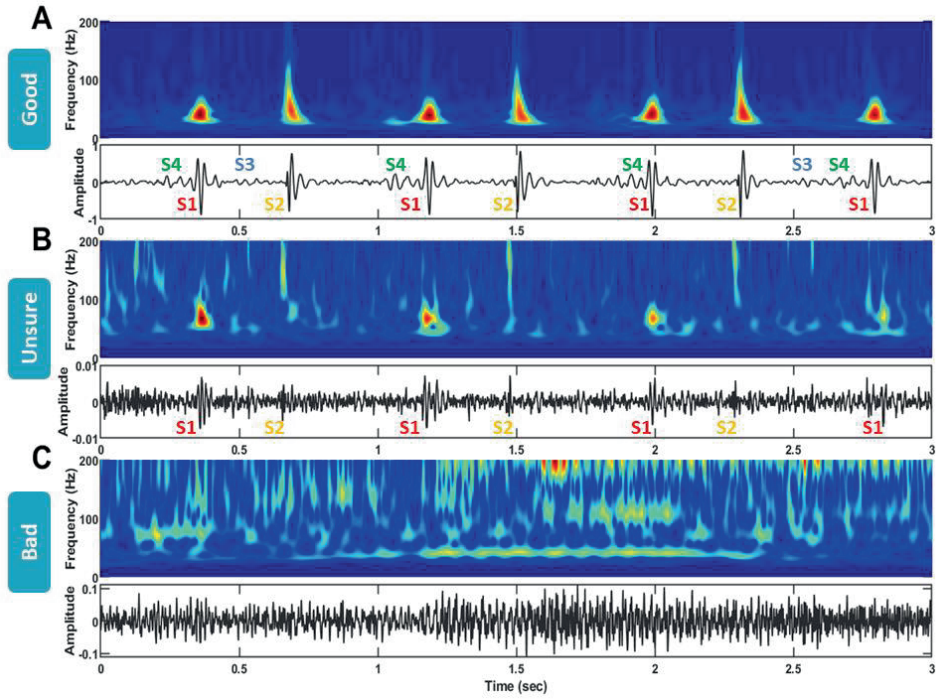

Figure 3. Time-frequency colormap (upper strip) and raw signal (lower strip)of good- (A), unsure- (B) and bad-quality (C) raw heart sound recordings

The time-frequency colormaps show how heart sound frequency (vertical axis) changes with time (horizontal axis), with heart sound energy ranging from low (in blue) to high (in red). In raw signals, locations of first- (S1), second- (S2), third- (S3), and fourth heart sound (S4) are labelled.

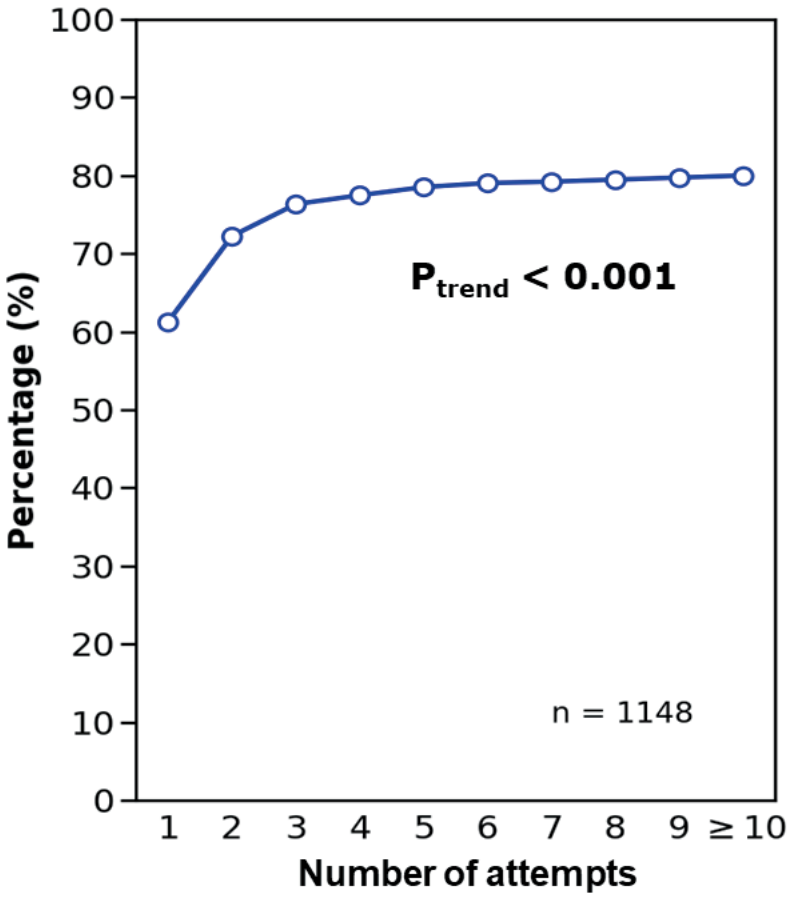

Figure 4. Change of success rate with number of attempts to record heart sound

Phone version

The relationship between iPhone version and proportion of users who succeeded in making a good-quality recording in 1 attempt (orange line) and in 3 attempts (red line) is shown in **Figure 5**. The proportion significantly increased when more recent iPhones were used for the first attempt (P = 0.03), but not for the first 3 attempts (P = 0.29). However, the significance was mainly driven by the lowest success rate in the users of iPhone 7 in both the first attempt and the first 3 attempts. Actually, the success rate did not change markedly from iPhone versions 8 to 13, fluctuating within 10% (for the first attempt: 55~65%; for the first 3 attempts: 70~80%). These numbers showed a good hardware support when using iPhone to record heart sounds.

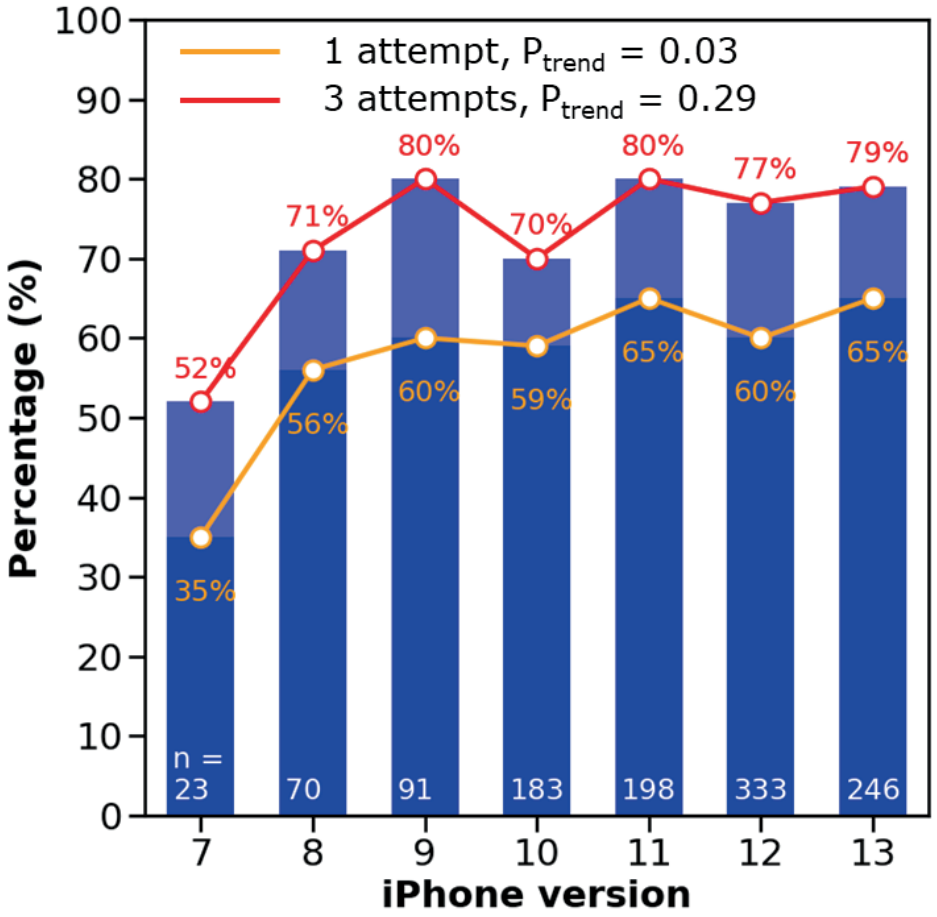

Figure 5. Version of smartphone and success rate

Orange line and dark blue boxes indicate the percentage of heart sound recordings rated with good quality in the first attempt by the users, while red line and light blue boxes in the first 3 attempts.

Sex and age

Sex was reported in 184 (16%) users, including 92 males and 92 females. Success rate did not differ between males and females in the first attempt (P = 0.41; **Figure 6A**) and in the first 3 attempts (P = 0.21). Compared with females, the users who did not report their sex had a significantly lower success rate in 1 attempt (P = 0.002) and in 3 attempts (P = 0.003). This might indicate that the ones who reported their sex and/or age might have done so because they were much more confident in their recordings (they had a higher success rate).

Age (35 ± 14 years; range: 10-69 years) was reported in 194 users. When grouping the users' age by every decade, in the first attempt, success rate of making a good-quality recording tended to decrease with age (P = 0.06; **Figure 6B**). However, this trend diminished when the first 3 attempts were taken into consideration, indicating good learning capability of more advanced-age users (P = 0.70).

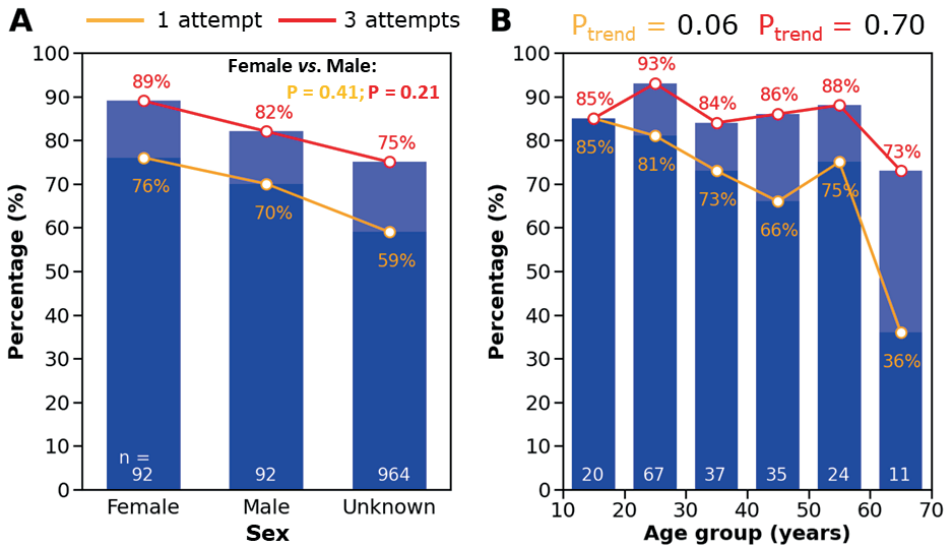

Figure 6. Changes of percentage of users having a good-quality heart sound recording with sex and age

Orange line and dark blue boxes indicate the percentage of heart sound recordings rated with good quality in the first attempt by the users, while red line and light blue boxes in the first 3 attempts.

BMI

Body weight and height were reported in 154 (13%) users. BMI (23.6 ± 4.2 kg/m^2; range: 15.1-34.5 kg/m^2) was calculated and grouped in 5 kg/m^2 bins (**Figure 7**). Success rate did not significantly decrease with BMI, neither in 1 attempt (P = 0.73) nor in 3 attempts (P = 0.14). However, success rate dropped for BMI >30 kg/m^2. In fact, the success rate did not change from the first attempt to the first 3 attempts in the highest BMI group (56% *vs*. 56%).

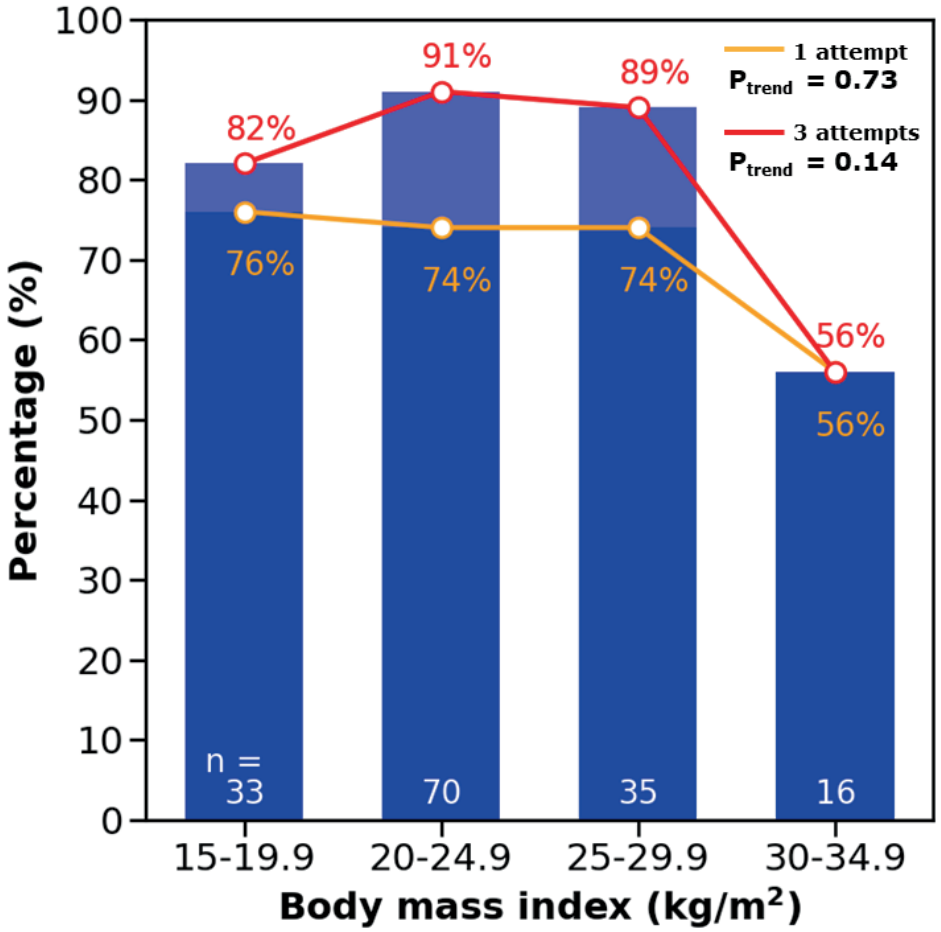

Figure 7. Changes of percentage of users having a good-quality heart sound recording with body mass index

Orange line indicates the values of the first recording. Red line indicates the values of the first 3 recordings.

Discussion

Principal findings

Three quarters of the participants from the general public can record good-quality heart sounds by means of a mobile phone. Principal findings of this study are that 1) it is feasible to use a smartphone microphone to record heart sounds in and by the general population; 2) approximately 3 out of 4 raw unfiltered heart sound recordings are of good-quality and ~ 4 of 5 users can finally manage to record a good-quality recording; 3) a maximum of 3 attempts is needed to obtain a good-quality recording of

heart sound; and 4) iPhone version and sex do not affect heart sound recordings, but BMI > 30 kg/m^2 and age > 60 years seem to lead to lower quality recordings.

Can smartphone be used to record heart sounds?

Nowadays, most smartphones are equipped with a high-quality microphone having a frequency response of 20 Hz - 20 kHz. This range is more than sufficient to cover the frequency range of heart sounds (20-200 Hz) [18]. A study tested the accuracy of smartphone sound measurement using signals between 20 Hz and 20 kHz, and found that even for the very early versions of iPhone (iPhone 3Gs to iPhone 5), the difference in sound pressure level recorded using a professional sound recorder and an iPhone microphone was not significant [19]. That finding was supported by a study that used an app (iStethoscope) to record heart sounds, though no data were shown regarding validity of each version of iPhone in recording heart sounds [8]. Our study extends these studies by showing that the more recent versions of iPhone from 7 to 13 also work for heart sound measurement. Therefore, it appears appropriate to conclude that the iPhone can be used for heart sound collection. The only study on Android phones for heart sound collection reported that heart sounds can be recorded in hospital settings using an app (CPstethoscope) on Samsung and LG phones [9]. Among the 46 patients enrolled, the researchers were able to distinguish among normal, third heart sound, fourth heart sound, systolic murmur and diastolic murmur. However, in this small-sample-size pilot study, the heart sounds were measured by researchers who had professional knowledge about cardiovascular anatomy. Our study was a large-scale study that distributed an app among over 1100 non-medical public users. The results showed that the smartphone could not only record the most distinctive components (S1 and S2) of heart sound, but also the low-amplitude and low-frequency extra heart sound components (S3 and S4) that are normally difficult to hear by experienced doctors using stethoscope. Moreover, our study shows good utilization of the app among the first-time users for heart sound measurement. Overall, smartphones, including both iPhone and Android, can be used to record heart sounds.

Factors affecting heart sound quality

We found that despite a high success rate (~ 80%) of recording a good-quality heart sound among the users, a few factors still affected the use of

our app. The fact that success rate increased with time of measurement, especially in the first 3 attempts, indicates the possibility of improving the app design to better guide the users to quickly learn how to use the app in the first few attempts in the future. For example, compared with the static user's guidance in the current app, we may use a video to guide the users how to use the app properly. Regarding hardware, iPhone version doesn't seem to relate to heart sound quality, indicating similar or even the same microphone sensor used in the series of products. Signal quality is not markedly different between sexes, showing a good understanding of the app in both sexes. The decreased proportion of users who were able to make a good-quality recording with age warranted a better design of the app to guide the old-age users to record heart sounds. However, despite the lower success rate among the elderly for the first attempt of the app, actually these users quickly learned how to correctly use the app in the next two attempts, as evidenced by the higher increase of success rate from the first attempt to the first 3 attempts compared to their younger counterparts. Yet this finding may need to be confirmed in a larger-scale study in the future.

Advantages of using smartphone for recording heart sounds

The huge amount of smartphone users (6.38 billion in 2021) provides a unique opportunity to turn the built-in microphone to an electronic stethoscope for both health education among the public and for medical purposes among the patients [20]. Since the solution does not incur any extra cost contrary to buying a professional electronic stethoscope, those who are living in underdeveloped or remote areas short of medical resources can use the app for health-related purposes. From this perspective, turning smartphone into an electronic stethoscope provides a solution to reduce health system costs in these areas. Our app may provide an immediate solution for auscultation in some urgent situations such as on a train or street, where a stethoscope may not be readily available but smartphones are likely to be present.

When comparing with conventional stethoscope, the smartphone app also allows storage, replay, analysis and comparison of heart sounds. Clinically, identification of pathological heart sounds (e.g., S3 and S4) relies on well-trained doctors' ears, and it is well known that a high interobserver variability exists in auscultation among doctors [21, 22]. Once heart sounds are recorded using our app, the signals may be analysed using more advanced signal processing techniques, like the

time-frequency spectrum analysis applied in this study, to better observe various heart sound components and to reduce the interobserver variability. Even for experienced doctors, it is challenging to assess differences in heart sounds from one day to another, making it difficult to track patient's status on a daily basis. By storing heart sound data in the cloud, our app allows replaying previous heart sounds to better compare subtle heart sound features.

The human ears' abilities may further be enhanced by combining with automatic algorithms including machine learning algorithms. For example, the PASCAL Classifying Heart Sounds Challenge using heart sounds collected from the iPhone-based app (iStethoscope Pro) has stimulated the development of multiple algorithms including convolutional neural network, deep learning algorithm and artificial neural network for automatic segmentation and classification of heart sounds [23-26].

Future perspectives

Our study was a preliminary analysis of an increasingly expanding heart sound dataset of the Echoes app. Our findings support further development of the app for not just public engagement purpose but also medical purposes. As a low-cost and easy-to-use solution, our app may be deployed on a large scale in areas with insufficient medical resources to help screen and monitor patients with cardiovascular diseases. An example is to use the app to screen for congenital and valvular heart diseases which mostly produce systolic and/or diastolic murmurs but which may be too late to be intervened at an advanced stage. Another potential application is to use the app for heart rate and rhythm managements in patients with chronic cardiovascular diseases such as atrial fibrillation. Atrial fibrillation creates the irregularities of not only rhythm but also amplitude of the heart sounds. In this respect, heart sounds may serve as a valuable tool in supporting electrocardiogram for evaluation of arrhythmias. In particular, our app enables the users' self-recording of transient arrhythmias in conditions like paroxysmal atrial fibrillation and premature ventricular contraction at home for further hospital consultation.

Since built-in microphone of smartphone is more sensitive to vibrations falling in audible frequency range (≥ 20 Hz), it may be combined with the built-in inertial measurement unit of the phone for a better measurement of lower-frequency vibrations such as seismocardiogram. For example, the

built-in accelerometer may be put on the chest of a patient in supine position to record seismocardiogram [27]. However, before applying the app to the patients, further preliminary tests in hospital settings may help improve the usability of the app and establish its role in conjunction with other existing monitoring methods such as electrocardiogram.

Limitations

Our study had a few limitations. Firstly, we assessed heart sound quality by eyeballing which might have introduced some subjective biases. However, currently there is no consensus on how to assess heart sound quality. It seems reasonable to state that a segment of heart sounds that looks noisy and bad-quality is also likely not be well heard by clinicians because human ears are more sensitive to high-frequency sounds (> 200 Hz) while most heart sound energies are located at low-frequency range (< 100 Hz). On the other hand, this eyeballing labelling of signal quality provides a gold reference to develop automatic algorithms such as machine learning to classify heart sounds [23, 25]. Secondly, the Echoes app was only available for iPhone, and the advertisement channels might limit our abilities to cover users of all educational backgrounds. In the future, we need to develop the app for Android users who account for more than half of overall smartphone users. Also, promotion of the app through channels such as Google Ads may help cover more diverse users. Whether some other factors such as dimensions or weight of the phone would affect heart sound quality may also be worthy of investigation. Our third limitation came from the low proportion of users who filled in their personal information (e.g., sex and age) or indicated the specific location for recording heart sounds on the chest wall. Improvements of the user interface are necessary to guide the users to submit these data. Furthermore, some modifications including enlargement of font size and simplification of texts are crucial since the users with heart diseases are frequently old. Lastly, our current version of the Echoes app only allows to record up to 7 seconds of heart sounds. This may be extended to a longer period of time such as 30 seconds for more robust evaluation of heart rhythm and rate.

Conclusions

A smartphone can be used to record heart sounds in general population. Users of older age and higher BMI are likely to have lower-quality heart

sound recordings. The app solution may be useful for monitoring heart health on a large scale in the future.

Conflict of Interest:

None declared

Funding:

We have received funding from the Wellcome Trust Senior Research Fellowship (g.a. 209450/Z/17/Z) and the European Union Horizon 2020 research and innovation program “Personalised In-silico Cardiology (PIC)” under the Marie Sklodowska-Curie grant agreement No 764738. We have also been supported by the British Heart Foundation and Evelina Children's Heart Organization.

References:

1. Bank I, Vliegen HW and Bruschke AV. The 200th anniversary of the stethoscope: Can this low-tech device survive in the high-tech 21st century? Eur Heart J 2016; 37(47):3536-3543. [doi: 10.1093/eurheartj/ehw034]
2. Abelson D. A high-fidelity electronic stethoscope. JAMA 1971; 218(5):741. [doi: 10.1001/jama.218.5.741b]
3. Blashkin II. Trends in the design of stethophonendoscopes. Biomedical engineering 1970; 4(6):335-337. [doi: 10.1007/BF00562413]
4. Harbison J. 'The old guessing tube': 200 years of the stethoscope. QJM 2017; 110(1):9-10. [doi: 10.1093/qjmed/hcw108]
5. Leng S, Tan RS, Chai KT, Wang C, Ghista D and Zhong L. The electronic stethoscope. Biomed Eng Online 2015; 14:66. [doi: 10.1186/s12938-015-0056-y]
6. Kalinauskiene E, Razvadauskas H, Morse DJ, Maxey GE and Naudziunas A. A comparison of electronic and traditional stethoscopes in the heart auscultation of obese patients. Medicina (Kaunas) 2019; 55(4). [doi: 10.3390/medicina55040094]
7. Behere S, Baffa JM, Penfil S and Slamon N. Real-World evaluation of the eko electronic teleauscultation system. Pediatr Cardiol 2019; 40(1):154-160. [doi: 10.1007/s00246-018-1972-y]
8. Bentley PJ. IStethoscope: A demonstration of the use of mobile devices for auscultation. Methods Mol Biol 2015; 1256:293-303. [doi: 10.1007/978-1-4939-2172-0_20]
9. Kang SH, Joe B, Yoon Y, Cho GY, Shin I and Suh JW. Cardiac auscultation using smartphones: Pilot study. JMIR mHealth uHealth 2018; 6(2):e49. [doi: 10.2196/mhealth.8946]
10. Echoes App. Information sheet _ Echoes. URL: https://www.echoesapp.org/information-sheet/ [accessed 2021-11-29]
11. Childs-Maidment J.Pyrebase - a simple python wrapper for the Firebase API. URL: https://github.com/thisbejim/Pyrebase [accessed 2021-11-29]
12. Stockwell RG, Mansinha L and Lowe RP. Localization of the complex spectrum: The S transform. Ieee T Signal Proces 1996; 44(4):998-1001. [doi: 10.1109/78.492555]
13. King's College London. One-of-a kind app, Echoes, records the beating of a user's heart with use of their mobile phone -- King's College London Twitter. URL: https://twitter.com/kingscollegelon/status/1395655208609501189 [accessed 2021-05-21]
14. King's College London. Researchers develop mobile app to record the sound of a beating heart. URL: https://www.kcl.ac.uk/news/researchers-develop-mobile-app-to-record-the-sound-of-a-beating-heart [accessed 2021-05-21]
15. CARIM newsletter. Echoes app Listen to your heart anytime, anywhere - CARIM Newsletter July 2021. URL: https://mailchi.mp/bf53a645392d/carim-newsletter-july2021?e=918045fa51 [accessed 2021-07-01]
16. Cellule Studio London. Echoes – cellule. URL:

https://www.cellule.co.uk/echoes/#:~:text=On%20May%2021st%2C%20Echoes%20was,with%20their%20own%20heart%20sounds. [accessed 2021-05-21]
17. Luo H. Examples of good-, unsure- and bad-quality heart sounds recorded using Echoes app. URL: https://github.com/hongxingluoUM/Echoes-app---heart-sound-examples [accessed 2021-11-29]
18. Wood JC, Buda AJ and Barry DT. Time-frequency transforms: A new approach to first heart sound frequency dynamics. IEEE Trans Biomed Eng 1992; 39(7):730-740. [doi: 10.1109/10.142648]
19. Kardous CA and Shaw PB. Evaluation of smartphone sound measurement applications. The Journal of the Acoustical Society of America 2014; 135(4):L186-L192. [doi: 10.1121/1.4865269]
20. Statista. Number of smartphone users from 2016 to 2021. URL: https://www.statista.com/statistics/330695/number-of-smartphone-users-worldwide/ [accessed 2021-11-29]
21. Lok CE, Morgan CD and Ranganathan N. The accuracy and interobserver agreement in detecting the 'gallop sounds' by cardiac auscultation. Chest 1998; 114(5):1283-1288. [doi: https://doi.org/10.1378/chest.114.5.1283]
22. Ishmail AA, Wing S, Ferguson J, Hutchinson TA, Magder S and Flegel KM. Interobserver agreement by auscultation in the presence of a third heart sound in patients with congestive heart failure. Chest 1987; 91(6):870-873. [doi: https://doi.org/10.1378/chest.91.6.870]
23. Gomes EF, Bentley PJ, Coimbra M, Pereira E and Deng Y. Classifying heart sounds approaches to the PASCAL challenge. Proceedings of the International Conference on Health Informatics (HEALTHINF-2013) 2013:337-340. [doi: 10.5220/0004234403370340]
24. Palm D, Burns S, Pasupathy T, Deip E, Blair B and Flynn M, et al. Artificial neural network analysis of heart sounds captured from an acoustic stethoscope and emailed using iStethoscopePro. Journal of Medical Devices 2010; 4(2). [doi: 10.1115/1.3443737]
25. Kayikci S. Cardiac sound analyzation using convolutional neural network. 2019: IEEE.
26. Gopika P, Sowmya V, Gopalakrishnan EA and Soman KP. Performance improvement of deep learning architectures for phonocardiogram signal classification using fast fourier transform. 2019: IEEE.
27. Landreani F, Faini A, Martin-Yebra A, Morri M, Parati G and Caiani EG. Assessment of Ultra-Short heart variability indices derived by smartphone accelerometers for stress detection. Sensors (Basel) 2019; 19(17). [doi: 10.3390/s19173729]

SUPPLEMENTARY MATERIALS

Figure S1. Step-by-step user's instructions on using the Echoes app

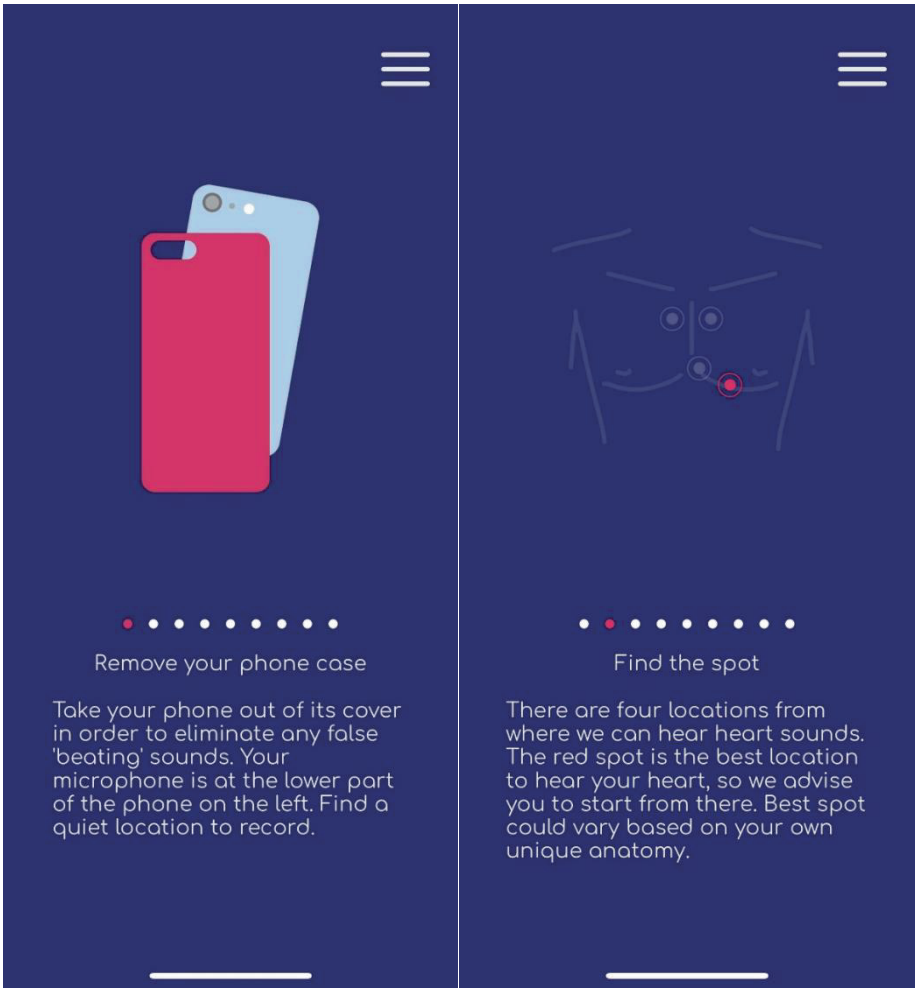

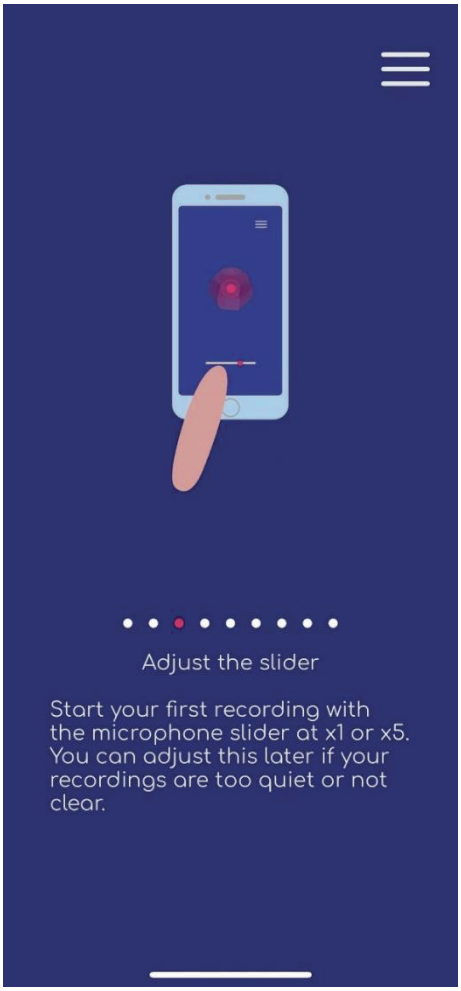
Adjust the slider
Start your first recording with the microphone slider at x1 or x5. You can adjust this later if your recordings are too quiet or not clear.

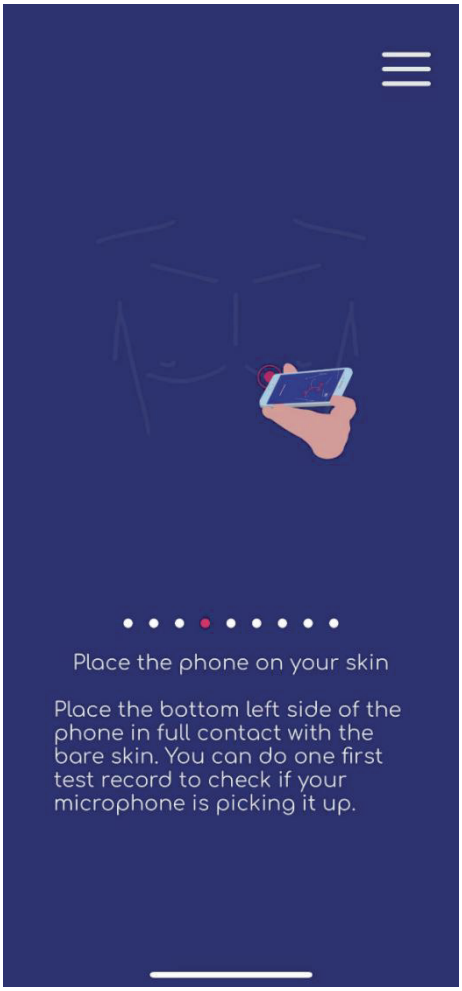
Place the phone on your skin
Place the bottom left side of the phone in full contact with the bare skin. You can do one first test record to check if your microphone is picking it up.

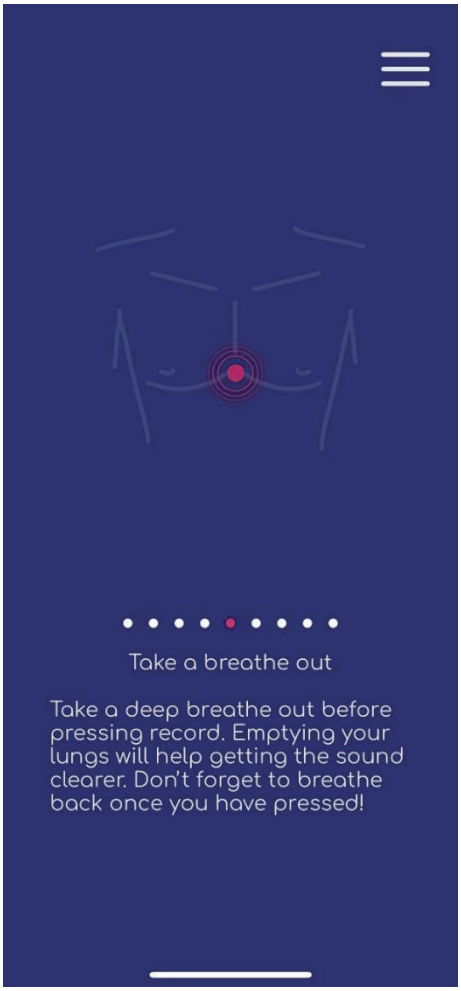
Take a breathe out
Take a deep breathe out before pressing record. Emptying your lungs will help getting the sound clearer. Don't forget to breathe back once you have pressed!

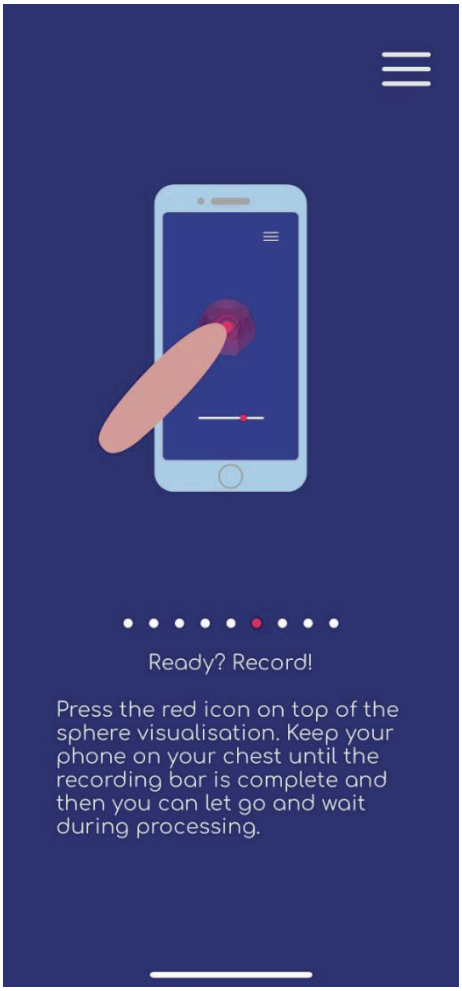
Ready? Record!
Press the red icon on top of the sphere visualisation. Keep your phone on your chest until the recording bar is complete and then you can let go and wait during processing.

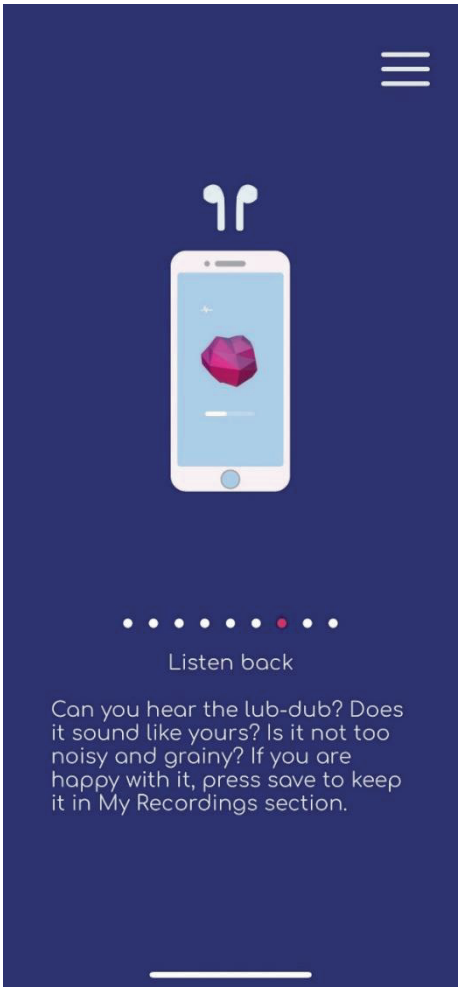
Listen back
Can you hear the lub-dub? Does it sound like yours? Is it not too noisy and grainy? If you are happy with it, press save to keep it in My Recordings section.

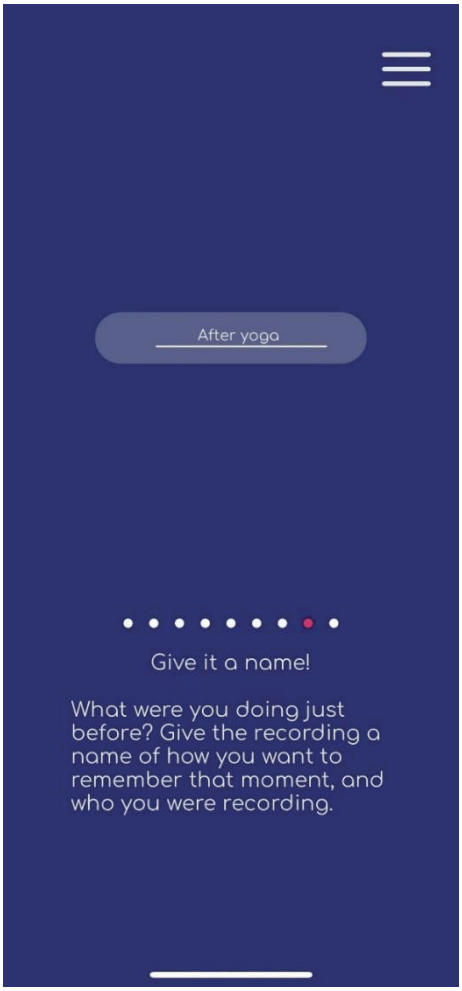
After yoga
Give it a name!
What were you doing just before? Give the recording a name of how you want to remember that moment, and who you were recording.

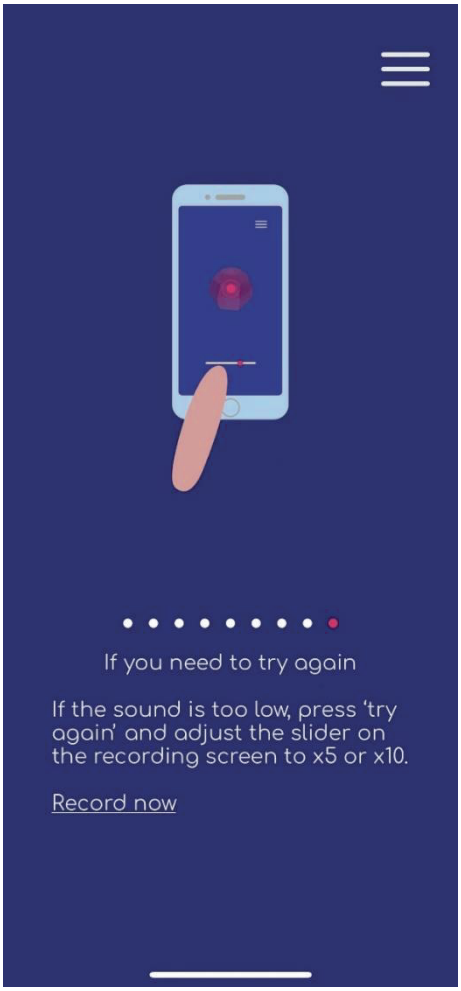
If you need to try again
If the sound is too low, press 'try again' and adjust the slider on the recording screen to x5 or x10.
Record now

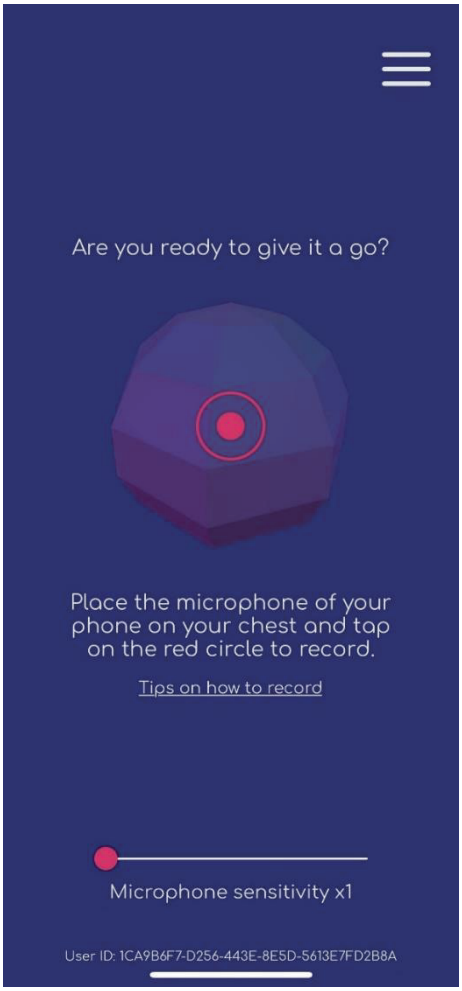
Are you ready to give it a go?
Place the microphone of your phone on your chest and tap on the red circle to record.
Tips on how to record
Microphone sensitivity x1
User ID: 1CA9B6F7-D256-443E-8E5D-5613E7FD2B8A

Table S1. Agreements of visual assessment of heart sound quality between two assessors (n = 1000)

		Assessor 2			
		Good	Unsure	Bad	
Assessor 1	Good	672	65	17	754 (75.4%)
	Unsure	8	25	28	61 (6.1%)
	Bad	6	29	150	185 (18.5%)
		686 (68.6%)	119 (11.9%)	195 (19.5%)	847 (84.7%)

Chapter 6

General discussion and impact

General discussion and impact

The overarching goal of this thesis is to provide insights into the relations between heart sound characteristics and hemodynamics in heart failure, and test feasibility of measuring heart sounds on a large scale using mobile phones.

We investigated the use of heart sounds for estimation of interventricular (VV) delay in **Chapter 2**, and for optimization of atrioventricular (AV) delay in **Chapter 3**. In **Chapter 2**, a novel algorithm was proposed for automatic calculation of VV delay from second heart sounds (S2) measured in open-chest porcine experiments. A close relation was observed between algorithm-estimated S2 splitting and invasively measured VV dyssynchrony. In **Chapter 3**, we investigated optimization of AV delay in a combined experimental-clinical study. In the experimental study, heart sounds were collected from pigs under baseline and myocardial depression. In the clinical study, heart sounds were collected from the patients using a microphone incorporated in a pulse generator of a cardiac resynchronization therapy (CRT) device. Both studies indicated close relations between heart sound-derived systolic time intervals (STIs) and left ventricular (LV) contractility indicators during varying paced AV delays. Loss of hemodynamics at optimal AV delays determined by heart sounds was minor. Thus, heart sound-derived STIs can probably serve as useful indicators for optimization of AV delay in CRT.

While CRT is indicated for patients with severely reduced ejection fraction, heart failure with preserved ejection fraction (HFpEF) is faced with a scarcity of treatments. Close monitoring of these patients is nonetheless important to identify symptoms at an early stage so that drugs can be utilized to relieve the patients' symptoms. In **Chapter 4**, we conducted a pilot study with a handheld digital stethoscope to explore associations between phonocardiography (PCG) and echocardiography in patients suspected of HFpEF. The study showed that heart sound frequency, STIs and occurrence of fourth heart sound were linked to the ratio of early diastolic mitral inflow to mitral annulus velocity (E/e'), a common echocardiographic indicator of elevated LV filling pressure and diastolic dysfunction. Furthermore, we proposed a combined score based on heart sound features to differentiate E/e' below and above 9, which showed good performance in both matched patients and all enrolled patients. The study may provide novel non-invasive markers for evaluation of HFpEF patients.

One major bottleneck in the widespread application of heart sounds for home monitoring is the lack of an affordable device to measure heart sounds. In **Chapter 5**, we tested the feasibility of using the microphone of smartphones as an electronic stethoscope. Nearly 80% of the users were able to record heart sounds by themselves, and around 3 out of 4 recordings were visually labelled as good quality. The quality of recorded heart sounds did not significantly differ by sex or phone version but tended to be lower in patients with an advanced age and a high body mass index. The study was the first in investigating factors affecting heart sound quality among general users. It provided evidence and confidence to further develop smartphone for daily remote monitoring of the patients, as one of basic components of mobile health (mHealth).

In this chapter, we will discuss our findings from a broader perspective. To do so, we first present a brief review of history of heart sound research, together with evolution of device for measurement of heart sounds. Then alterations of heart sounds in heart failure are analyzed, and the novelty of our research results is evaluated. The past two decades have seen emergence of novel tools for measurement and algorithms for analysis of heart sounds. These advancements will be discussed in the broad context of mHealth. This chapter is wrapped up with discussion on scientific and social impacts of the findings of this thesis.

1. Three waves of heart sound research

Literature search for publications on heart sounds has clearly shown three waves of research enthusiasm (**Figure 1**). The first wave started from early 19th century and spanned across the whole 20th and beginning of the 21th century. Early days of heart sound research were centered on how to develop a simple tool for auscultation. History of auscultation is generally thought to start from an accidental finding by René Laennec who was able to listen to sounds of the heart by rolling a squire of paper to a cylinder and applying it to the patient's precordial area in 1816 [1]. Since then, the instruments for auscultation have greatly evolved. An important landmark is the invention of the binaural stethoscope by Arthur Leared in 1851, which has been the prototype for all stethoscopes used nowadays [2]. However, human ears may not serve as the best detector of low-frequency vibrations like heart sounds. Boosted by progresses in electronic engineering, PCG machines were developed that used electronic modules for sensing vibrations and an

oscillograph for displaying signals [3]. Indeed, the first wave of heart sound research was initiated by the popularity of the PCG machine in 1950s, contributing to most (88%) of all publications on heart sounds. During this first wave, two major research topics were origin of heart sounds and applications of heart sounds to diagnosis of diseases.

Investigations on the first topic resulted in several theories on the origin of heart sounds. While early studies hypothesized that sudden tensing of ventricular muscles or cardiac valves gives rise to heart sounds, later studies tended to support the idea of vibrations of the whole cardiohemic system including valves, myocardia, blood mass and adjacent tissues as origin of heart sounds [4-7]. The recent simulation study in our group, based on the cardiohemic hypothesis, appeared quite consistent with previous observations of heart sounds in normal condition, heart failure and exercise [8]. **Chapter 4** showed a higher frequency of heart sounds in patients with elevated LV filling pressure. This was likely caused by the vibrations of a blood column encapsulated in a stiffened structure consisted of myocardia, valves and adjacent tissues.

The second distinctive feature of the first wave of heart sound research is the large number of observations on heart sounds in various diseases. The study on alterations of heart sounds in heart failure is an example and will be discussed below in **Section 2**.

The first wave of heart sound research waned at the emergence of a novel imaging technique, echocardiography. The first course dedicated to cardiac ultrasound was in 1968 and the first book on echocardiography in 1972 [9]. Virtually in parallel, researchers' interest in heart sounds has faded from the 1970s to 2000, with the number of annual publications drastically decreasing from over 400 to less than 40.

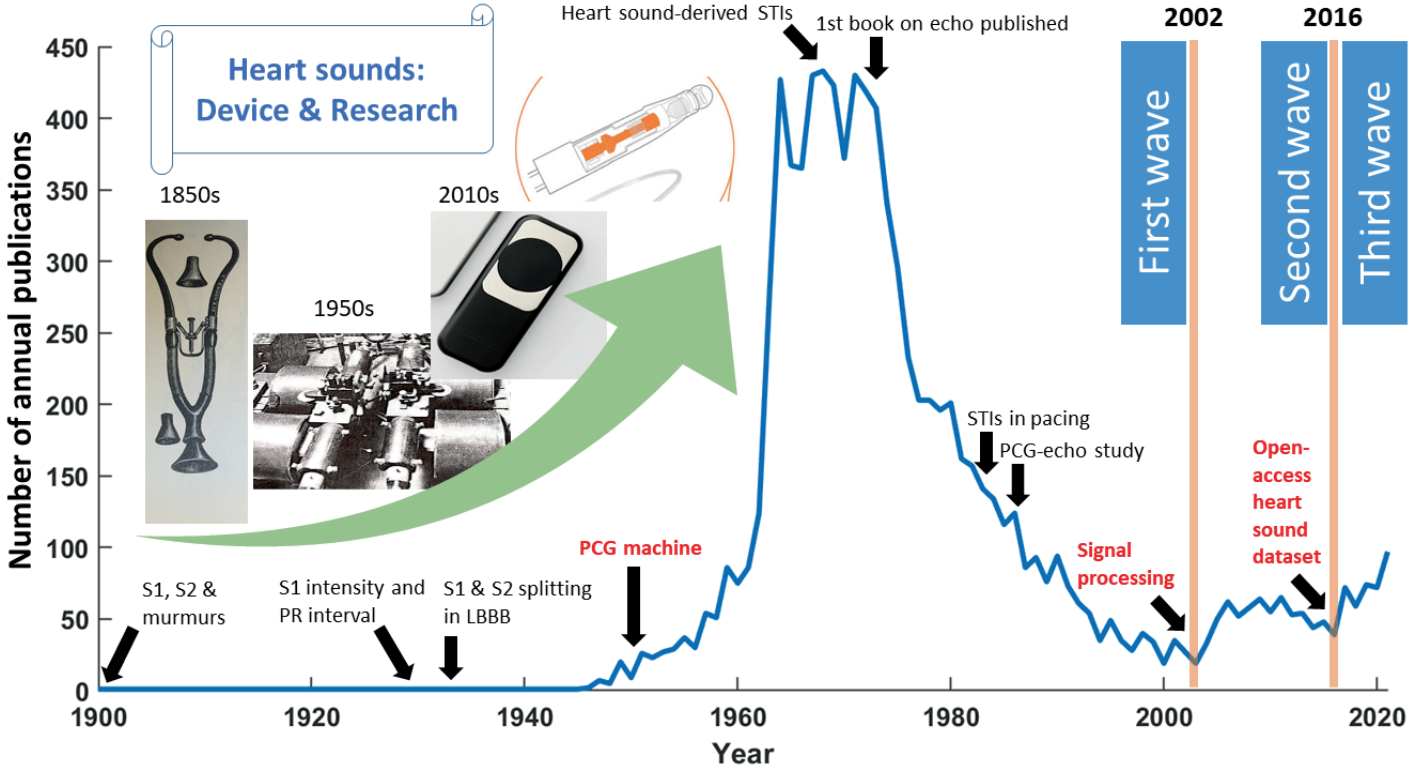

Figure 1. Trends of heart sound measurement devices and research publications *Number of annual publications was retrieved from a PubMed search on 23 February 2022 using the following search query: phonocardiogr* OR "heart sound". Only data between the years 1900 and 2021 are shown. Echo, echocardiography; LBBB, left bundle branch block; PCG, phonocardiography; S1, first heart sound; S2, second heart sound; STIs, systolic time intervals.*

In the first two decades of the 21st century, the second wave of heart sound research occurred because of advancements in signal processing techniques. The most important progress is the development and enhancement of multiple time-frequency representation algorithms for heart sound analysis, including short-time Fourier transform, wavelet transform, Hilbert-Huang transform and Wigner distribution, which are still widely used nowadays [10-13]. These time-frequency representation algorithms allow to project one-dimensional time-series signals such as heart sounds to a two-dimensional map for better observations of changes of frequency and energy with time. One of important applications of time-frequency projection is for estimation of heart sound splitting. In **Chapter 2**, S2 was projected to a time-frequency map using S-transform to allow automatic tracking of aortic and pulmonic components. The S2 splitting interval was calculated from the timing difference between the two components. The algorithm was validated in simulated conditions and showed a close relation to the invasively-measured "gold standard" of VV dyssynchrony. In contrast, previous studies on S2 splitting using time-frequency representation algorithms were neither validated in simulation nor shown to be related to ventricular activities in experiments [14-18].

The past 5 years have seen the commencement of a third wave of heart sound research, boosted by open-access heart sound datasets and machine learning algorithms. The most-cited heart sound dataset is the PhysioNet Heart Sound Database released in 2016 which contains over 2400 heart sound recordings from nearly 1300 healthy volunteers and patients [19]. The dataset has stimulated studies on algorithms for automatic segmentation, feature extraction and classification of heart sounds [20-22]. All these three tasks can be achieved using machine learning, which is discussed in **Section 3**.

The above-mentioned progress on heart sound research has benefited from continuous evolutions of heart sound measurement tools. This topic will also be covered in **Section 3**.

2. Heart sounds in heart failure

The origin of heart sounds dictates that any alterations of cardiac mechanical activities during diseased conditions may affect morphologies and timing of heart sounds. In this thesis, we focus on the alterations of heart sounds in heart failure in **Chapters 2, 3 and 4**. Heart failure may be caused by either systolic or diastolic dysfunction, or both. The former is also referred to as heart failure with reduced

ejection fraction, while the latter is called HFpEF [23]. This section will discuss the relations of various heart sound features including STIs, dominant frequency and splitting interval to heart failure. Furthermore, values of heart sounds in predicting heart failure patients' outcomes are discussed.

2.1 STIs

STIs are time intervals within the cardiac systole that can be derived from simultaneous heart sound and electrocardiogram (ECG) measurements, including time interval from onset of QRS to onset of S1 (QS1) and time interval between onsets of S1 and S2 (S1S2). Several studies reported a longer QS1 in heart failure patients compared with normal subjects [24-28]. Findings regarding S1S2 in heart failure were inconsistent [26, 28]. This was likely caused by differences in confounding factors between the studies, such as heart rate, gender and body mass index of the patients. **Chapter 3** circumvented these factors by using animals as their own controls while varying paced AV delays with a fixed heart rate. The study found close relations between STIs (QS1 and S1S2) and myocardial contractility evaluated using invasive pressure indicators including the maximal rate of rise of LV pressure.

In addition to myocardial contractility, atrial pressure also seems to play a crucial role in determining QS1. **Chapter 4** shows that patients with an enlarged left atrial volume and elevated LV filling pressure tend to have a longer QS1. It is likely that elevated atrial pressure at a given rate of rise of LV pressure delays the timing of atrio-ventricular pressure cross-over and thus the onset of S1 [29]. Overall, QS1 and S1S2 may serve as useful timing indicators of ventricular systolic and diastolic (dys)function.

2.2 Frequency of heart sounds

Little is known about changes of heart sound frequency in heart failure. This may have been caused by complexity of frequency calculation during the first wave of heart sound research when computers were either unavailable or primitive. From a physics perspective, frequency of a harmonic oscillator is equal to the square root of material elasticity divided by the mass of the system. An early observational study reported S1 energies shifted toward low-frequency range in patients with cardiomyopathy [30]. The authors hypothesized that decreased myocardial elasticity and volume overload together may have resulted

in reduced S1 frequency. However, myocardial elasticity is also likely increased in these patients due to more stretched myocardium by enlarged LV end-diastolic volume. This idea is supported by data from a recent porcine study showing that the dominant frequency of S1 increases with end-diastolic volume [31]. In patients suspected of HFpEF, S1 frequency tends to increase with elevated LV filling pressure (**Chapter 4**). The structural cause may come from LV hypertrophy, as evidenced by a heavier LV mass in patients with a higher E/e' ratio.

Our study is the first to demonstrate relationship between heart sound frequencies and echocardiographic parameters. In addition to S1 frequency, S2 and S4 frequencies have also been found higher in patients with elevated LV filling pressure, suggesting a stiffened cardiohemic system in these patients. However, these findings still need to be confirmed in more extensive studies.

2.3 Splitting of heart sounds

Heart sounds are initiated by valve closure, with S1 containing mitral and tricuspid components, while S2 containing aortic and pulmonic components. Measuring this heart sound splitting may be of value for evaluation of VV dyssynchrony which is not uncommon in heart failure patients. A pulsed-wave Doppler imaging study in patients with reduced LV ejection fraction (< 35%) showed that up to 72% of patients with left bundle branch block and QRS duration over 150 ms have a mechanical VV delay greater than 40 ms, which remained above 50% in patients with a QRS duration between 120 – 150 ms [32]. The benefits of correcting for VV dyssynchrony in these patients have been widely validated in large clinical trials, but the selection of eligible candidates for CRT is mainly based on electrical dyssynchrony assessed using ECG criteria such as QRS duration and LBBB morphology [23]. Addition of heart sounds to current criteria may provide an extra layer of information on mechanical dyssynchrony. In the Markers and Response to CRT (MARC) study, mechanical VV delay was shown to contribute to patient selection [33]. Following CRT implantation, splitting of heart sounds may also be useful for regular evaluation of VV contraction. The Cardiac Resynchronisation in Heart Failure (CARE-HF) study showed that CRT significantly reduced VV mechanical delay by 21 ms during 3 months follow-up, which persisted up to 18 months [34]. While the study had to rely on echocardiography for follow-up of the patients, heart sounds can be regularly recorded by the patients at

home, or using a microphone in the implanted device in combination with automated adjustment, as is the case in the SonR system.

Moreover, computer simulation studies in our group showed that S2 splitting is a promising tool for evaluation of type and evolution of heart failure. S2 splitting interval is prolonged as LV function worsens at constant RV function, while shortened or even reversed as only RV function worsens [8]. Therefore, S2 splitting interval, used alone or combined with other heart sound components such as third heart sound, may be helpful for titration of drugs such as diuretics and beta-blocker, as well as optimization of pacemaker therapy in heart failure patients.

The findings in **Chapter 2** confirm that S2 splitting can be determined reliably. Several aspects of this experimental study are noteworthy. Firstly, signal-to-noise ratio of S2 in our study is much higher than previous studies because heart sounds were measured epicardially on the right ventricular outflow tract close to the pulmonic and aortic valves. In comparison, most previous studies collected heart sounds on the chest and thus might have suffered from interference by noises such as respiratory sounds. Moreover, the pulmonic component was likely poorly recorded in previous studies due to its low amplitude and damping during its transmission to the chest. Secondly, an advanced automatic signal processing technique was utilized to calculate splitting interval of S2, while previous studies had to rely on eyeballing to identify heart sound components. Each of S2 components (aortic or pulmonic) consists multiple peaks and nadirs before the signal gradually damps, creating challenges for visual inspection of heart sound components. Lastly, S2 splitting interval showed a close relation to VV mechanical dyssynchrony measured invasively with catheter, which has not been reported in any previous studies.

In **Chapter 2**, we only investigated splitting of S2 rather than S1 because the epicardial sensor on right ventricular outflow tract was assumed to optimally record S2. Nonetheless, S1 splitting may similarly provide useful information on VV dyssynchrony, as indicated in previous roentgenkymographic and echophonocardiographic studies in patients with left and right bundle branch block [35-37]. The most distinctive advantage of evaluation of S1 splitting compared to S2 splitting is the close proximity of S1 with the time to ventricular contraction, which is crucial for evaluation of cardiac function. Future studies are warranted to study in more detail the relationship between S1 splitting and VV dyssynchrony.

2.4 Relations between heart sounds and patient outcome

The close relationship between heart sounds and hemodynamics makes it reasonable to hypothesize that heart sounds can serve as useful prognosticators in heart failure. Several studies have investigated the relationship between heart sounds and patient outcome. The third heart sound (S3) detected during physical examination on hospital admission is associated with higher in-hospital all-cause mortality and cardiac death in acute heart failure [38]. During a mean follow-up of 32 months, S3 is an independent predictor of hospitalization for heart failure and death from pump failure [39]. Recently, an S3 score calculated automatically from timing, duration, intensity and frequency of S3 has been reported as prognosticator of all-cause mortality in patients with chronic heart failure [40]. In contrast, S4 is only reported in a study as an indicator of favourable outcomes in patients with hypertrophic cardiomyopathy plus sinus rhythm [41]. The finding seems contrary to most previous studies reporting S4 as a specific marker of elevated end-diastolic pressure [42-44]. Our findings in **Chapter 4** also demonstrated that S4 is more frequently observed in patients with increased LV filling pressure. The contradiction likely arises from small sample size (only 9 patients enrolled in the S4-absent group) and composite outcome (a combination of cardiac death, stroke, hospitalization for worsening heart failure, and newly developed atrial fibrillation) of the hypertrophic cardiomyopathy study [41]. Interestingly, no reports have been found on the impacts of S1 and S2 properties on patient outcomes, though they are the most distinctive parts of a heart sound recording. The results obtained on the relations between hemodynamic factors and S2 splitting (**Chapter 2**), STIs (**Chapters 3 and 4**) and dominant frequency (**Chapter 4**) indicate that studies on how S1 and S2 relate to patient outcome may be worthwhile to perform.

3. Heart sounds in the 21st century

The past two decades have seen increasing interest in research of heart sounds, as demonstrated in **Figure 1**. These studies are driven by a few key factors including emergence of new tools for recording heart sounds, advancements of digital signal processing and popularity of artificial intelligence. Furthermore, the coronavirus disease 2019 (COVID-19) pandemics in the past two years have greatly accelerated the adoption of mHealth techniques in clinical practice. The possibility

of using heart sounds for mHealth purposes in post-COVID era is also discussed in this section.

3.1 Evolution of tools for measurement of heart sounds

In the past two decades, miniaturization of sensors and data processing units gives rise to portable, implantable and wearable digital stethoscopes for recording heart sounds [28, 45, 46]. Various ways of measuring heart sounds have been explored in this thesis. In **Chapter 2**, heart sounds were measured using a miniaturized accelerometer that can be further incorporated in a pacing lead like the SonR system [46]. In **Chapter 3**, heart sounds were measured by a microphone implemented in a pulse generator. In **Chapter 4**, a handheld digital stethoscope was utilized for simultaneous measurements of heart sounds and ECG on the skin. In **Chapter 5**, a smartphone was turned into an electronic stethoscope to enable a large-scale collection of heart sounds. All these measurement techniques are considerably better than the early studies with PCG machine. An important feature of all the newly developed tools is that they allow data collection both at hospital and at home, enabling continuous monitoring of patients' conditions. This may have implications for reducing healthcare costs and hospital visits in the future.

3.2 Advancements of digital signal processing

Digital signal processing aims to enhance features of a given signal using mathematical calculation. It is crucial for heart sound analysis because heart sounds are noisy (often mixed with lung sounds and baseline noise), impulsive (all heart sound components occurring within tens of millisecond) and low-frequency (most energies < 100 Hz). Human ears are not well adapted to listen to heart sounds.

In the past two decades, three central tasks of signal processing are heart sound denoising (**Chapters 2, 3, 4 and 5**), splitting identification (**Chapter 2**), and frequency analysis (**Chapters 2 and 5**). Bandpass filtering is the most commonly and earliest used technique for denoising heart sounds with a frequency range between 20 – 250 Hz [6, 47]. Recently, wavelet transform has been proposed to better suit to impulsive signals such as heart sounds. However, no consensus has been reached on selection of mother wavelet, level of decomposition or thresholding type during wavelet denoising [48, 49]. Since heart sounds are mixed with relatively stable sources of noises such as

respiratory sounds, a technique named harmonic regeneration noise reduction was applied to remove baseline noises in **Chapter 3** [50].

Splitting detection of heart sounds has been performed with eyeballing in early studies [51, 52]. The drawbacks of this approach are obvious: it is subject to human judgements and vulnerable to noise interference. To better observe heart sound splitting, the one-dimensional time-series signals must be projected to a two-dimensional time-frequency map. An example is provided in **Chapter 2** in which S2 is projected to a time-frequency spectrum using S-transform. The results showed that heart sound splitting can be automatically traced on time-frequency spectrum and the algorithm is robust to factors such as baseline noises. A recent progress on time-frequency analysis is the development of synchrosqueezing techniques which squeeze time-frequency components to their ridges, like our proposed S-transform amplitude ridge tracking algorithm [53, 54]. While time-frequency analysis provides better observations of signals, frequency analysis alone such as Fast Fourier analysis also provides valuable information including dominant frequency of signals. In **Chapter 4**, dominant frequencies of S1 and S2 are higher in patients with elevated LV filling pressure, suggesting increased myocardial stiffness. Overall, advancements of signal processing have greatly enhanced our abilities to extract useful information from heart sounds.

3.3 Machine learning for heart sound

Machine learning is a statistical method that "learns" implicit patterns of given data mostly based on prespecified features [55]. It has been reported for heart sound-based classification of cardiovascular diseases including aortic stenosis, heart failure and various congenital heart diseases [56-60]. The first step of machine learning is usually to identify heart sound features for training the classification model. Though many features including timing, frequency and amplitude may be calculated using heart sounds, some of them are heavily influenced by confounding factors (e.g., gender, body mass index and heart rate) rather than by the disease of interest. To minimize the effect of confounding factors, we obtained patients of similar baseline characteristics by "matching" these confounding factors (**Chapter 4**). Then these patients were divided by echocardiographic parameter of interest such as E/e' ratio into low and high groups. Heart sound features were compared between these two groups, and only features that significantly differed between the two groups were eligible for our

combined diagnostic score of E/e'. This "match-and-compare" strategy quickly shrinks the number of heart sound features to those relevant to research question of interest. Our proposed procedures may contribute to "explainability" of machine learning by fine-tuning selection of features for training the model, which is crucial for high-stakes decision-making scenarios in health care where machine learning has been criticized for its nature of "black box" [61]. In addition to heart sound features, patients' baseline characteristics such as age and sex may be directly fed into machine learning algorithm, but this has not been applied in most current heart sound classification algorithms which have solely been based on heart sound signals [56-60]. Inclusion of this information may help to further fine-tune the algorithms to assess the patients' status more precisely. Furthermore, the algorithms have the chance to become more powerful as more data become available for training during their use. The fact that automatic speech recognition is probably one of the most successful applications of machine learning indicates that similar success may also be achieved for "speech recognition" of the heart in the near future [62].

3.4 Heart sound for mHealth

Driven by rapidly expanding number of phone users in the past decades, mHealth has been proposed to take the advantage of mobile phone for health care purposes. In the past two years, a crucial driving force of mHealth is the need for remote and/or large-scale monitoring of patients during the COVID-19 pandemics. The power of even a simple mHealth approach was demonstrated by us in a study performed during the first few weeks of the COVID-19 outbreak in China. In order to assist the general population, we designed and released an online questionnaire for surveillance of COVID-19 (see **Appendix**) [63]. A total of 18161 questionnaires were returned, including 6% (1171) from Wuhan City in around 3 weeks. This first surveillance study of COVID-19 showed that the percentage of users reporting fever peaked in 2 weeks following the governmentally-enforced lockdown, consistent with official daily monitoring of COVID-19 confirmed cases. While the study only collected data via an online questionnaire, more data can be obtained by utilizing built-in sensors of mobile phone.

The applications of mHealth can be roughly divided by the type of sensor for data collection into camera-, inertial measurement unit-, and microphone-related. Camera-related applications, usually termed photoplethysmography, make use of pulsatile blood flow-caused subtle

colour changes of skin on sites such as finger and face [64, 65]. The inertial measurement unit is a built-in element of smartphone that combines accelerometer, gyroscope, and sometimes magnetometer. To measure heart rate, the user is required to lay down and put the smartphone on the chest so that any body vibrations can cause movements of the phone [66]. Drawbacks of this approach are: 1) the low-energy vibrations caused by cardiac mechanical activities might not induce visible movements of the phone, and 2) built-in inertial measurement unit generally has a low sampling rate (≤ 100 Hz) and signal resolution.

These two drawbacks are avoided by using the smartphone microphone for heart sound measurement. After nearly 150-year development, the microphone equipped in mobile phones has a high sampling rate (mostly 44100 Hz) and signal resolution (16 bit or higher). In comparison, most energies of heart sound lie in the range below 250 Hz. The ability of smartphone microphones to record heart sounds has also been confirmed in **Chapter 5** that shows nearly 3/4 of all recordings collected by participants from the general public are identifiable for S1 and S2. These findings have clinical implications for turning smartphone microphone into a digital stethoscope for daily monitoring of patients. More importantly, heart sounds provide more information than only heart rate and rhythm compared with either camera- or inertial measurement unit-based applications. As discussed above, long before the invention of the mobile phone (since 1973), heart sounds have been widely used as a simple tool for evaluation of cardiovascular diseases such as congenital heart disease, valvular abnormalities, arrhythmias and heart failure. Ongoing studies on heart sounds for mHealth will greatly benefit from these previous findings.

Impact

Scientific: revival of an old art for new applications

Auscultation is a technique with a history of over 200 years but has been overlooked in the past decades. One of the reasons is probably the unreliability of human ears to discern subtle changes of heart sounds. While this issue can be addressed by registering heart sounds on paper for visual analysis, PCG machines in early days were mostly clumsy and limited to hospital use. A key innovative feature of this thesis is the multiple ways we could measure digital recordings of heart sounds using implantable (**Chapters 2 and 3**) and portable (**Chapters 4 and 5**) devices. These studies provided preliminary experience for future researchers to work on heart sounds using new tools.

Revival of the old auscultation technique has also benefited from advancements of digital signal processing which enables detailed analyses of heart sounds. For example, the time-frequency representation algorithm utilized in **Chapter 2** showed clearly two components of S2 with different timing, frequencies and energies when VV dyssynchrony occurs. Algorithms for analysis of heart sounds may be automated to avoid biases introduced by conventional auscultation by humans. Furthermore, these algorithms may be deployed using mHealth techniques for automatic monitoring of heart sounds in real-time.

Findings from this thesis also show that heart sounds may provide useful information for evaluation of less consistently defined diseases such as HFpEF. For the first time, we demonstrated the potential link between elevated LV filling and dominant frequency of heart sounds in HFpEF (**Chapter 4**). Moreover, a combined score was proposed to differentiate E/e' below and above 9, which may serve as a novel tool for non-invasive screening of patients suspected with HFpEF.

Societal: remote monitoring for reducing healthcare cost

Heart failure affected 33.5 million people worldwide in 1990, which nearly doubled to 64.3 million in 2017 [67]. An economic estimation showed the global cost of heart failure in 2012 to be 108 billion US dollars [68]. For hospitalizations with first-time heart failure, the estimated mean cost was 11 552 dollars per patient in 2014, totaling an estimated 11 billion dollars in the United States alone [69]. The situation is worsened by the fact that as a chronic disease, heart failure recurs frequently in patients with a poor management. Around 24% of cases are rehospitalized within 30 days of discharge, which rises to over

50% within 6 months [70]. To reduce rehospitalization, closely monitoring the patients' conditions is necessary to detect and manage early signs of disease worsening at home.

To enable remote monitoring of heart failure, the patients have to be given a simple tool so that they can collect daily data. **Chapter 5** provides a low-cost tool for measuring heart sounds on a daily basis by turning smartphone to digital stethoscope. Considering the wide use of mobile phone nowadays, this finding will generate considerable societal impacts by combining patients' self-monitoring with doctors' remote guidance. A similar example is the use of mobile phone camera for assessment of heart rhythm during teleconsultations between patients and doctors in TeleCheck-AF project, which reduced hospital visits of the patients during COVID-19 pandemics [65]. These mHealth techniques have been reported to reduce cost of healthcare in most economic studies [71]. However, whether remote monitoring using heart sounds measured from mobile phone helps reduce the cost of healthcare remains to be clarified in the future.

Heart sounds for the public

Our studies have drawn the public's interest in heart sounds and more broadly on medicine, as evidenced by the large number of users (over 1100) who used our Apps named Echoes with only a few advertisements via social media of the universities in less than 5 months (**Chapter 5**). The fact that around 4/5 of general users were able to record good-quality heart sounds justifies the use of smartphone as a tool for measuring heart sounds on a large scale. Thus, the public can not only actively gain knowledge about their health but also contribute to scientific research. The solution of using smartphone for health monitoring may be particularly valuable for underdeveloped and/or remote areas with insufficient healthcare resources.

Medical education can also benefit from turning smartphone into digital stethoscope. For example, medical students can use the App to record and replay heart sounds of typical cases to learn heart sounds of diseased conditions. Since some components of heart sounds such as S3 and S4 are low-frequency and low-amplitude and difficult to be heard by human ears in some cases, recorded heart sounds allow visualizing these components so that they are more easily identified. Similar advantages also apply to S2 splitting which generally occurs in tens of millisecond. The use of smartphones for measuring heart sounds is also a cost-effective solution for medical students.

Conclusions

This thesis contributes to the revival of heart sound measurements for evaluation of patients with cardiovascular diseases. Features like systolic time intervals, frequency and splitting of heart sounds proved to contain important information. These features can be measured by a range of techniques from implanted sensors to "ordinary" mobile phones. As also evidenced in this thesis, with the progress in measurement tools, signal processing and machine learning, heart sounds are likely to become important tool in the mHealth era.

References:

1. S Minelli MR and Minelli S. The first 200 years of cardiac auscultation and future perspectives. Journal of multidisciplinary healthcare 2019; 12:183-189. [doi: 10.2147/JMDH.S193904]
2. Harbison J. 'The old guessing tube': 200 years of the stethoscope. QJM 2017; 110(1):9-10. [doi: 10.1093/qjmed/hcw108]
3. Leatham A, Auscultation of the Heart and Phonocardiography (Second edition). 1976, Edinburgh, London and New York: Churchill Livingstone.
4. Dock W. Mode of production of the first heart sound. Archives of Internal Medicine 1933; 51(5):737. [doi: 10.1001/archinte.1933.00150240096007]
5. Eckstein RW. Sounds due to muscular contraction and their importance in auscultatory qualities of the first heart sound. American Journal of Physiology-Legacy Content 1937; 118(2):359-367. [doi: 10.1152/ajplegacy.1937.118.2.359]
6. Adolph RJ, Stephens JF and Tanaka K. The clinical value of frequency analysis of the first heart sound in myocardial infarction. Circulation 1970; 41(6):1003-1014. [doi: 10.1161/01.cir.41.6.1003]
7. Luisada AA and Portaluppi F. The main heart sounds as vibrations of the cardiohemic system: Old controversy and new facts. The American Journal of Cardiology 1983; 52(8):1133-1136. [doi: https://doi.org/10.1016/0002-9149(83)90547-7]
8. Shahmohammadi M, Luo H, Westphal P, Cornelussen RN, Prinzen FW and Delhaas T. Hemodynamics-driven mathematical model of first and second heart sound generation. Plos Comput Biol 2021; 17(9):e1009361. [doi: 10.1371/journal.pcbi.1009361]
9. Feigenbaum H. Evolution of echocardiography. Circulation 1996; 93(7):1321-1327. [doi: 10.1161/01.CIR.93.7.1321]
10. A. Djebbari and F. Bereksi Reguig. Short-time Fourier transform analysis of the phonocardiogram signal. 7th IEEE International Conference on Electronics, Circuits and Systems (Cat. No.00EX445). 2000. [doi: 10.1109/ICECS.2000.913008]
11. Cherif LH, Debbal SM and Bereksi-Reguig F. Choice of the wavelet analyzing in the phonocardiogram signal analysis using the discrete and the packet wavelet transform. Expert Syst Appl 2010; 37(2):913-918. [doi: https://doi.org/10.1016/j.eswa.2009.09.036]
12. Tseng YL, Ko PY and Jaw FS. Detection of the third and fourth heart sounds using Hilbert-Huang transform. Biomed Eng Online 2012; 11:8. [doi: 10.1186/1475-925X-11-8]
13. Debbal SM and Bereksi-Reguig F. Time-frequency analysis of the second cardiac sound in phonocardiogram signals. Med Phys 2005; 32(9):2911-2917. [doi: 10.1118/1.2008427]
14. Al-Naami B, Al-Nabulsi J, Amasha H and Torry J. Utilizing wavelet transform and support vector machine for detection of the paradoxical splitting in the second heart sound. Med Biol Eng Comput 2010; 48(2):177-184. [doi: 10.1007/s11517-009-0548-7]
15. Barma S, Chen BW, Man KL and Wang JF. Quantitative measurement of split of the second heart sound (S2). IEEE/ACM Trans Comput Biol Bioinform 2015; 12(4):851-860. [doi: 10.1109/TCBB.2014.2351804]

16. Debbal SM and Bereksi-Reguig F. Analysis and study of the variation of splitting in the second heartbeat sound of wavelet transform. Journal of Medical Engineering & Technology 2006; 30(5):298-305. [doi: 10.1080/03091900500256164]
17. Debbal SM and Bereksi-Reguig F. Automatic measure of the split in the second cardiac sound by using the wavelet transform technique. Comput Biol Med 2007; 37(3):269-276. [doi: https://doi.org/10.1016/j.compbiomed.2006.01.005]
18. Djebbari A and Bereksi-Reguig F. Detection of the valvular split within the second heart sound using the reassigned smoothed pseudo Wigner-Ville distribution. Biomed Eng Online 2013; 12:37. [doi: 10.1186/1475-925X-12-37]
19. Liu C, Springer D, Li Q, Moody B, Juan RA and Chorro FJ, et al. An open access database for the evaluation of heart sound algorithms. Physiol Meas 2016; 37(12):2181-2213. [doi: 10.1088/0967-3334/37/12/2181]
20. Liu C, Springer D and Clifford GD. Performance of an open-source heart sound segmentation algorithm on eight independent databases. Physiol Meas 2017; 38(8):1730-1745. [doi: 10.1088/1361-6579/aa6e9f]
21. Chakraborty D, Bhattacharya S, Thakur A, Gosthipaty AR and Datta C. Feature Extraction and Classification of Phonocardiograms using Convolutional Neural Networks. 2020 IEEE 1st International Conference for Convergence in Engineering (ICCE). 2020: [doi: 10.1109/ICCE50343.2020.9290565]
22. Clifford GD, Liu C, Moody B, Springer D, Silva I and Li Q, et al. Classification of normal/abnormal heart sound recordings: The PhysioNet/Computing in Cardiology Challenge 2016. in 2016 Computing in Cardiology Conference (CinC). 2016.
23. McDonagh TA, Metra M, Adamo M, Gardner RS, Baumbach A and Bohm M, et al. 2021 ESC Guidelines for the diagnosis and treatment of acute and chronic heart failure. Eur Heart J 2021; 42(36):3599-3726. [doi: 10.1093/eurheartj/ehab368]
24. Weissler AM, Harris WS and Schoenfeld CD. Systolic time intervals in heart failure in man. Circulation (New York, N.Y.) 1968; 37(2):149-159. [doi: 10.1161/01.CIR.37.2.149]
25. N De Oliveira Neto MPAC. Abnormalities of the systolic time intervals obtained by electronic stethoscope in heart failure. The Internet Journal of Cardiology 2007; 5(2):1-7.
26. Wang S, Lam Y, Liu M, Fang F, Wang J and Shang Q, et al. Acoustic cardiography helps to identify heart failure and its phenotypes. Int J Cardiol 2013; 167(3):681-686. [doi: https://doi.org/10.1016/j.ijcard.2012.03.067]
27. Shitara J, Kasai T, Murata N, Yamakawa N, Yatsu S and Murata A, et al. Temporal changes of cardiac acoustic biomarkers and cardiac function in acute decompensated heart failure. ESC Heart Fail 2021; 8(5):4037-4047. [doi: 10.1002/ehf2.13492]
28. Li X, Liu X, Liu L, Li S, Wang Y and Mead RH. Evaluation of left ventricular systolic function using synchronized analysis of heart sounds and the electrocardiogram. Heart Rhythm 2020; 17(5, Part B):876-880. [doi: https://doi.org/10.1016/j.hrthm.2020.01.025]

29. Wells BG, Prediction of mitral pressure gradient from heart sounds. Br Med J 1957; 1(5018): 551–554. [doi: 10.1136/bmj.1.5018.551]
30. Adolph RJ, Stephens JF and Tanaka K. The clinical value of frequency analysis of the first heart sound in myocardial infarction. Circulation 1970; 41(6):1003-1014. [doi: 10.1161/01.cir.41.6.1003]
31. Krogh MR, Halvorsen PS, Grymyr O, Bergsland J, Elle OJ and Fosse E, et al. Continuous estimation of acute changes in preload using epicardially attached accelerometers. IEEE Trans Biomed Eng 2021; 68(7):2067-2075. [doi: 10.1109/TBME.2020.3020358]
32. Ghio S, Constantin C, Klersy C, Serio A, Fontana A and Campana C, et al. Interventricular and intraventricular dyssynchrony are common in heart failure patients, regardless of QRS duration. Eur Heart J 2004; 25(7):571-578. [doi: 10.1016/j.ehj.2003.09.030]
33. Maass AH, Vernooy K, Wijers SC, van T Sant J, Cramer MJ and Meine M, et al. Refining success of cardiac resynchronization therapy using a simple score predicting the amount of reverse ventricular remodelling: Results from the Markers and Response to CRT (MARC) study. EP Europace 2018; 20(2):e1-e10. [doi: 10.1093/europace/euw445]
34. Cleland JGF, Daubert J, Erdmann E, Freemantle N, Gras D and Kappenberger L, et al. The effect of cardiac resynchronization on morbidity and mortality in heart failure. New Engl J Med 2005; 352(15):1539-1549. [doi: 10.1056/NEJMoa050496]
35. Burggraf GW. The first heart sound in left bundle branch block: An echophonocardiographic study. Circulation 1981; 63(2):429-435. [doi: 10.1161/01.cir.63.2.429]
36. Wolferth CC and Margolies A. Asynchronism in contraction of the ventricles in the so-called common type of bundle-branch block: Its bearing on the determination of the side of the significant lesion and on the mechanism of split first and second heart sounds. Am Heart J 1935; 10(4):425-452. [doi: 10.1016/S0002-8703(35)90213-7]
37. Brooks N, Leech G and Leatham A. Complete right bundle-branch block: Echophonocardiographic study of first heart sound and right ventricular contraction times. Br Heart J 1979; 41(6):637-646. [doi: 10.1136/hrt.41.6.637]
38. Minami Y, Kajimoto K, Sato N, Aokage T, Mizuno M and Asai K, et al. Third heart sound in hospitalised patients with acute heart failure: Insights from the ATTEND study. Int J Clin Pract 2015; 69(8):820-828. [doi: 10.1111/ijcp.12603]
39. Drazner MH, Rame JE, Stevenson LW and Dries DL. Prognostic importance of elevated jugular venous pressure and a third heart sound in patients with heart failure. New Engl J Med 2001; 345(8):574-581. [doi: 10.1056/NEJMoa010641]
40. Wang S, Liu M, Fang F, Shang Q, Sun JP and Sanderson JE, et al. Prognostic value of acoustic cardiography in patients with chronic heart failure. Int J Cardiol 2016; 219:121-126. [doi: https://doi.org/10.1016/j.ijcard.2016.06.004]
41. Sakai C, Kawasaki T, Kawamata H, Harimoto K, Shiraishi H and Matoba S. Absent fourth heart sound as a marker of adverse events in hypertrophic cardiomyopathy with sinus rhythm. Ann Noninvasive Electrocardiol 2022:e12932. [doi: 10.1111/anec.12932]

42. Shah SJ, Nakamura K, Marcus GM, Gerber IL, McKeown BH and Jordan MV, et al. Association of the fourth heart sound with increased left ventricular end-diastolic stiffness. J Card Fail 2008; 14(5):431-436. [doi: 10.1016/j.cardfail.2008.01.010]
43. Goldblatt A, Aygen MM and Braunwald E. Hemodynamic-phonocardiographic correlations of the fourth heart sound in aortic stenosis. Circulation 1962; 26:92-98. [doi: 10.1161/01.cir.26.1.92]
44. Gupta S and Michaels AD. Relationship between accurate auscultation of the fourth heart sound and the level of physician experience. Clin Cardiol 2009; 32(2):69-75. [doi: 10.1002/clc.20431]
45. Behere S, Baffa JM, Penfil S and Slamon N. Real-World evaluation of the eko electronic teleauscultation system. Pediatr Cardiol 2019; 40(1):154-160. [doi: 10.1007/s00246-018-1972-y]
46. Brugada J, Delnoy PP, Brachmann J, Reynolds D, Padeletti L and Noelker G, et al. Contractility sensor-guided optimization of cardiac resynchronization therapy: Results from the RESPOND-CRT trial. Eur Heart J 2017; 38(10):730-738. [doi: 10.1093/eurheartj/ehw526]
47. Yoganathan AP, Gupta R, Udwadia FE, Miller JW, Corcoran WH and Sarma R, et al. Use of the fast Fourier transform for frequency analysis of the first heart sound in normal man. Med Biol Eng 1976; 14(1):69-73. [doi: 10.1007/BF02477093]
48. Ali MN, El-Dahshan EA and Yahia AH. Denoising of heart sound signals using discrete wavelet transform. Circuits, Systems, and Signal Processing 2017; 36(11):4482-4497. [doi: 10.1007/s00034-017-0524-7]
49. Cherif LH, Debbal SM and Bereksi-Reguig F. Choice of the wavelet analyzing in the phonocardiogram signal analysis using the discrete and the packet wavelet transform. Expert Syst Appl 2010; 37(2):913-918. [doi: https://doi.org/10.1016/j.eswa.2009.09.036]
50. Plapous C, Marro C and Scalart P. Improved Signal-to-Noise ratio estimation for speech enhancement. IEEE transactions on audio, speech, and language processing 2006; 14(6):2098-2108. [doi: 10.1109/TASL.2006.872621]
51. Boyer SH and Chisholm AW. Physiologic splitting of the second heart sound. Circulation 1958; 18(5):1010-1011. [doi: 10.1161/01.cir.18.5.1010]
52. Castle RF and Jones KL. The mechanism of respiratory variation in splitting of the second heart sound. Circulation 1961; 24:180-184. [doi: 10.1161/01.cir.24.2.180]
53. Yu G, Lin T, Wang Z and Li Y. Time-Reassigned multisynchrosqueezing transform for bearing fault diagnosis of rotating machinery. IEEE T Ind Electron 2021; 68(2):1486-1496. [doi: 10.1109/TIE.2020.2970571]
54. Yu G and Lin TR. Second-order transient-extracting transform for the analysis of impulsive-like signals. Mech Syst Signal Pr 2021; 147:107069. [doi: https://doi.org/10.1016/j.ymssp.2020.107069]
55. Jordan MI and Mitchell TM. Machine learning: Trends, perspectives, and prospects. Science 2015; 349(6245):255-260. [doi: 10.1126/science.aaa8415]
56. Chorba JS, Shapiro AM, Le L, Maidens J, Prince J and Pham S, et al. Deep learning algorithm for automated cardiac murmur detection via a digital stethoscope

platform. J Am Heart Assoc 2021; 10(9):e19905. [doi: 10.1161/JAHA.120.019905]
57. Liu J, Wang H, Yang Z, Quan J, Liu L and Tian J. Deep learning-based computer-aided heart sound analysis in children with left-to-right shunt congenital heart disease. Int J Cardiol 2022; 348:58-64. [doi: https://doi.org/10.1016/j.ijcard.2021.12.012]
58. Lv J, Dong B, Lei H, Shi G, Wang H and Zhu F, et al. Artificial intelligence-assisted auscultation in detecting congenital heart disease. European Heart Journal - Digital Health 2021; 2(1):119-124. [doi: 10.1093/ehjdh/ztaa017]
59. Gjoreski M, Gradisek A, Budna B, Gams M and Poglajen G. Machine learning and End-to-End deep learning for the detection of chronic heart failure from heart sounds. Ieee Access 2020; 8:20313-20324. [doi: 10.1109/ACCESS.2020.2968900]
60. Gjoreski M, Simjanoska M, Gradišek A, Peterlin A, Gams M and Poglajen G. Chronic heart failure detection from heart sounds using a stack of Machine-Learning classifiers. 2017 International Conference on Intelligent Environments (IE). 2017. [doi: 10.1109/IE.2017.19]
61. Rudin C. Stop explaining black box machine learning models for high stakes decisions and use interpretable models instead. Nature Machine Intelligence 2019; 1(5):206-215. [doi: 10.1038/s42256-019-0048-x]
62. Deng L and Li X. Machine learning paradigms for speech recognition: An overview. IEEE transactions on audio, speech, and language processing 2013; 21(5):1060-1089. [doi: 10.1109/TASL.2013.2244083]
63. Luo H, Lie Y and Prinzen FW. Surveillance of COVID-19 in the General Population Using an Online Questionnaire: Report From 18,161 Respondents in China. JMIR Public Health Surveill 2020; 6(2):e18576. [doi: 10.2196/18576]
64. Kwon S, Kim H and Park KS. Validation of heart rate extraction using video imaging on a built-in camera system of a smartphone. Annu Int Conf IEEE Eng Med Biol Soc 2012; 2012:2174-2177. [doi: 10.1109/EMBC.2012.6346392]
65. van der Velden RMJ, Verhaert DVM, Hermans ANL, Duncker D, Manninger M and Betz K, et al. The photoplethysmography dictionary: Practical guidance on signal interpretation and clinical scenarios from TeleCheck-AF. European Heart Journal - Digital Health 2021; 2(3):363-373. [doi: 10.1093/ehjdh/ztab050]
66. Lahdenoja O, Hurnanen T, Iftikhar Z, Nieminen S, Knuutila T and Saraste A, et al. Atrial Fibrillation Detection via Accelerometer and Gyroscope of a Smartphone. IEEE J Biomed Health Inform 2018; 22(1):108-118. [doi: 10.1109/JBHI.2017.2688473]
67. Bragazzi NL, Zhong W, Shu J, Abu MA, Lotan D and Grupper A, et al. Burden of heart failure and underlying causes in 195 countries and territories from 1990 to 2017. Eur J Prev Cardiol 2021; 28(15):1682-1690. [doi: 10.1093/eurjpc/zwaa147]
68. Cook C, Cole G, Asaria P, Jabbour R and Francis DP. The annual global economic burden of heart failure. Int J Cardiol 2014; 171(3):368-376. [doi: https://doi.org/10.1016/j.ijcard.2013.12.028]
69. Jackson SL, Tong X, King RJ, Loustalot F, Hong Y and Ritchey MD. National Burden of Heart Failure Events in the United States, 2006 to 2014. Circulation. Heart failure 2018; 11(12):e4873. [doi: 10.1161/CIRCHEARTFAILURE.117.004873]
70. Desai AS and Stevenson LW. Rehospitalization for heart failure. Circulation

2012; 126(4):501-506. [doi: 10.1161/CIRCULATIONAHA.112.125435]
71. Iribarren SJ, Cato K, Falzon L and Stone PW. What is the economic evidence for mHealth? A systematic review of economic evaluations of mHealth solutions. Plos One 2017; 12(2):e170581. [doi: 10.1371/journal.pone.0170581]

Summary

中文摘要

Summary

Heart sounds are a series of vibrations arising from impacts of blood on cardiovascular structures including valves, myocardium and blood vessels. The two most obvious heart sounds are: the first heart sound (S1) occurring at end-diastole and the second heart sound (S2) occurring at end-systole. S1 contains mitral and tricuspid components, while S2 contains aortic and pulmonic components. Splitting of heart sounds refers to a significant interval between the two components of S1 or S2. Systolic time intervals derived from combined electrocardiogram and heart sound analysis consist of QS1 (the interval between onsets of QRS on the electrocardiogram and S1) and S1S2 (the interval between onsets of S1 and S2).

Heart sounds have been used in diagnosis for over two centuries, boosted by the emergence of the stethoscope 200 years ago. Novel developments like digital stethoscopes and advanced signal analysis create new opportunities for the use of heart sounds. Heart sound-derived parameters are likely useful for evaluation of heart failure with reduced (HFrEF) and preserved ejection fraction (HFpEF).

HFrEF patients with interventricular dyssynchrony may need to be treated with cardiac resynchronization therapy. Selection of candidate and post-implant optimization of cardiac resynchronization therapy are likely improved by using splitting interval of heart sounds for adjustment of interventricular delay. In **Chapter 2**, a novel algorithm has been developed to automatically identify splitting interval between S2 components. The algorithm was tested in simulated signals and in experimental studies that showed a good relation between S2 splitting and an invasively measured indicator of interventricular mechanical dyssynchrony.

In **Chapter 3**, we analyzed data from a combined experimental-clinical study aiming to find the relationship between heart sound-derived systolic time intervals and myocardial contractility. Varying atrioventricular delays were induced using pacing and left ventricular (LV) pressure was invasively recorded. VS1, an indicator close to QS1, shortened as myocardial contractility improved during optimization of atrioventricular delay, associated with prolongation of S1S2. Using VS1 and S1S2 to predict optimal atrioventricular delay resulted in a minor loss of optimal hemodynamics judged by maximal LV pressure and maximal rate of rise of LV pressure. These findings showed that heart sound-derived systolic time intervals may be useful for optimization of

atrioventricular delay in cardiac resynchronization therapy, possibly performed using a microphone in the implanted device.

HFpEF is becoming an increasingly prevalent disease in ageing population. However, discrepancies exist in current guidelines regarding evaluation of diastolic dysfunction and elevated LV filling pressure. In **Chapter 4**, we explored the relationship between heart sounds and echocardiographic parameters in a group of outpatients suspected of HFpEF. To reduce the confounding effects of sex, body mass index and heart rate, these factors were first matched to result in two groups of patients of similar baseline characteristics. Then heart sounds and echocardiographic parameters were compared between these two groups. The results showed that patients with a higher ratio between early mitral inflow velocity and mitral annular early diastolic velocity (E/e') presented higher heart sound frequencies, a longer QS1 interval and a more frequent occurrence of S4. By assigning a score to each of these factors, we proposed a combined score for differentiation of E/e' below and above 9. The combined score demonstrated better performance than a common serological biomarker of elevated LV filling pressure. The association between heart sounds and echocardiography makes it likely to use heart sounds for simple non-invasive screening of patients with HFpEF.

With the recent progress in sensor and communication technologies, the smartphone becomes a potential candidate to help health evaluation of the patients. Mobile health (mHealth) is increasingly recognized as part of the healthcare system, boosted by the coronavirus-19 pandemic. To enable large-scale application of heart sounds for health purposes, we explored the feasibility of turning the smartphone microphone to an electronic stethoscope in **Chapter 5**. An App named Echoes was developed for iPhone and was distributed to general users, which resulted in >1100 respondents with limited advertisement. Heart sounds and basic information of the users were collected anonymously. Visual assessment of quality of heart sound showed that about 3 out of 4 recordings had clear S1 and S2. Most users were able to make a good-quality recording of heart sounds within the first 3 attempts. Factors that tended to negatively influence heart sounds quality were age and body mass index. The findings suggest the possibility of recording heart sounds by general users using their mobile phone.

In **Chapter 6**, we summarized our findings and discussed the scientific and societal impacts. In a history of over 200 years,

auscultation has undergone three waves of research enthusiasm, along with rapid development of measurement tools. Heart failure is one of central research topics in heart sound, but little is known about how splitting and frequency of heart sounds change during disease evolution. More importantly, the relationship between heart sounds and patient outcome needs to be clarified in more extensive follow-up studies. Advancements in mobile phone technology enable turning the smartphone microphone to a digital stethoscope for recording heart sounds on a large scale, which has the potential to remotely monitor the patients' status. In the 21st century, signal processing techniques, open-access heart sound datasets and machine learning algorithms are laying foundations for the third wave of heart sound research and applications.

In conclusion, this thesis explored the relationship between heart sounds and hemodynamics using animal and human studies, and preliminarily investigated the potential to use heart sound recordings for mHealth applications. These findings help facilitate the use of heart sounds as a simple, non-invasive and low-cost tool for monitoring patients remotely and in hospital.

中文摘要

心音是血流冲击心血管相关组织包括瓣膜、心肌和血管引起的一系列振动。心音的两个主要成分是第一心音（S1）和第二心音（S2）。前者发生在心室舒张末期，后者发生在心室收缩末期。S1 由二尖瓣和三尖瓣分量构成。S2 由主动脉瓣和肺动脉瓣分量构成。S1 或 S2 的两个分量如果发生时间相距较远，则产生心音分裂。此外，心音可以联合心电图进行分析，其中最常见的指标是收缩时间参数。它包含两个指标，分别是 QS1（从心电图 QRS 波起始至心音 S1 起始的时间差）和 S1S2（心音 S1 起始至 S2 起始的时间差）。

从二百余年前起，医生即开始用心音来协助诊断疾病。随后，听诊器的出现更促进了心音在临床上的应用。新近出现的一些技术，比如电子听诊器和数字信号处理技术，使得心音的采集和分析更为便捷。本论文主要探讨心音相关参数在评估心力衰竭，包括射血分数降低的心力衰竭（HFrEF）和射血分数保留的心力衰竭（HFpEF）中的应用。

HFrEF 的患者如果被查出双心室收缩不同步，则有可能需要接受心室再同步化治疗。在这种情况下，心音分裂间期可以反映双心室收缩不同步的时间，有助于选择心室再同步化治疗的人群以及调整术后起搏器参数。在本书**第二章**中，我们提出了一种新算法自动计算 S2 的分裂时间。信号仿真实验和动物实验结果均证实了该算法得到的 S2 分裂时间和侵入性导管测得的双心室机械收缩不同步之间，存在良好的相关性。

在**第三章**中，我们联合了动物实验和临床研究，探讨心音收缩时间参数与心肌收缩力的关系。我们通过起搏的方式逐步延长心房-心室耦合时间，并同时测量左心室（LV）内压。通过联合心音和心电图，我们计算了 VS1 间期，即从心室刺激电位开始至心音 S1 产生的时间差。结果表明，该指标随着起搏过程中，心肌收缩力的改善而逐步缩短，同时伴随着 S1S2 间期逐步延长。进一步分析表明，这两个指标对心房-心室优化起搏治疗的最佳参数之估计误差较小，同时血流动力学参数的预测吻合度较高。该发现有助于促进心音收缩时间参数在起搏器治疗参数优化中的应用。

近些年，HFpEF 的流行率逐渐上升，特别是在老年群体中。但是，目前医学指南对该病的相关评估，比如心室舒张功能障碍和 LV 内压升高均未达成共识。在**第四章**中，我们初步探讨了心音和彩超在评估 HFpEF 疑似患者方面是否存在相关性。为了减少性别、体重指数和心率这些混杂因素的影响，我们首先匹配了这三个因素，从而获得两组基线数据相似的患者。通过比较这两组患者的心音和彩超数据，我们发现若患者的舒张早期跨二尖瓣血流最大速度/二尖瓣环最大速度的比值（E/e’比值）较高，则心音频率也较高，同时 QS1 间期延长，第四心音的发生率升高。通过对这些因素进行加权，我们提出了一种基于积分的方法来区分 E/e’比值是否大于 9。该方法比常规血清学检查更能反映 LV 灌注压力升高。该研究发现的心音和彩超相关性，为进一步发展心音用于无创筛查 HFpEF 奠定了基础。

随着近年传感技术和通信技术的快速发展，智能手机逐渐成为一个健康评估的工具。移动医疗（mHealth）日益受到重视，特别是在过去两年新冠疫情的阴霾下。为了将心音大规模应用于健康监测，我们初步探讨了用手机麦克风来测量心音的可能性（**第五章**）。我们基于 iPhone 平台开发了一款 App（Echoes），并将其分发给普通用户。我们让这些用户自己采集心音，并提供简单的个人数据。随后，我们分析了超过 1100 名用户的 7500 条心音数据。结果表明，大约 3/4 患者的心音数据质量较好，可以用于分析 S1 和 S2，而多数患者可以在前 3 次成功采集心音。年龄较大和体重指数较高的患者，心音质量偏差。这些结果提示，普通用户可以通过智能手机来采集心音。

在**第六章**中，我们总结了本书的发现，并分析了这些发现的科学价值和社会价值。心音听诊有着 200 多年的历史，并正在经历第三轮研究浪潮。这些发展得益于近年飞速发展的心音测量技术。心力衰竭是心音研究的中心课题之一，但目前对于心音分裂及心音频率如何随着心力衰竭变化，仍知之甚少。更重要的是，目前缺乏随访研究来证实这些心音参数与患者预后之间的关系。随着移动技术的发展，智能手机可以被用作电子听诊器，来帮助大规模采集心音数据，使远程监测患者状况成为可能。在目前的第三波心音研究浪潮中，三大基石分别是电子信号处理、开源心音数据库和人工智能算法。

总之，本书通过动物实验和人体研究，探讨了心音与血流动力学的关系，并初步研究了心音在移动医疗方面的应用。在未来，心音有可能作为一种简单、无创和廉价的工具，用于医院内和家庭患者监测。

Appendix

Surveillance of COVID-19 in the General Population Using an Online Questionnaire: Report From 18,161 Respondents in China

Hongxing Luo[1]; Yongchan Lie[2]; Frits W. Prinzen[1]

JMIR Public Health Surveill. 2020 Apr 27;6(2):e18576. doi: 10.2196/18576.

[1]Department of Physiology, Cardiovascular Research Institute Maastricht (CARIM), Maastricht University, Maastricht, the Netherlands
[2]Department of Health Ethics and Society, Faculty of Health Medicine and Life Sciences (FHML), Maastricht University, Maastricht, the Netherlands

Abstract

Background:

The recent outbreak of coronavirus disease 2019 (COVID-19) has become an international pandemic. So far little is known about the role of an internet approach in COVID-19 surveillance.

Objective:

We aim to investigate whether an online survey can provide population-level information for observing prevalence trends during early phase of outbreak and identifying potential risk factors of COVID-19 infection.

Methods:

A 10-item online questionnaire was developed according to medical guidelines and relevant publications. It was distributed between 24 January and 17 February 2020. Characteristics of respondents and temporal changes of various questionnaire-derived indicators were analyzed.

Results:

A total of 18161 questionnaires were returned, including 6% (1171) from Wuhan City. Geographical distributions of the respondents were consistent with population per province (R^2 = 0.61, $P < .001$). History of contact significantly decreased with time, both outside Wuhan City (R^2 = 0.35, $P = .002$) and outside Hubei Province (R^2 = 0.42, $P < .001$). Percentage of fever respondents peaked around February 8 (R^2 = 0.57, $P < .001$) and increased with history of contact in the areas outside Wuhan City (risk ratio: 1.31, 95% confidence interval: 1.13 - 1.52, $P < .001$). Male sex, advanced age, and lung diseases were associated with a higher risk of fever in the general population with history of contact.

Conclusions:

This study shows the usefulness of an online questionnaire for surveillance of outbreaks like COVID-19 by providing information about trends of the disease and aiding in identifying potential risk factors.

Introduction

The recent outbreak of 2019 coronavirus disease (COVID-19) has caused over 752 thousand confirmed cases and 36 thousand deaths by March 30, 2020 [1-4]. Despite a proactive policy of identifying and treating patients with infected symptoms, it remains resource-intensive to screen the general population that is at risk of infection [5, 6]. Moreover, inequality of healthcare system among different areas also brings challenges to cover remote areas which are also at risk of the COVID-19 infection. Therefore, a new way to surveil the general population is likely to contribute to our understanding of COVID-19 [7]. The wide use of internet throughout China, and in the rest of the world, may be sufficient to provide such information. Participatory disease surveillance has been increasingly investigated in recent years as a promising tool to complement traditional facility-based surveillance platforms [8]. It has the advantage of quick coverage of a large population during disease outbreak. Because of this, an online survey may be valuable in monitoring disease trends in community and providing information for policy-making.

Here we report the results of the first online questionnaire of COVID-19, released since 24 January and with data collected up to 17 February 2020. Our study aims to investigate 1) how history of contact and fever, both defined according to relevant medical guidelines, have evolved during the early phase of government policy of lockdown, and 2) whether an online questionnaire can be used to identify certain risk factors related to fever among those reporting history of contact.

Methods

Questionnaire development and distribution

The first version of questionnaire was developed on 24 January 2020. By that time, little evidence was known about COVID-19. Our anonymous questionnaire was primarily developed from the following 3 sources: 1) the Diagnosis and Treatments of COVID-19 (Third Version) guideline; 2) clinical courses of the first 17 death cases, both of which released by the National Health Commission of China; and 3) an article which first analyzed the clinical features of 41 cases with COVID-19 [9-11]. The guideline requires a suspected case to satisfy the following criteria: 1) any history of contact: living in Wuhan or having travelled to Wuhan within 2 weeks of disease onset; being in contact with any person with fever and respiratory symptoms from Wuhan within 2 weeks of disease onset; belonging to a cluster of infected cases; 2)

clinical manifestations: fever, defined as body temperature ≥ 37.3 ℃ (99.1 ℉); imaging evidence of COVID-19; normal white blood cell count or leukopenia or lymphopenia. A confirmed case is further established by positive findings of real-time polymerase chain reaction or viral gene sequencing. The descriptions of the guideline are in good consistency with the clinical features of the first 17 death cases and later 41 infected cases reported on 24 January [9, 10]. Therefore, our questionnaire evaluated the risk of COVID-19 in general population from the following aspects:

1) History of contact: living in Wuhan, or having travelled to Wuhan in the past 2 weeks; or had any close contact (lived, studied or worked together, or had any other close contact) in the past 2 weeks with a person with fever and cough who came from Wuhan; or workplace, school or family has at least 2 confirmed cases. Other history of contact with wildlife animals within 2 weeks of disease onset was also considered.

2) Body temperature: having a fever with body temperature higher than 37.3 ℃ (99.1 ℉).

3) Symptoms: We classified symptoms by their relative importance into the following 3 groups: 1. Chief symptoms related to pulmonary infection, i.e., cough without sputum or with little sputum, and shortness of breath; 2. Secondary symptoms related to systemic changes probably caused by viral infection, i.e., fatigue, headache, and myalgia; and 3. Probably unrelated symptoms, i.e., nasal obstruction, rhinorrhea, sneezing, sore throat, and diarrhea.

4) Comorbidities: Lung diseases, cardiovascular diseases, hypertension, diabetes, stroke and chronic kidney dysfunction.

5) Basic information: age and gender.

We did not include laboratory examinations (e.g. real-time polymerase chain reaction, lymphopenia, white blood cell count) or thoracic imaging results (e.g., multiple patchy consolidation and interstitial changes) in our questionnaire because in general they are unlikely obtained by general population.

By 17 February 2020 we had developed and released three versions of Chinese questionnaires to the public. They were essentially similar, with the following three major revisions: 1) We divided the age group of ≤ 40 years, used in the first version, into age groups of ≤ 30 years and 31 – 40 years in the following two versions for better risk stratification; 2) History of contact with wildlife animals was removed from the third version because we considered it to have a low value for

diagnosis in general population; and 3) the question, initially included for evaluating shortness of breath ("I feel extremely short of breath when climbing upstairs or walking at a fast speed", modified from the Medical Research Council Breathlessness scale) was removed from the third version, and added as an item named "shortness of breath" to the question about symptoms of COVID-19. This was done, because we found an exceptionally high percentage of respondents reporting shortness of breath in the first 2 versions of questionnaires (26.5% and 32.9%, respectively).

After completing the questionnaire, the respondents would be classified into one of the following 4 risk groups and given different suggestions: 1) High risk group having history of contact and fever: they were suggested to measure their body temperature after 30 minutes and immediately visit hospital to screen for potential COVID-19; 2) Moderate risk group having history of contact but without fever: they were suggested to daily monitor their body temperature and screen for potential COVID-19 if fever or respiratory symptoms occur; 3) Low risk group without history of contact but with fever: this group probably had a common cold, and was suggested to make an appointment with general practitioner for help if necessary; 4) Very low risk group without history of contact or fever: they were unlikely to have COVID-19 at the time they completed the questionnaire and were suggested to take necessary measures such as putting on a facemask to prevent the infection.

The questionnaire was developed using a professional online questionnaire website Wenjuanxing (Questionnaire Star) [12]. It is the most popular website for online survey in China with over 4.2 billion questionnaires recycled and over 59 million users by 21 February 2020. Questionnaires were distributed online by 1) WeChat, the most popular instant message application in China, and 2) sharing the link of the questionnaire. Since our aim was to have an overview of situations in China during COVID-19 outbreak, we did not target any specific groups of respondents of interest. Distribution and filling of the questionnaires were voluntary behaviors, making our study a convenience sampling study.

According to the World Health Organization Guidelines on Ethical Issues in Public Health Surveillance, a surveillance study in emergency outbreak situations is clearly exempted from ethical review and oversight [13]. Indeed, our online questionnaire was designed on 23 January when the lockdown of Wuhan City was officially announced and

released on the day followed, so it could not await the formal approval of an ethical review of committee. All users were informed at the beginning of the questionnaire that their questionnaire data would be used only for medical education and research purposes. If the informed consent was rejected by the users, they still could continue the questionnaire and obtain their results.

Data collection

The questionnaire was released on 24 January and recycled on 17 February. All questionnaire results were downloaded from the website for our analysis. In addition to the items of the questionnaire, the downloaded data also included date of submission of all respondents as well as respondents' location on city level.

We also collected population data of each province from China Statistical Abstract 2019 published by the National Bureau of Statistics of China [14]. The number of confirmed cases was followed up on a daily basis since release of the questionnaire using the NetEase News website, the largest Chinese hub for real-time collection of COVID-19-related data and news [15]. The statistics of confirmed cases per province used in this study were collected until midnight of February 11, because at that time also clinically diagnosed cases without positive real-time polymerase chain reaction results were included in the officially confirmed number of cases.

Statistical analysis

Count data were expressed as number (percentage). Skewed continuous data (time to complete questionnaire) were expressed as median (25th percentile – 75th percentile). Geographical distributions were drawn using Microsoft Excel Visual Basic. Pearson's correlation analysis was used to analyze the relationship between two variables of interest (mainly between date and percentage of respondents of interest per day). Comparison of respondents' basic characteristics between inside and outside Wuhan was performed using *chi-squared* test or Fisher's exact test if sample size < 40. Risk of fever in respondents with history of contact was evaluated using risk ratio (95% confidence interval) [RR (95% CI)]. All statistical analyses were performed using Stata 14.0 and MATLAB R2018b. Statistical significance was defined as a two-tailed *P* value smaller than .05.

Results

By 17 February 02:33 AM, a total of 19449 individuals completed the questionnaires, 97% from China. After removing 385 questionnaires from overseas countries, 575 lacking informed consent, 55 missing age, 31 missing temperature, 38 missing comorbidities, and 4 missing symptoms information, 18161 anonymous questionnaires were analyzed. Overall, it took 52 (41 - 67) seconds to complete the questionnaire. Most questionnaires were accessed by clicking on the link of the questionnaire (11337, 62%) and by visiting WeChat miniApp (6800, 37%).

Geographical distributions

Figure 1A shows the geographical distributions of the questionnaire respondents in China. The questionnaire covered all 34 province-level administrative regions. For Hubei Province, 69% (1171) of respondents came from Wuhan City which was mostly affected by COVID-19. A positive relation was found between the number of respondents and the population size per province (**Figure 1B**), demonstrating good coverage of the questionnaire across China.

Basic characteristics

Table 1 summarizes the demographics and basic characteristics of respondents. The population in Wuhan had similar age and comorbidities to that of outside Wuhan. Age was negatively correlated with the number of respondents (R^2 = 0.95, P < .001). As expected, history of contact was more frequent among the respondents living in Wuhan (all P < .001). The percentage of fever was significantly lower among respondents inside versus outside Wuhan. Symptoms were reported in a rather high percentage (65%) of respondents. When restricting the symptoms to at least 1 main symptom and 1 secondary symptom, the number of respondents with symptoms dropped to 13% (2292).

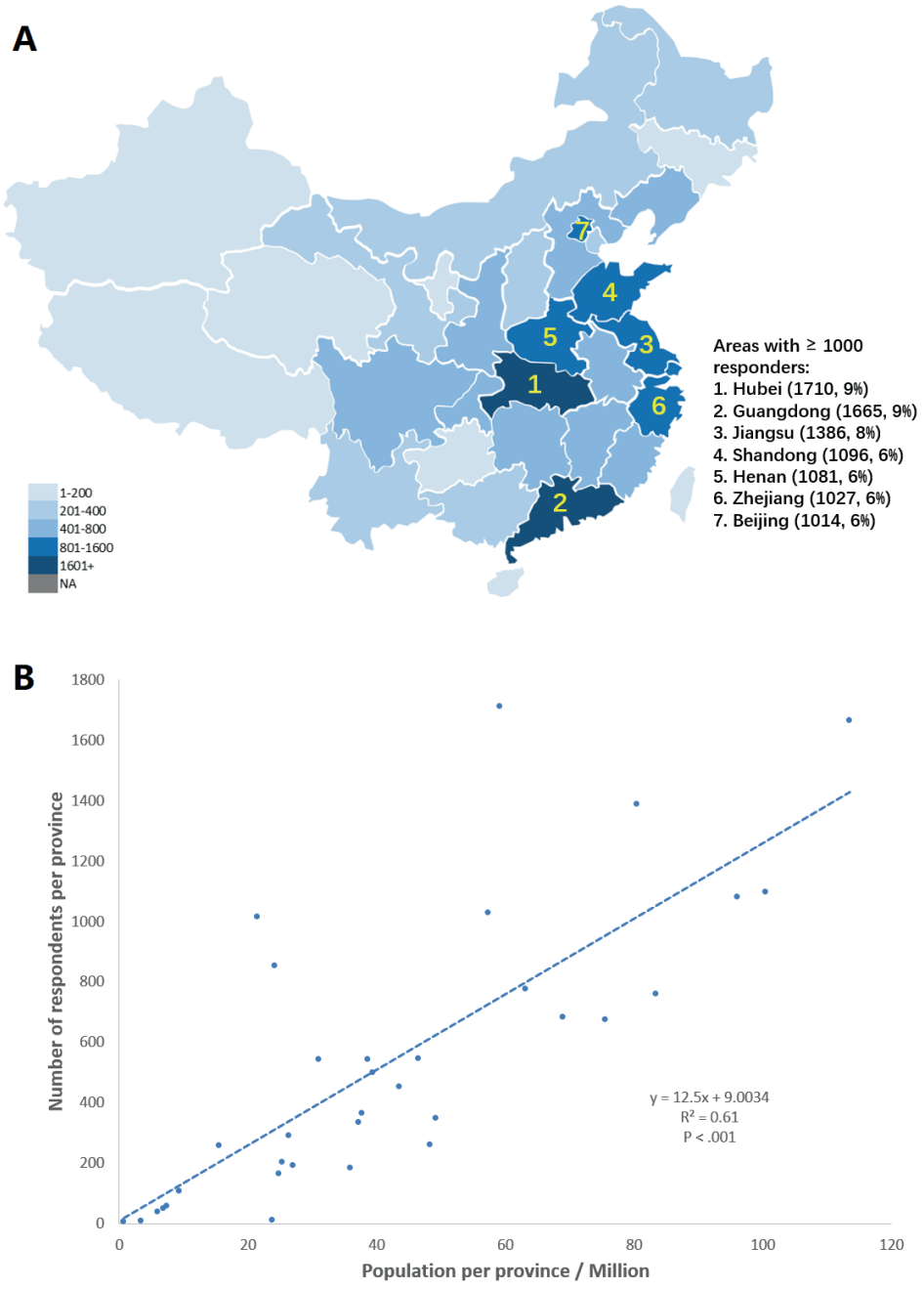

Figure 1 A) Geographical distributions of questionnaire respondents in China. B) A positive correlation between the number of respondents and the size of the population of each province.

Table 1. Demographics and basic characteristics of respondents

	All respondents (n = 18161)	Wuhan (n = 1171)	Outside Wuhan (n = 16990)	*P* value
Women	10801 (59%)	762 (65%)	10039 (59%)	< .001
Age, years				
≤ 30	12504 (69%)	782 (67%)	11722 (69%)	.11
31 – 40	3757 (21%)	282 (24%)	3475 (20%)	.003
41 – 50	1154 (6%)	70 (6%)	1084 (6%)	.59
51 – 60	532 (3%)	28 (2%)	504 (3%)	.26
61 – 70	147 (0.8%)	6 (0.5%)	141 (0.8%)	.24
≥ 71	67 (0.4%)	3 (0.3%)	64 (0.4%)	.51
Any comorbidity	1593 (9%)	95 (8%)	1498 (9%)	.41
Hypertension	655 (4%)	38 (3%)	617 (4%)	.49
Lung diseases	468 (3%)	24 (2%)	444 (3%)	.24
Cardiovascular diseases	375 (2%)	21 (2%)	354 (2%)	.50
Diabetes	223 (1%)	16 (1%)	207 (1%)	.66
Chronic kidney disease	135 (0.7%)	5 (0.4%)	130 (0.8%)	.19
Stroke	34 (0.2%)	4 (0.3%)	30 (0.2%)	.21
Any history of contact	2631 (14%)	1171 (100%)	1460 (9%)	< .001
Living in Wuhan now or having gone to Wuhan in the past 2 weeks	1950 (11%)	1171 (100%)	779 (5%)	< .001
Contacts with a person with fever and cough from Wuhan in the past 2 weeks	938 (5%)	298 (25%)	640 (4%)	< .001
At least 2 confirmed cases in workplace, school or family	532 (3%)	122 (10%)	410 (2%)	< .001
Fever	1653 (9%)	56 (5%)	1597 (9%)	< .001
Any symptom	11796 (65%)	699 (60%)	11097 (65%)	< .001
Cough	5242 (29%)	314 (27%)	4928 (29%)	.11
Shortness of breath	4393 (24%)	263 (22%)	4130 (24%)	.15
Nasal obstruction, rhinorrhea, or sneezing	4376 (24%)	237 (20%)	4139 (24%)	.001
Sore throat	3397 (20%)	201 (18%)	3196 (20%)	.16
fatigue	3245 (18%)	148 (12%)	3097 (18%)	< .001
headache or myalgia	2072 (11%)	87 (7%)	1985 (12%)	< .001
Diarrhea	1360 (8%)	70 (6%)	1290 (8%)	.04

History of contact

History of contact was reported in 2631 (14%) respondents. However, the high percentage might have been confounded by considering all

respondents living in Wuhan City as having history of contact according to the definition of official guideline, so we excluded these respondents from our analysis and divided the remaining respondents by every 8 days into 3 phases: 1) phase 1: 24 to 31 January; 2) phase 2: 1 to 8 February; and 3) phase 3: 9 to 16 February. Despite heterogeneous responses of different provinces, proportion of respondents reporting history of contact had markedly decreased over these 3 phases in most provinces (**Figures 2A, B, C**). This observation was further confirmed by correlation analysis between the proportion of respondents reporting history of contact and date in areas outside Wuhan City and Hubei Province (**Figure 2D**). These findings indicate the efficacy of current policies adopted to reduce the history of contact among general population since a lockdown in Wuhan and other areas on January 23.

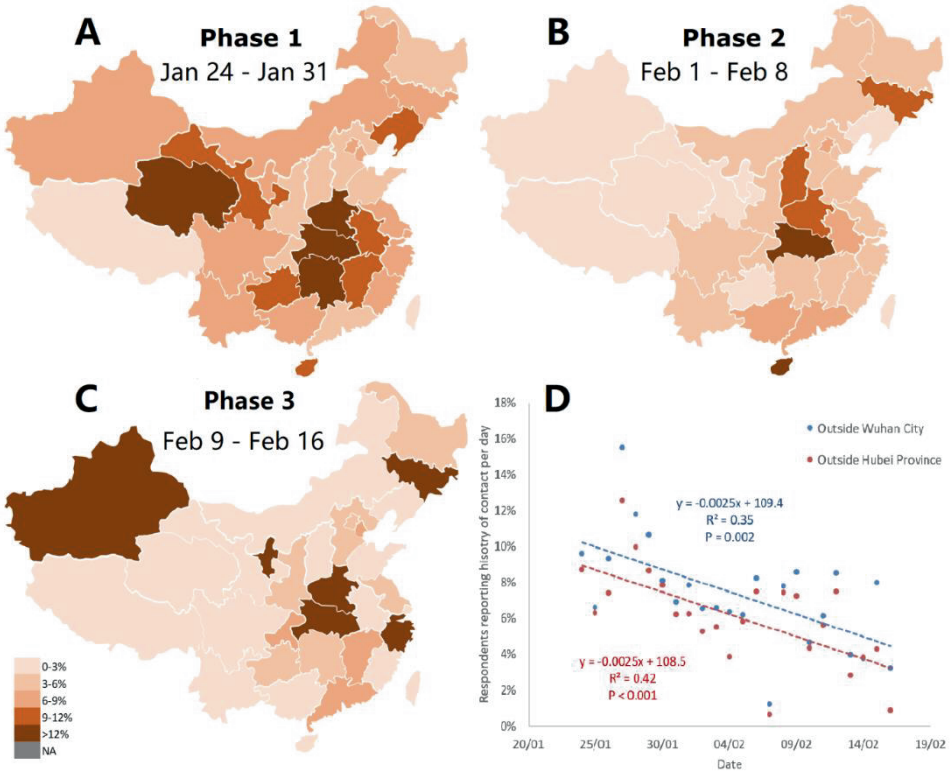

Figure 2. Geographic spread of the proportion of respondents reporting history of contact in three phases of the COVID-19 outbreak (A, B, C) and its time course in all regions outside Wuhan City and outside Hubei Province (D).

Body temperature

Body temperature was measured in 77% (14073) of respondents, with a higher percentage in Wuhan City (85%, 990) and Hubei Province (84%, 1431), respectively. Overall, fever was reported in 9% (1653) of respondents. Unexpectedly, a lower percentage was found for Wuhan City and Hubei Province (5% for both). This might be due to that as COVID-19 developed to a further stage in Wuhan, fever cases were identified early and sent to hospitals without access to internet. We further analyzed how the percentage of respondents with fever evolved with time. The trend seemed to peak on around February 8 (**Figure 3**).

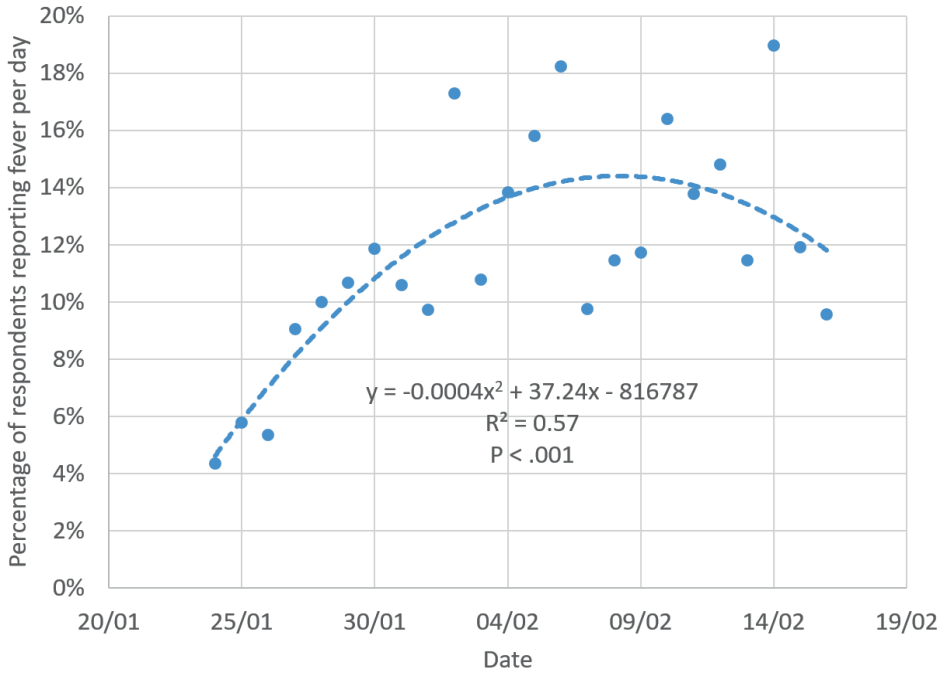

Figure 3. Proportion of respondents reporting fever over time.

Fever in respondents with history of contact

To analyze the relationship between fever and history of contact may help develop population-based strategies for prevention purpose. For the respondents living outside Wuhan, we found a significant relation between any history of contact and fever (RR: 1.31, 95% CI: 1.13-1.52, *P* < .001). Travelling to Wuhan, having any close contact with confirmed case, and having at least 2 confirmed cases at workplace in the past 2 weeks conferred a significantly higher risk of fever (RR: 1.47, 95% CI: 1.23-1.77, *P* < .001; RR: 1.98, 95% CI: 1.67 - 2.24, *P* < .001; and RR:

2.12, 95% CI: 1.74 – 2.58, *P* < .001, respectively). Moreover, there was a significant positive relation between the number of officially confirmed cases and the number of respondents reporting fever (R^2 = 0.41, *P* < .001) or the number of respondents reporting fever plus history of contact (R^2 = 0.35, *P* < .001) on a province basis. Regarding risk stratification based on history of contact and fever, most respondents (14264, 79%) were classified to very low risk group, followed by moderate (1883, 10%) and low risk group (1428, 8%), whereas only 1% (225) to high risk group.

Furthermore, comparison of fever rates among groups of various characteristics was likely to help identify risk factors (**Figure 4**). Males were at a higher risk of fever than females (P < .001). There was a positive trend between age and fever (P < .001). Respondents reporting fatigue and headache/myalgia were more likely to report fever (P < .001). Comorbidities showed various associations with fever, among which history of lung diseases seemed to confer a higher risk of fever than the others. However, the relationship needs to be further validated by larger-sample studies because of a relatively small number of respondents in each group.

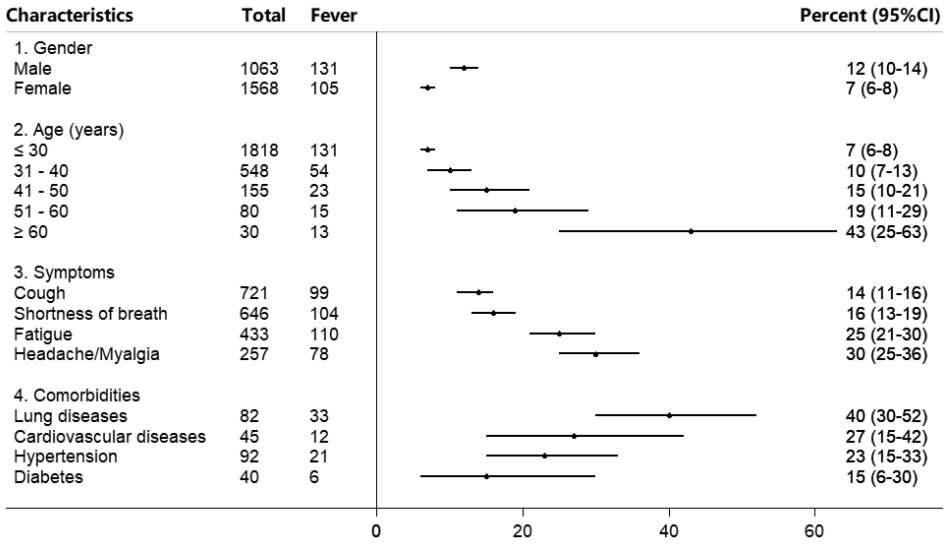

Figure 4. Fever in various subgroups of respondents with history of contact

Discussion

To the best of our knowledge, this is the first large-sample online surveillance of COVID-19 outbreak in general population. Our major findings are: 1) our questionnaire had a good coverage of all provinces of China in a relatively short period of time (~3 weeks); 2) history of contact among population outside Wuhan and Hubei Province significantly decreased during the early phase of government policy of lockdown; 3) fever reported by respondents significantly increased in short term of disease outbreak and levelled off in 2 to 3 weeks; and 4) among those with history of contact, some factors (male, an advanced age and history of lung diseases) seemed to be associated with a higher risk of fever.

Values of online questionnaire

An online questionnaire is likely to serve as a complementary way of disease surveillance in general population, especially during the emergent outbreak of an infectious disease [5]. It takes the advantage of low-cost and efficient delivery to all areas even the most remote areas where internet access is better than health care resources [16, 17]. Our questionnaire included 3% (385) Chinese respondents from 38 overseas countries, including developed (the United States, Japan, Canada, the United Kingdom), developing (Brazil, Russia, India, South Africa) and underdeveloped countries (Laos, Uganda, Cambodia). Translation of the questionnaire to other languages may further increase the coverage across the world and improve surveillance of COVID-19 outbreak and comparable epidemics.

Compared with the conventional way of disease surveillance, the online questionnaire covers the population generally with less severe conditions but nevertheless is under risk of infection [7, 18]. Taking into account this population helps to establish the full spectrum of COVID-19 epidemiology. It may also facilitate the early triage and diagnosis of high-risk groups when combining with other digital health measures such as online physician consultation which has been widely adopted since COVID-19 outbreak in China. For the low-risk population, the questionnaire can also be adapted to reduce unnecessary anxiety and hospital visits and thus greatly relieve the workloads of healthcare facilities especially when an emergent public health event occurs [19].

The questionnaire approach is advantageous compared with other approaches of online disease surveillance using data from the Google Trends, Twitter, or Facebook [20-22]. It provides richer information of

the respondents because most items can be designed according to medical guidelines and characteristics of target population. Therefore, it is a more active approach than other infosurveillance methods using social media. The information such as symptoms, history of contact and comorbidities provided by an online questionnaire can be further combined with vital data such as body temperature, heart rate, respiratory rate, oxygenation level and activity level obtained from wearable devices to have a more comprehensive and reliable estimation of respondent's risk of disease [23]. For the high-risk group identified using an online questionnaire, a case can be further confirmed by sending a home testing kit and instructing the respondents to perform a rapid diagnostic test, as shown in the GoViral study [24]. Additionally, self-reported data from an online questionnaire can be linked with electronic medical records to build a long-term monitoring system [8].

Use of questionnaire to observe trends

An online survey is likely to be used to observe the trends of disease prevalence in community and thus support government policy evaluation. In our study, the date February 8 when the percentage of fever respondents peaked was 16 days following lockdown of Wuhan City, close to the 14 days of the maximum incubation period of coronavirus [25]. The delay of fever peak might be associated with delayed quarantine policies in other cities in China. Overall, our data support the efficacy of current policies (quarantine, social distancing, and isolation of infected population) for containing the spread of COVID-19 from Wuhan City to the other areas of China [6, 26, 27]. However, the period and efficacy of quarantine may differ by country [28]. It depends on not only government policies but also local culture and more importantly active supports from general population. For the other countries which may not have quarantine policies as strict as that of China the time to fever peak is probably longer among general population. Moreover, integration of survey data in a model for real-time and long-term forecasting of disease trends is likely to provide richer information for policy-making [29]. Of note, our questionnaire is more applicable to those living in China than abroad. Definition of history of contact has been mostly relied on contact with a confirmed case from Wuhan. However, this can be further modified according to the earliest and generally most severely affected area of a country of interest, such as Lombardy in Italy.

Use of questionnaire to identify risk factors

Our survey also indicates that some factors such as male, an advanced age and history of lung disease are likely to relate to a higher risk of infection and thus these groups should be under close observations. Indeed, these risk factors identified from our study are consistent with the clinical features of infected cases in previous publications [9, 30-33]. Opportunities are that with a quick dissemination of an online questionnaire during the early phase of disease outbreak, risk factors can be identified at a much earlier phase than when enough severe cases have been collected and analyzed using a conventional surveillance method. This further allows for an earlier protection of vulnerable groups from potential infection and thus reducing the number of cases. Internet-based surveillance approach based on Twitter has been demonstrated to detect Ebola, avian influenza and thunderstorm asthma at an early stage, even before the first official report [20-22].

Limitations of the approach

The approach undoubtedly has the bias of sampling primarily internet users and their relatives. As a consequence, the population included in our study is relatively young. Previous study demonstrated that both too young (age 0 – 10 years) and too old (age over 81 years) populations are under-represented in an internet-based monitoring survey [34]. A better coverage of general population with high representativeness generally requires a more complicated study design together with robust supports from an official institution [8]. The questionnaire can also be distributed through other web platforms such as Sina Weibo (the most popular microblogging website in China) and news media (NetEase and Xinhua) which have a wider reach of respondents in China. Also, this study does not include a follow-up of individual patients. This choice was made in order to respect the respondents' privacy. However, in future studies it may be acceptable to allot an individual code to each individual, thereby allowing follow-up, although systematic follow-up will remain a problem with internet questionnaires. Follow-up may be further compromised by the lack of internet access when the individual is hospitalized.

Unlike hospitals which diagnose COVID-19 using a comprehensive set of laboratory and imaging examinations, we did not include diagnostic tests such as real-time polymerase chain reaction or lung computed tomography results in our questionnaire. Therefore,

evaluating the respondents' risk of viral infection from history of contact, body temperature, symptoms and comorbidities may have the risk of underestimating some asymptomatic or presymptomatic patients who are not uncommon [35, 36].

Based on this study, we have updated our fourth version of Chinese questionnaire [37] and released the English questionnaire [38] (also see the **online appendix** for Word format files). Both questionnaires follow the Attribution 4.0 International (CC BY 4.0) license, meaning that they are free to be shared and adapted under the condition that current work has been properly cited. Considering privacy purpose, the survey data of this study can be obtained from the corresponding author at request.

Conclusions:

In conclusion, this study shows that an online questionnaire may help monitor current prevalence, evaluate government policy and identify high-risk population during COVID-19 outbreak. The online questionnaire approach can also be adapted to monitor other types of infectious diseases depending on areas of interest.

References:

1. Wu JT, Leung K and Leung GM. Nowcasting and forecasting the potential domestic and international spread of the 2019-nCoV outbreak originating in Wuhan, China: A modelling study. The Lancet 2020; 395(10225):689-697. [doi: 10.1016/S0140-6736(20)30260-9]

2. Hui DS, I Azhar E, Madani TA, Ntoumi F, Kock R and Dar O, et al. The continuing 2019-nCoV epidemic threat of novel coronaviruses to global health — the latest 2019 novel coronavirus outbreak in Wuhan, China. Int J Infect Dis 2020; 91:264-266. [doi: 10.1016/j.ijid.2020.01.009]

3. World Health Organization. WHO announces COVID-19 outbreak a pandemic. URL: http://www.euro.who.int/en/health-topics/health-emergencies/coronavirus-covid-19/news/news/2020/3/who-announces-covid-19-outbreak-a-pandemic [accessed 2020-03-12]

4. Worldometer. COVID-19 coronavirus pandemic. URL: https://www.worldometers.info/coronavirus/ [accessed 2020-03-30]

5. Lipsitch M, Swerdlow DL and Finelli L. Defining the epidemiology of covid-19 — studies needed. New Engl J Med 2020. [doi: 10.1056/NEJMp2002125]

6. Cheng VCC, Wong S, To KKW, Ho PL and Yuen K. Preparedness and proactive infection control measures against the emerging Wuhan coronavirus pneumonia in China. J Hosp Infect 2020. [doi: https://doi.org/10.1016/j.jhin.2020.01.010]

7. Cowling BJ and Leung GM. Epidemiological research priorities for public health control of the ongoing global novel coronavirus (2019-nCoV) outbreak. Euro surveillance : bulletin Europeen sur les maladies transmissibles = European communicable disease bulletin 2020; 25(6). [doi: 10.2807/1560-7917.ES.2020.25.6.2000110]

8. Smolinski MS, Crawley AW, Olsen JM, Jayaraman T and Libel M. Participatory disease surveillance: Engaging communities directly in reporting, monitoring, and responding to health threats. JMIR Public Health Surveill 2017; 3(4):e62. [doi: 10.2196/publichealth.7540]

9. Huang C, Wang Y, Li X, Ren L, Zhao J and Hu Y, et al. Clinical features of patients infected with 2019 novel coronavirus in Wuhan, China. The Lancet 2020; 395(10223):497-506. [doi: 10.1016/S0140-6736(20)30183-5]

10. National Health Commission of China. Report of situations about 2019 coronavirus disease on 23 January 2020. URL: http://www.nhc.gov.cn/xcs/yqtb/202001/5d19a4f6d3154b9fae328918ed2e3c8a.shtml [accessed 2020-01-23]

11. National Health Commission of China. Diagnosis and treatments of new coronavirus pneumonia (Third version). URL: http://www.nhc.gov.cn/xcs/zhengcwj/202001/f492c9153ea9437bb587ce2ffcbee1fa.shtml [accessed 2020-03-05]

12. Questionnaire Star. Questionnaire star. URL: https://www.wjx.cn/ [accessed 2020-03-05]

13. WHO guidelines on ethical issues in public health surveillance. Geneva: World Health Organization; 2017. Licence: CC BY-NC-SA 3.0 IGO.
14. National Bureau of Statistics China, China Statistical Abstract 2019. 2019: China Statistics Press.
15. NetEase News. Real-time COVID-19 tracking. URL: https://wp.m.163.com/163/page/news/virus_report/index.html?_nw_=1&_anw_=1 [accessed 2020-03-05]
16. Flahault A, Utzinger J, Eckerle I, Sheath DJ, de Castañeda RR and Bolon I, et al. Precision global health for real-time action. The Lancet Digital Health 2020; 2(2):e58-e59. [doi: https://doi.org/10.1016/S2589-7500(19)30240-7]
17. Gilbert M, Pullano G, Pinotti F, Valdano E, Poletto C and Boëlle P, et al. Preparedness and vulnerability of African countries against importations of COVID-19: A modelling study. The Lancet 2020. [doi: 10.1016/S0140-6736(20)30411-6]
18. Zhao S, Musa SS, Lin Q, Ran J, Yang G and Wang W, et al. Estimating the unreported number of novel coronavirus (2019-nCoV) cases in china in the first half of january 2020: A Data-Driven modelling analysis of the early outbreak. J Clin Med 2020; 9(2):388. [doi: 10.3390/jcm9020388]
19. Wong JEL, Leo YS and Tan CC. COVID-19 in singapore—current experience. JAMA 2020. [doi: 10.1001/jama.2020.2467]
20. Yousefinaghani S, Dara R, Poljak Z, Bernardo TM and Sharif S. The assessment of twitter's potential for outbreak detection: Avian influenza case study. Sci Rep-Uk 2019; 9(1). [doi: 10.1038/s41598-019-54388-4]
21. Odlum M and Yoon S. What can we learn about the Ebola outbreak from tweets? Am J Infect Control 2015; 43(6):563-571. [doi: 10.1016/j.ajic.2015.02.023]
22. Joshi A, Sparks R, McHugh J, Karimi S, Paris C and MacIntyre CR. Harnessing tweets for early detection of an acute disease event. Epidemiology 2020; 31(1):90-97. [doi: 10.1097/EDE.0000000000001133]
23. Radin JM, Wineinger NE, Topol EJ and Steinhubl SR. Harnessing wearable device data to improve state-level real-time surveillance of influenza-like illness in the USA: A population-based study. The Lancet Digital Health 2020; 2(2):e85-e93. [doi: https://doi.org/10.1016/S2589-7500(19)30222-5]
24. Goff J, Rowe A, Brownstein JS and Chunara R. Surveillance of acute respiratory infections using Community-Submitted symptoms and specimens for molecular diagnostic testing. PLoS Curr 2015; 7. [doi: 10.1371/currents.outbreaks.0371243baa7f3810ba1279e30b96d3b6]
25. Backer JA, Klinkenberg D and Wallinga J. Incubation period of 2019 novel coronavirus (2019- nCoV) infections among travellers from Wuhan, China, 20 – 28 January 2020. Euro surveillance : bulletin Europeen sur les maladies transmissibles = European communicable disease bulletin 2020; 25(5). [doi: 10.2807/1560-7917.ES.2020.25.5.2000062]
26. Anderson RM, Heesterbeek H, Klinkenberg D and Hollingsworth TD. How will country-based mitigation measures influence the course of the COVID-19 epidemic? The

Lancet 2020; 395(10228):931-934. [doi: https://doi.org/10.1016/S0140-6736(20)30567-5]
27. Tang B, Xia F, Tang S, Bragazzi NL, Li Q and Sun X, et al. The effectiveness of quarantine and isolation determine the trend of the COVID-19 epidemics in the final phase of the current outbreak in China. Int J Infect Dis 2020. [doi: 10.1016/j.ijid.2020.03.018]
28. The Lancet. COVID-19: Too little, too late? The Lancet 2020; 395(10226):755. [doi: https://doi.org/10.1016/S0140-6736(20)30522-5]
29. Brownstein JS, Chu S, Marathe A, Marathe MV, Nguyen AT and Paolotti D, et al. Combining participatory influenza surveillance with modeling and forecasting: Three alternative approaches. JMIR public health and surveillance 2017; 3(4):e83. [doi: 10.2196/publichealth.7344]
30. Chen N, Zhou M, Dong X, Qu J, Gong F and Han Y, et al. Epidemiological and clinical characteristics of 99 cases of 2019 novel coronavirus pneumonia in Wuhan, China: A descriptive study. The Lancet 2020; 395(10223):507-513. [doi: 10.1016/S0140-6736(20)30211-7]
31. Wang D, Hu B, Hu C, Zhu F, Liu X and Zhang J, et al. Clinical Characteristics of 138 Hospitalized Patients with 2019 Novel Coronavirus–Infected Pneumonia in Wuhan, China. JAMA 2020. [doi: 10.1001/jama.2020.1585]
32. Xu X, Wu X, Jiang X, Xu K, Ying L and Ma C, et al. Clinical findings in a group of patients infected with the 2019 novel coronavirus (SARS-Cov-2) outside of Wuhan, China: Retrospective case series. BMJ 2020:m606. [doi: 10.1136/bmj.m606]
33. Yang X, Yu Y, Xu J, Shu H, Xia J and Liu H, et al. Clinical course and outcomes of critically ill patients with SARS-CoV-2 pneumonia in Wuhan, China: A single-centered, retrospective, observational study. The Lancet Respiratory Medicine 2020((online first)). [doi: 10.1016/S2213-2600(20)30079-5]
34. Marquet RL, Bartelds AI, van Noort SP, Koppeschaar CE, Paget J and Schellevis FG, et al. Internet-based monitoring of influenza-like illness (ILI) in the general population of the Netherlands during the 2003-2004 influenza season. Bmc Public Health 2006; 6:242. [doi: 10.1186/1471-2458-6-242]
35. Pan X, Chen D, Xia Y, Wu X, Li T and Ou X, et al. Asymptomatic cases in a family cluster with SARS-CoV-2 infection. The Lancet Infectious Diseases 2020. [doi: 10.1016/S1473-3099(20)30114-6]
36. Bai Y, Yao L, Wei T, Tian F, Jin D and Chen L, et al. Presumed asymptomatic carrier transmission of COVID-19. JAMA 2020. [doi: 10.1001/jama.2020.2565]
37. Luo H, Lie Y and Prinzen F.Coronavirus Infection Risk Self-Assessment Questionnaire (CIRSAQ 4.0, Chinese Simplified). URL: https://ks.wjx.top/jq/59735934.aspx [accessed 2020-03-05]
38. Luo H, Lie Y and Prinzen F.Coronavirus Infection Risk Self-Assessment Questionnaire (CIRSAQ 4.0, English version). URL: https://ks.wjx.top/jq/59730857.aspx [accessed 2020-03-05]

Acknowledgements

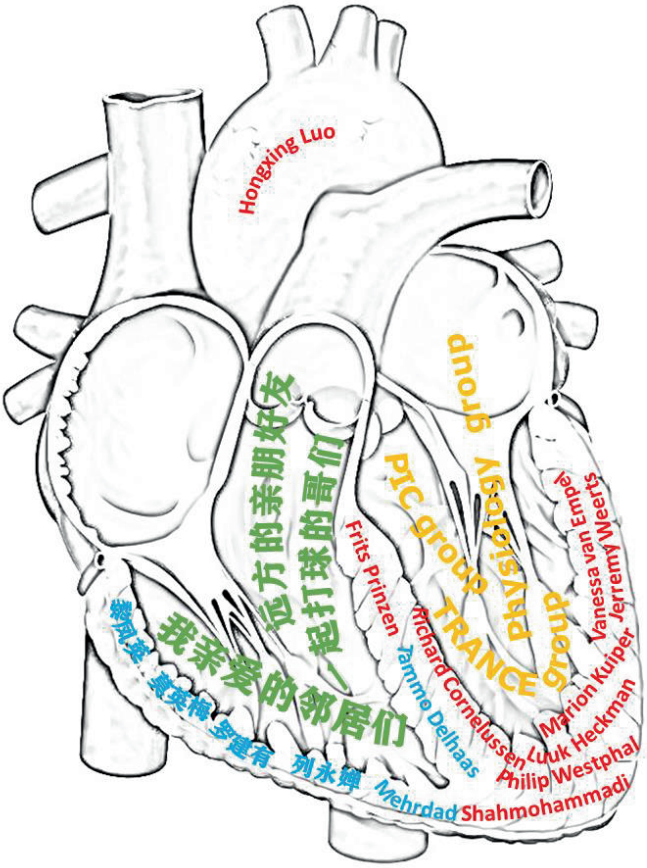

LV for work,
RV for life.
You are in
my heart.

Hongxing Luo
25.02.2022

Finally, it is time to write some words about the people who have helped me a lot in my past 3.75 years.

Frits Prinzen has been my role model.

Tammo Delhaas always checks my manuscript word-by-word, and hopefully he will find this Acknowledgements section free of any grammatical mistakes.

Richard Cornelussen inspires me with his unique opinions on academia and industry.

Mehrdad Shahmohammadi is energetic and enthusiastic about his life and (more importantly) about heart sounds.

Philip Westphal is ready to help at any time with his engineering perspective.

Luuk Heckman provides me his great helps in animal experiments, together with Marion Kuiper who has been the support of many other PhD students as usual.

Biweekly TRANCE meeting held on Monday afternoon is stressful for the speakers while joyful for the others. By combining both Physiology and Biomedical Engineering Departments, it gives me a privileged chance to taste different topics of cardiovascular research from engineering, physiological and clinical perspectives. Among the whole TRANCE team, I would like to extend my special thanks to Joost Lumens, Kevin Vernooy, Frans van Nieuwenhoven, Mohammed Ghossein, Jolijn Lubrecht, Floor Salden, Nienke Verzaal, Meike Ploeg, Erik Willemen and Tim van Loon, for their valuable comments and inspiring talks.

Arne van Hunnik and Vladimir Sobota helped a lot in goat experiments though we have not managed to publish it.

Jolanda Gulpen and Bianca Gorski-Feenstra have constantly freed me from annoying unknown things popped up in my works and life.

Jaeson Bang gave me a precious chance to understand business, and showed me how to translate scientific ideas to an industrial product.

Jerremy Weerts has helped collected heart sound data from heart failure patients in hospital. He also provides valuable comments on the study. Without him, the success of EKO HFpEF study is impossible. Also, Vanessa van Empel has greatly supported this study.

Personalised In-silico Cardiology (PIC) project has been supported by the European Union's Horizon 2020 research and Innovation programme under the Marie Sklodowska-Curie grant agreement No. 764738. Without this funding, I would not be able to study in the Netherlands and learn the diversity of the world.

Pablo Lamata has been leading the project with his great enthusiasms, together with helps from David Jordan. I will remember the happy time of staying with the other PIC fellows including Yingjing Feng, Joao Fernandes, Filip Loncaric, Hassaan Bukhari, Ali Wajdan, Manuel Villegas Martinez, Andrew Gilbert, Cristobal Rodero, Jorge Corral-Acero, Valeria Galli, Francesca Margara, Maciej Marciniak and Mariana Sousa Santos. Moreover, Espen W Remme, Peter Mortier and Blanca Rodriguez had some happy talks with me at some moments.

Salomé Bazin has helped managed the development of Echoes App and been responsible for design of user interface.

My Chinese friends have been making my life colorful in the past years.

Yiping Huang(黄一平), Guangyao Wu (吴光耀), Min Deng (邓敏), Zhilong Chen (陈志龙), Rui Wang (王锐), Yiwen Yu (余艺文) and Zhenwei Shi (石镇维) have been playing basketball with me during the weekend every now and then. I also joined some sports together with my neighbors including Xiuxiang Tan (檀秀香), Xingzhen Zhang (张幸真), Jinmi Zou (邹今幂) and Qian Luo (罗倩). Jun Wan (万俊) and Shanshan Wang (王珊珊) are a nice couple who have been helping me a lot.

My wife and I had some fun times staying with Wenting You (油文婷), Tao Zhou (周涛), YoYo Zhou (周泽楷), Qing Xu (徐青), Shenghua Zong (宗盛华) and Yumi Zong (小玉米). The kids YoYo Zhou (周泽楷) and Yumi Zong (小玉米) are so cute.

Kongyuan Wei (魏孔源) has been my friend for over 10 years, and hope he can publish his first paper in Nature or Science one day in the near future.

Yong Qin (秦涌), Yiqiang Liu(刘毅强) and Zhengpu Qin (秦峥浦) are hospitable in The Hague. Looking forward to their visit to Maastricht.

Yi Wu (吴怡) and Chunxiao Fan (范春晓) are unique girls who offer my wife and I valuable guidance in the past years. Letao Li (李乐涛) and I had some nice sports and talks together. Best wishes to his research and life in Erasmus. Sunny Jiang (Brightlands China Center) is always ready to help when I have questions about industry.

During my later days of PhD, new friends have brought many joys to my life, including Minsi Cai (蔡敏思), Rui Zhang (张瑞), Fangzhou Lu (卢方舟), Yan Sun (孙妍), Jinzhe Ju (剧锦哲) and Lei He (何磊). Great thanks to Fangzhou Lu (卢方舟) and Lei He (何磊) for teaching me how to swim. Best wishes to your research and living in Maastricht.

Xianwei Zhang (张献伟) has been in contact with me since Simula courses in Oslo in June 2018. We shared our thoughts on research and life every now and then.

I also would like to thank my friends who are living in mainland China. Shuo Zhang (张硕) is an excellent optical engineer who is enthusiastic about research and life. Kunfei Liang (梁坤飞) and Xingdong Mai (麦兴东) have helped me build some hardware to test my preliminary ideas. Shijie Ding (丁世杰) is the first Chinese I met in Physiology Department, and best hope to his ambition of building a great company of cultured meat in China. Ying Gong (龚英) was my senior guide in life and research in Maastricht. Wanli Liang (梁万利), Yixiong Wu (吴艺雄) and Cong Zhang (张聪) had some nice remote talks with me. Hongzhi Liu (刘洪智), Xiaoliang Li (李晓亮) and Song Lin (林松) always offered me nice thoughts from clinical perspective. Ting Cui(崔婷) had some nice times with my wife and me. Best wishes to her new career in China. Gang Yu (于刚) has provided me his selfless and expert guidance in signal processing. I really appreciate that.

My family members give me the strongest supports during my PhD period, including Jianyou Luo (罗建有), Yingmei Mo (莫英梅), Hongyun Luo (罗鸿运) and Fengying Li (黎凤英). My beloved wife Yongchan Lie (列永婵) has offered me her greatest supports in my life and research. Great thanks to Jinfeng Gan (甘进凤) and Jiafang Lie (列家芳) for their nice talks with my wife and me every now and then. We also had a nice trip with Eli Xie (谢娥丽) in Europe before the COVID-19 outbreak. Looking forward to the next visit when everything gets better.

Lastly, I would like to thank some unseen workers on heart sound and signal processing researches, some of whom may have passed away, including Aldo A. Luisada, Louis-Gilles Durand, Frans van de Werf, Hani N. Sabbah, Paul D. Stein, John C. Wood, Yukio Ozawa, Hiroshi Kanai, Charles C. Wolferth, Alexander Margolies, Victor A. McKusick, Robert G Stockwell and Hong Tang. Their wisdoms are shining my path on heart sound research.

About the Author

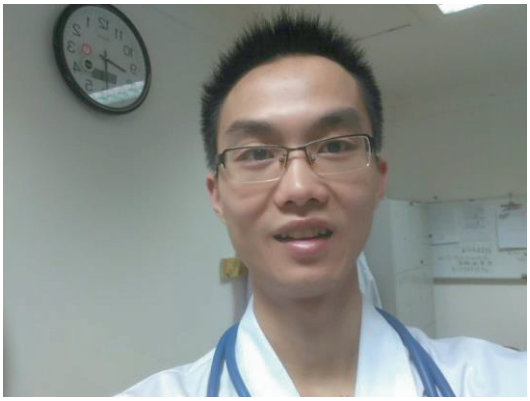

Hongxing Luo was born on 15 August, 1991 in Guangdong, China. After completing his secondary education at Guangdong Gaozhou Middle School, he started to study clinical medicine in Lanzhou University from September 2010. In June 2015, he completed his bachelor study and was enrolled as a master student in Department of Heart Failure, Zhengzhou University Renmin Hospital, under supervision of dr. prof. Yu Xu. The 3-year master program was a combination of research and clinical trainings at various departments of hospital. During this period, he grew interests in clinical trials and the use of technology for solving clinical issues. He obtained his Chinese medical practice license and graduated as one of "Top 10 Graduate Students" in Zhengzhou University.

Since July 2018, he has been sponsored by European Union's Horizon 2020 Research and Innovation Programme under the Marie Sklodowska-Curie grant to work as a PhD candidate at Department of Physiology, Cardiovascular Research Institute (CARIM), Maastricht University, under supervision of prof. dr. Frits W. Prinzen. His project is about the use of heart sounds for disease monitoring such as the optimization of pacemaker in heart failure patients. During the period, he has been learning how to translate engineering techniques to solve unmet clinical needs. He works together with other engineers to build tools for measurement and simulation of cardiac signals, and also with King's College London and Cellule Design Studio to develop an App to record heart sounds using smartphone microphone. In the meantime, he has been active in reviewing for renowned journals in the fields of mHealth and cardiology such as the *JMIR* series, *European Heart Journal – Digital Health* and *ESC Heart Failure*.

As of January 2022, he is working together with prof. dr. Frits W. Prinzen as a postdoctoral research fellow at the Department of Physiology in Maastricht University.

List of Publications

List of publications

Hemodynamics-driven mathematical model of third heart sound generation.
Shahmohammadi M, Huberts W, **Luo H**, Westphal P, Cornelussen RN, Prinzen FW, Delhaas T. Front Physiol. 2022 July 25. doi: 10.3389/fphys.2022.847164.

Left Ventricular Pressure Estimation Using Machine Learning-Based Heart Sound Classification.
Westphal P, **Luo H**, Shahmohammadi M, Heckman LIB, Kuiper M, Prinzen FW, Delhaas T, Cornelussen RN. Front Cardiovasc Med. 2022 May 25;9:763048. doi: 10.3389/fcvm.2022.763048. eCollection 2022.

Hemodynamics-driven mathematical model of first and second heart sound generation.
Shahmohammadi M, **Luo H**, Westphal P, Cornelussen RN, Prinzen FW, Delhaas T. PLoS Comput Biol. 2021 Sep 22;17(9):e1009361. doi: 10.1371/journal.pcbi.1009361. eCollection 2021 Sep.

Second heart sound splitting as an indicator of interventricular mechanical dyssynchrony using a novel splitting detection algorithm.
Luo H, Westphal P, Shahmohammadi M, Heckman LIB, Kuiper M, Cornelussen RN, Delhaas T, Prinzen FW. Physiol Rep. 2021 Jan;9(1):e14687. doi: 10.14814/phy2.14687.

Surveillance of COVID-19 in the General Population Using an Online Questionnaire: Report From 18,161 Respondents in China.
Luo H, Lie Y, Prinzen FW. JMIR Public Health Surveill. 2020 Apr 27;6(2):e18576. doi: 10.2196/18576.

The 'Digital Twin' to enable the vision of precision cardiology.
Corral-Acero J, Margara F, Marciniak M, Rodero C, Loncaric F, Feng Y, Gilbert A, Fernandes JF, Bukhari HA, Wajdan A, Martinez MV, Santos MS, Shamohammdi M, **Luo H**, Westphal P, Leeson P, DiAchille P, Gurev V, Mayr M, Geris L, Pathmanathan P, Morrison T, Cornelussen R, Prinzen F, Delhaas T, Doltra A, Sitges M, Vigmond EJ, Zacur E, Grau V, Rodriguez B, Remme EW, Niederer S, Mortier P, McLeod K, Potse M, Pueyo E, Bueno-Orovio A, Lamata P. Eur Heart J. 2020 Dec 21;41(48):4556-4564. doi: 10.1093/eurheartj/ehaa159.

Manuscripts under revision:

Smartphone as an electronic stethoscope: Factors influencing heart sound quality. **Luo H**, Lamata P, Bazin S, Bautista T, Barclay N, Shahmohammadi M, Lubrecht JM, Delhaas T, Prinzen FW. Eur Heart J - Digit Health.

Association between phonocardiography and echocardiography in heart failure patients with preserved ejection fraction. **Luo H**, Weerts J, Bekkers A, Achten A, Lievens S, Smeets K, van Empel VPM, Delhaas T, Prinzen FW. Eur Heart J - Digit Health.

Heart sound-derived systolic time intervals for atrioventricular delay optimization in cardiac resynchronization therapy. **Luo H**, Westphal P, Shahmohammadi M, Heckman LIB, Kuiper M, Cornelussen RN, Delhaas T, Prinzen FW. Heart Rhythm.

Conference presentations

Dutch Physiology Days 2021, Online event, February 2021, oral presentation: ***Splitting of second heart sound as measure of ventricular dyssynchrony***.

CARIM Symposium 2020, Maastricht, November 2020, Winner of the best poster presentation: ***Heart sounds for cardiac resynchronization therapy optimization***.

Mobile App

Echoes App, available at Apple App Store (https://apps.apple.com/gb/app/echoes/id1529300249) and on the Echoes website (https://www.echoesapp.org/).